



Università degli Studi di Cagliari

## **DOTTORATO DI RICERCA**

Scuola di Dottorato di Ricerca in Ingegneria Civile e Architettura

Dottorato in Tecnologie per la conservazione dei beni architettonici e ambientali

Ciclo XXVII

### **TITOLO TESI**

**AMBIENT VIBRATION MEASUREMENTS FOR NON-DESTRUCTIVE  
EVALUATION OF STRUCTURES BY MEANS OF SEISMIC METHODS  
AND GROUND-BASED MICROWAVE INTERFEROMETRY**

Settore scientifico disciplinare di afferenza

GEO/11 Geofisica applicata

Presentata da: Sergio Vincenzo Calcina

Coordinatore Dottorato Prof. Ulrico Sanna

Tutor/Relatore Prof. Gaetano Ranieri

Esame finale anno accademico 2013 – 2014



Unione europea  
Fondo sociale europeo



REGIONE AUTONOMA DELLA SARDEGNA



FSE 2007-2013  
obiettivo competitività regionale e occupazione



<b>SOMMARIO .....</b>	<b>1</b>
<b>SUMMARY .....</b>	<b>5</b>
<b>CHAPTER 1.....</b>	<b>9</b>
<b>AMBIENT VIBRATION ANALYSIS FOR THE STUDY OF THE MODAL BEHAVIOUR OF STRUCTURES .....</b>	<b>11</b>
1.1 RANDOM PROCESSES .....	11
1.1.1 CORRELATION FUNCTIONS.....	12
1.1.2 ERGODIC PROCESSES .....	13
1.2 POWER SPECTRAL DENSITY FUNCTIONS .....	14
1.3 TRANSFER FUNCTION .....	16
1.3.1 IMPULSE RESPONSE FUNTION.....	17
1.4 DETERMINATION OF THE NORMAL MODE SHAPES BY MEANS OF OUTPUT-ONLY MEASUREMENTS .....	20
1.5 ANALYSIS METHODS.....	20
1.5.1 BASIC PEAK-PICKING METHOD.....	21
1.5.2 FREQUENCY DOMAIN DECOMPOSITION METHOD .....	23
1.5.3 RANDOM DECREMENT TECHNIQUE .....	24
REFERENCES .....	26
<b>CHAPTER 2.....</b>	<b>27</b>
<b>GROUND-BASED RADAR INTERFEROMETRY AND REMOTE SENSING FOR STRUCTURAL MONITORING.....</b>	<b>29</b>
1.1 INTRODUCTION TO THE GROUND-BASED RADAR INTERFEROMETRY.....	30
2.2 INSTRUMENTAL FEATURES AND CAPABILITIES OF THE RADAR INTERFEROMETER IBIS-S.....	31
2.2.1 INTERFEROMETRY: WORKING PRINCIPLES .....	31
2.2.2 RADAR RESOLUTION.....	33
2.2.3 STEPPED FREQUENCY-CONTINUOUS WAVES RADAR TECHNIQUE.....	33
2.2.4 RADAR BEAM .....	35
REFERENCES .....	36
<b>CHAPTER 3.....</b>	<b>39</b>
<b>DYNAMIC CONTROL OF HISTORICAL BUILDINGS THROUGH INTERFEROMETRIC RADAR TECHNIQUES: A USEFUL APPROACH FOR STRUCTURAL HEALTH MONITORING ON EARTHQUAKE DAMAGED STRUCTURES .....</b>	<b>41</b>
3.1 INTRODUCTION .....	42
3.2 DESCRIPTION OF THE STUDY AND METHOD .....	43

3.2.1 THE TOWER: A BRIEF HISTORICAL OVERVIEW AND DESCRIPTION OF THE DAMAGE ....	43
3.2.2 SENSOR INSTALLATION AND DATA PROCESSING.....	44
3.3 RESULTS AND DISCUSSION.....	45
3.4 DISCRETE MODEL OF THE TOWER.....	48
3.5 CONCLUSIONS .....	50
REFERENCES .....	51

**CHAPTER 4..... 53**

COMPARISON OF NATURAL AND ARTIFICIAL FORCING TO STUDY THE DYNAMIC BEHAVIOUR OF BELL TOWERS IN LOW WIND CONTEXT BY MEANS OF GROUND-BASED RADAR INTERFEROMETRY: THE CASE OF THE LEANING TOWER OF PISA..... 55

4.1 INTRODUCTION.....	56
4.2 APPLICATIONS AND RESULTS .....	56
4.3 CONCLUSIONS .....	64
REFERENCES .....	65

**CHAPTER 5..... 67**

NON-DESTRUCTIVE EVALUATION OF THE DYNAMIC BEHAVIOUR OF HISTORIC BELL TOWERS BY INTEGRATING CONTACT AND REMOTE SENSING MEASUREMENTS..... 69

5.1 INTRODUCTION.....	70
5.2 DESCRIPTION OF THE STRUCTURE.....	71
5.3 DESCRIPTION OF THE EXPERIMENTAL VIBRATION TESTS AND RESULTS .....	72
5.3.1 MICROTREMOR MEASUREMENTS .....	72
5.3.2 EXPERIMENTAL RESULTS AND DISCUSSION.....	76
5.3.3 EXPERIMENTAL MODAL SHAPES.....	87
5.4 FINITE ELEMENT ANALYSIS AND VALIDATION OF EXPERIMENTAL RESULTS.....	89
5.4.1 FINITE ELEMENT MODEL.....	89
5.4.2 CALIBRATION AND VALIDATION .....	93
5.5 CONCLUSIONS .....	95
REFERENCES .....	96

**CHAPTER 6..... 99**

AMBIENT VIBRATION TESTS OF AN ARCH DAM WITH DIFFERENT RESERVOIR WATER LEVELS: EXPERIMENTAL RESULTS AND COMPARISON WITH FINITE ELEMENT MODELLING..... 101

6.1 INTRODUCTION.....	102
6.2 THE SITE OF STUDY .....	104

6.3 EXPERIMENTAL VIBRATION TESTS AND RESULTS .....	105
6.3.1 DESCRIPTION OF DATA ACQUISITION AND PROCESSING .....	105
6.3.2 TESTS RESULTS AND DISCUSSION.....	108
6.4 FINITE ELEMENT MODELLING AND ANALYSIS .....	115
6.4.1 DISCRETE MODEL OF PUNTA GENNARTA DAM .....	115
6.4.2 NUMERICAL RESULTS.....	115
6.5 CONCLUSIONS .....	117
REFERENCES .....	119



## SOMMARIO

Il presente lavoro raccoglie i risultati delle ricerche sviluppate durante il percorso del dottorato in “Tecnologie per la conservazione dei beni architettonici e ambientali” all’interno della Scuola di Dottorato in Ingegneria Civile e Architettura dell’Università di Cagliari. Le ricerche si sono concentrate sull’analisi dinamica sperimentale degli edifici. In tal senso un’attenzione prevalente, ma non esclusiva, è stata rivolta a strutture di rilevanza storica, caratterizzate da un considerevole sviluppo verticale, come le torri campanarie. La ricerca affronta, caso per caso, problematiche inerenti sia gli aspetti sperimentali sia le relazioni tra le proprietà di vibrazione e le caratteristiche costruttive dei manufatti.

La tesi si articola in una parte introduttiva, sviluppata all’interno dei primi capitoli, in cui vengono esposti e sintetizzati i principi dei metodi di analisi dinamica sperimentale delle strutture, con particolare riferimento alle tecniche passive basate sulla registrazione di vibrazioni ambientali.

Una parte sempre introduttiva è invece dedicata alla presentazione e alla descrizione delle caratteristiche della tecnica Ground-based Radar Interferometry per la misura da remoto delle vibrazioni di oggetti presenti all’interno dello scenario radar, utilizzando la differenza di fase tra segnali riflessi dalla superficie del medesimo bersaglio. Questa tecnica, sviluppata in tempi relativamente recenti, ha assistito ad una crescente diffusione soprattutto grazie alla rapidità delle misure e alla possibilità di ricavare serie di spostamento senza la necessità di accedere alle strutture per l’installazione dei sensori. Caratteristica che si rivela di estremo vantaggio proprio in caso di analisi di strutture danneggiate o pericolanti.

Per quanto concerne quindi l’aspetto sperimentale, particolare interesse è stato rivolto al confronto tra i dati di vibrazione acquisiti con sistemi classici (quali sensori sismici, velocimetri, accelerometri, etc.) e quelli ricavati utilizzando il sensore radar IBIS-S (Image By Interferometry Survey), il cui funzionamento è appunto basato sulla tecnica interferometrica.

I diversi casi di studio presi in esame sono analizzati e discussi criticamente all’interno dei capitoli successivi. Il terzo capitolo si concentra sull’analisi delle proprietà di vibrazione di una struttura campanaria lesionata per effetto di un terremoto, anche attraverso il confronto tra le condizioni, rispettivamente, *ex ante* ed *ex post* il danneggiamento. La struttura, localizzata in prossimità dell’area epicentrale del terremoto emiliano del 2012, è stata oggetto di un rilievo radar interferometrico poco dopo l’evento sismico che ha permesso di descriverne il comportamento dinamico in presenza di un importante quadro fessurativo e di ingenti lesioni strutturali che tuttavia non hanno compromesso in modo irreparabile il manufatto. La risposta dinamica della struttura precedente la condizione di danneggiamento è stata invece simulata attraverso la realizzazione di un modello numerico agli elementi finiti.

Il quarto capitolo descrive lo studio finalizzato alla valutazione dell'influenza delle vibrazioni, indotte artificialmente dal movimento coordinato di venti persone all'interno di una struttura, nell'estrazione delle principali proprietà di vibrazione. In questo caso le misure sono state eseguite utilizzando diverse stazioni radar disposte intorno alla struttura oggetto di studio, la torre pendente di Pisa. Le misure sono state eseguite sia in presenza di sole vibrazioni ambientali che in presenza dell'azione forzante generata artificialmente nella parte più elevata della torre.

Il quinto capitolo descrive uno studio teso a valutare l'influenza delle proprietà meccaniche dei materiali e delle caratteristiche costruttive sui principali parametri dinamici delle strutture. A tale scopo è stata presa in esame una struttura caratterizzata da una doppia torre campanaria. Le due torri si ergono simmetricamente in corrispondenza delle parti laterali del prospetto principale dell'edificio, ma sono realizzate utilizzando materiali costruttivi differenti. Infatti, la struttura più antica si presenta in muratura di conci lapidei, la seconda, successiva di circa un secolo, è costruita con setti in cemento armato. In questo caso le analisi sono state eseguite integrando misure di vibrazione, realizzate con entrambi i sistemi a disposizione, ossia il sensore radar IBIS-S per le misure relative alle parti più elevate della struttura (non direttamente accessibili) e i trasduttori sismici, posizionati all'interno dell'edificio.

Infine l'ultimo capitolo si concentra sulle misure di vibrazione eseguite su una diga a doppio arco in diverse condizioni di invaso, analizzando in che modo le variazioni del livello d'acqua, sequestrata a monte dello sbarramento artificiale, modificano le proprietà dinamiche della struttura.

Alcuni degli argomenti trattati nell'ambito della ricerca sono stati oggetto di pubblicazione, o sono stati recentemente sottomessi per la pubblicazione su rivista internazionale e su atti di convegno. In particolare, si ricordano i seguenti lavori:

*Calcina S. V., Piroddi L., Ranieri G. (2013). "Interferometric radar applications for the monitoring of vibrations of cultural heritage buildings and comparison with 3D velocimeter measurements", in Proceedings of the 4<sup>th</sup> EARSel Workshop on Cultural and Natural Heritage, Session 3.3 SAR for Archaeology, Matera, Italy, 6<sup>th</sup>-7<sup>th</sup> June 2013. ISBN 978-8-88-9693254*

*Calcina S.V., Piroddi L., Ranieri G. (2013). "Dynamic control of historical buildings through interferometric radar technique: a useful approach for Structural Health Monitoring on earthquake damaged structures", in Proceedings of the 32° Congresso Nazionale GNGTS, Sessione 3.2 - Metodi elettromagnetici e gravimetrici, 19-21 novembre 2013, Trieste, Italia. ISBN: 978-88-902101-8-1*

*Calcina S.V., Piroddi L., Ranieri G. (2013). "Fast dynamic control of damaged historical buildings: a new useful approach for Structural Health Monitoring after an earthquake", ISRN Civil Engineering, vol. 2013, Article ID 527604, 6 pages.*



*doi:10.1155/2013/527604*

*Marchisio M., Piroddi L., Ranieri G., Calcina S.V., Farina P. (2014). Comparison of natural and artificial forcing to study the dynamic behaviour of bell towers in low wind context by means of Ground-based Radar Interferometry: the case of the Leaning Tower in Pisa, Journal of Geophysics and Engineering, 11, 5, 055004 (10pp).*

*doi:10.1088/1742-2132/11/5/055004*

*Calcina S.V., Eltrudis L., Piroddi L., Ranieri G. (2014). “Ambient Vibration Tests of an arch dam with different reservoir water levels: experimental results and comparison with Finite Element modelling”, The Scientific World Journal, vol. 2014, Article ID 692709, 12 pages.*

*doi:10.1155/2014/692709*

*Calcina S.V., Piroddi L., Ranieri G., Non-destructive evaluation of the dynamic behaviour of historic bell towers integrating contact and remote sensing measurements, submitted to Nondestructive testing and evaluation.*



## SUMMARY

This thesis collects the results of the researches carried out during the Ph.D. course in “Technologies for the Conservation of Architectural and Environmental Heritage” into the School of Civil Engineering and Architecture of the University of Cagliari. The main topics of this research are focused on the experimental dynamic analysis of the structures with prevalent, but not exclusive, interest for the analyses of historic structures. The research deals with several issues concerning both the experimental measurements and the relationships between vibration properties and structural features and materials.

The study starts with an introduction, developed into the first chapter, where the general principles of the experimental dynamic analysis methods of structures are presented and summarised, especially for the passive techniques based only on ambient vibrations records.

The next chapter presents and describes the main features of the Ground-based Radar Interferometry to perform remote measurements of vibrations, using the phase difference between reflected signals coming from the surface of the same object inside the radar scenario. This technique has been developed in relatively recent years and has seen a considerable spread thanks to the short time need for the measurements and for the capability to retrieve reliable time series of displacement without any contact sensors above the structures. Furthermore the vibration data, acquired with both conventional systems (such as seismic sensors, velocimeters, accelerometers, etc.) and the microwave interferometer IBIS-S (Image By Intereferometry Survey), have been compared.

Different case studies have been examined and critically discussed in the following chapters.

In particular, chapter three is focused on the analysis of the vibration properties of an earthquake damaged bell tower located near the epicenter of the Emilia earthquake. Both *ex ante* and *ex post* conditions respect to the seismic induced damage have been compared. For this purpose a non-contact dynamic survey has been carried out by means of the radar interferometry method. The campaign of measurements has been conducted after the earthquake to describe the dynamic behaviour of the structure with open fractures pattern and with significant structural damages. Finally, a Finite Element model of the structure has been done in order to compare the actual dynamic response of the tower with that one of the undamaged structure.

Chapter four looks at the influence of the vibration artificially induced by the coordinated movement of twenty people to improve main dynamic properties identification of the structure. In this case, the measurements have been carried out using the radar sensor by means of four stations located around the examined structure, the Leaning Tower of Pisa. The measurements have been performed in both operational mode using only wind induced vibrations and also with the artificial human forcing, applied at the top floor of the tower.

Chapter five describes both the experimental measurements and the numerical modelling carried out in order to derive the dynamic features of two similar bell towers. The comparison between the dynamic behaviour of the towers is aimed at studying the influence of the mechanical properties of different construction materials. In fact, the towers are symmetrically built on both sides of the main façade of a church but the two structures are made using different materials and with different construction techniques. The oldest tower is a stone masonry building and the second one is a Reinforced Concrete structure. In this case, the analyses have been carried out using vibration data acquired by means of both available systems, i.e. the IBIS-S radar interferometer for the measurements related to the upper parts of the structure (not easily accessible) and some seismic transducers for the stations located inside of the building.

Chapter six finally presents the vibration measurements performed on a double curvature arch dam with different reservoir water level in order to analyse the variation of the linear dynamic response of the structure related to the water level height on the upstream side of the dam. The experimental surveys are described and the comparison with a numerical modelling is shown.

Some topics discussed in the text have been published, or have recently been submitted for publication on international journals and conference proceedings. In particular, the following papers may be mentioned:

*Calcina S. V., Piroddi L., Ranieri G. (2013). "Interferometric radar applications for the monitoring of vibrations of cultural heritage buildings and comparison with 3D velocimeter measurements", in Proceedings of the 4th EARSel Workshop on Cultural and Natural Heritage, Session 3.3 SAR for Archaeology, Matera, Italy, 6th-7th June 2013. ISBN 978-8-88-9693254*

*Calcina S.V., Piroddi L., Ranieri G. (2013). "Dynamic control of historical buildings through interferometric radar technique: a useful approach for Structural Health Monitoring on earthquake damaged structures", in Proceedings of the 32° Congresso Nazionale GNGTS, Sessione 3.2 - Metodi elettromagnetici e gravimetrici, 19-21 novembre 2013, Trieste, Italia. ISBN: 978-88-902101-8-1*

*Calcina S.V., Piroddi L., Ranieri G. (2013). "Fast dynamic control of damaged historical buildings: a new useful approach for Structural Health Monitoring after an earthquake", ISRN Civil Engineering, vol. 2013, Article ID 527604, 6 pages.*

*doi:10.1155/2013/527604*

*Marchisio M., Piroddi L., Ranieri G., Calcina S.V., Farina P. (2014). Comparison of natural and artificial forcing to study the dynamic behaviour of bell towers in low wind context by means of Ground-based Radar Interferometry: the case of the Leaning Tower in Pisa, Journal of Geophysics and Engineering, 11, 5, 055004 (10pp). doi:10.1088/1742-2132/11/5/055004*

*Calcina S.V., Eltrudis L., Piroddi L., Ranieri G. (2014). "Ambient Vibration Tests of an arch dam with different reservoir water levels: experimental results and comparison with Finite Element modelling", The Scientific World Journal, vol. 2014, Article ID 692709, 12 pages.*

*doi:10.1155/2014/692709*

*Calcina S.V., Piroddi L., Ranieri G., Non-destructive evaluation of the dynamic behaviour of historic bell towers integrating contact and remote sensing measurements, submitted to Nondestructive testing and evaluation.*



## ***CHAPTER 1***





**Abstract**

*This chapter deals with the fundamental mathematical frame used for the random vibration analysis. The basic theory of the random processes is briefly described, especially about its typical applications to the study of the linear system response. Finally the key elements of the Operational Modal Analysis are introduced and the main techniques implemented for these purposes, working in time and in frequency domain, are summarised.*

**1.1 RANDOM PROCESSES**

Deterministic signals theory can be used when a physical phenomenon may be described using explicit mathematical relationships. Conversely the probabilistic approach allows one to study random phenomena which are characterised by unknown exact features at a determined time instant. Thus, the statistical methods provide the main tools suitable to analyse random data as ambient vibrations, microseisms, wind forces, sea waves, etc. A random or stochastic process is defined as the ensemble of all possible realizations of a random phenomenon. For example by considering the picture of Figure 1.1, we can see several time series of ambient vibration: the collection of all time histories represents the *random process*, whereas each trace is called *sample function* and it represents one single realization of the random process.

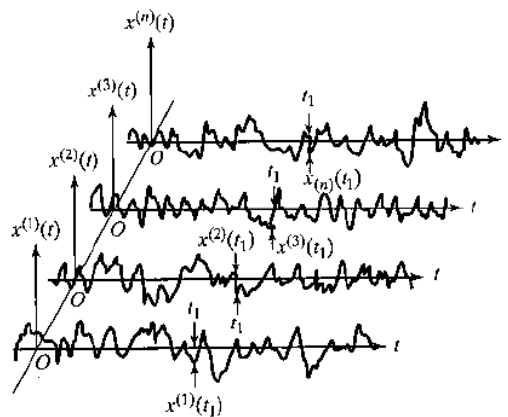


Figure 1.1: Example of random signals (by Bendat and Piersol, 2000).

Random processes are usually classified as:

- 1) *Sensu stricto stationary processes* when the statistics do not depend over time;
- 2) *Sensu lato stationary processes* if the mean and the auto-correlation do not depend over time;
- 3) Finally, *ergodic processes* when overall statistics may be calculated starting from time averages.

In the following paragraphs, main attention will be focused on Stationary Random Processes (SRP) and in particular on Stationary and Ergodic Random Processes (SERP).

### 1.1.1 Correlation functions

The correlation function is a fundamental tool used in many experimental dynamic identification techniques, especially for the output-only procedures. If we consider the sample functions  $x_k(t)$  and  $y_k(t)$  of two stationary random processes, the mean values are given by the following formulas:

$$\mu_x = E[x_k(t)] = \int_{-\infty}^{\infty} xp(x)dx \quad (1.1)$$

$$\mu_y = E[y_k(t)] = \int_{-\infty}^{\infty} yp(y)dy \quad (1.2)$$

Where  $p(x)$  and  $p(y)$  indicate the probability density functions of  $x(t)$  and  $y(t)$ , respectively. The covariance functions assume the expressions:

$$C_{xx}(\tau) = E[(x_k(t) - \mu_x)(x_k(t + \tau) - \mu_x)] \quad (1.3)$$

$$C_{yy}(\tau) = E[(y_k(t) - \mu_y)(y_k(t + \tau) - \mu_y)] \quad (1.4)$$

$$C_{xy}(\tau) = E[(x_k(t) - \mu_x)(y_k(t + \tau) - \mu_y)] \quad (1.5)$$

If the mean value is zero for both variables, the previous relationships can be simplified as:

$$C_{xx}(\tau) = R_{xx}(\tau) = E[x_k(t)x_k(t + \tau)] \quad (1.6)$$

$$C_{yy}(\tau) = R_{yy}(\tau) = E[y_k(t)y_k(t + \tau)] \quad (1.7)$$

$$C_{xy}(\tau) = R_{xy}(\tau) = E[x_k(t)y_k(t + \tau)] \quad (1.8)$$

The equations (1.6) and (1.7) represent the auto-correlation functions of  $x(t)$  and  $y(t)$ . Instead the equation (1.8) indicates the cross-correlation function computed between  $x(t)$  and  $y(t)$ . In particular the last correlation function denotes how much the considered sample functions are correlated

between them. Conversely when the mean values are not zero the covariance functions are related to the correlation functions by means of the equations:

$$C_{xx}(\tau) = R_{xx}(\tau) - \mu_x^2 \quad (1.9)$$

$$C_{yy}(\tau) = R_{yy}(\tau) - \mu_y^2 \quad (1.10)$$

$$C_{xy}(\tau) = R_{xy}(\tau) - \mu_x\mu_y \quad (1.11)$$

By considering both correlation and covariance functions the following inequalities can be written:

$$|C_{xy}(\tau)|^2 \leq C_{xx}(0) \cdot C_{yy}(0) \quad (1.12)$$

and

$$|R_{xy}(\tau)|^2 \leq R_{xx}(0) \cdot R_{yy}(0) \quad (1.13)$$

Furthermore, observing that:

$$|C_{xx}(\tau)| \leq C_{xx}(0) \quad (1.14)$$

$$|R_{xx}(\tau)| \leq R_{xx}(0) \quad (1.15)$$

It possible to derive that the maximum values of the auto-correlation and auto-covariance functions are obtained for  $\tau=0$  and they coincide with:

$$R_{xx}(0) = E[x_k^2(t)] \quad (1.16)$$

$$C_{xx}(0) = \sigma_x^2 \quad (1.17)$$

where  $E[x^2(t)]$  indicates the mean square value and  $\sigma_x^2$  represents the variance of  $x(t)$ .

### 1.1.2 Ergodic processes

Stationary random processes are defined weakly ergodic when their mean values can be calculated using time averages derived for a pair of sample records. This means that the statistical properties of a weakly stationary random process can be derived using a pair of sample records only. Thus the mean values of each sample function may be determined by means of time averages, as follows:

$$\mu_x(k) = \lim_{T \rightarrow \infty} \frac{1}{T} \int_0^T x_k(t) dt = \mu_x \quad (1.18)$$

$$\mu_y(k) = \lim_{T \rightarrow \infty} \frac{1}{T} \int_0^T y_k(t) dt = \mu_y \quad (1.19)$$

In the equations (1.18) and (1.19) the index  $k$  indicates that the  $k$ -th sample function has been used to derive the mean value by means of the integral formulation. For ergodic processes the sample function used to calculate the statistical values don't affect the results. In other words the statistical parameters are not influenced by the particular sample function considered for the calculus. Under the above conditions the auto-covariance and the cross-covariance functions can be written in this way:

$$C_{xx}(\tau, k) = \lim_{T \rightarrow \infty} \frac{1}{T} \int_0^T [x_k(t) - \mu_x][x_k(t + \tau) - \mu_x] dt = R_{xx}(\tau, k) - \mu_x^2 \quad (1.20)$$

$$C_{yy}(\tau, k) = \lim_{T \rightarrow \infty} \frac{1}{T} \int_0^T [y_k(t) - \mu_y][y_k(t + \tau) - \mu_y] dt = R_{yy}(\tau, k) - \mu_y^2 \quad (1.21)$$

$$C_{xy}(\tau, k) = \lim_{T \rightarrow \infty} \frac{1}{T} \int_0^T [x_k(t) - \mu_x][y_k(t + \tau) - \mu_y] dt = R_{xy}(\tau, k) - \mu_x \mu_y \quad (1.22)$$

For the aforementioned reasons it possible to express the auto-correlation and the cross-correlation functions in the following forms:

$$R_{xx}(\tau) = \lim_{T \rightarrow \infty} \frac{1}{T} \int_0^\infty x(t)x(t + \tau) dt \quad (1.23)$$

$$R_{yy}(\tau) = \lim_{T \rightarrow \infty} \frac{1}{T} \int_0^\infty y(t)y(t + \tau) dt \quad (1.24)$$

$$R_{xy}(\tau) = \lim_{T \rightarrow \infty} \frac{1}{T} \int_0^\infty x(t)y(t + \tau) dt \quad (1.25)$$

Ergodic random processes are an important class of random processes. For these processes a single sample function allows to compute statistical quantities instead of an ensemble of sample functions. From a general point of view in practical applications, stationary random processes are usually also ergodic.

## 1.2 POWER SPECTRAL DENSITY FUNCTIONS

Omitting here more deepened theoretical derivations, we can define the Fourier transforms of two sample records  $x_k(t)$  and  $y_k(t)$ , characterised by finite duration  $T$ , in the following form:

$$X_k(f, T) = \int_0^T x_k(t) e^{-i2\pi f t} dt \quad (1.26)$$

$$Y_k(f, T) = \int_0^T y_k(t) e^{-i2\pi f t} dt \quad (1.27)$$

and the two-sided auto- and cross-spectral density functions are described by the equations:

$$S_{xx}(f) = \lim_{T \rightarrow \infty} E \left[ \frac{1}{T} X_k^*(f, T) X_k(f, T) \right] \quad (1.28)$$

$$S_{yy}(f) = \lim_{T \rightarrow \infty} E \left[ \frac{1}{T} Y_k^*(f, T) Y_k(f, T) \right] \quad (1.29)$$

$$S_{xy}(f) = \lim_{T \rightarrow \infty} E \left[ \frac{1}{T} X_k^*(f, T) Y_k(f, T) \right] \quad (1.30)$$

where the symbol \* indicates the complex conjugate. The above functions are defined for both positive and negative frequencies  $f$  from  $-\infty$  to  $+\infty$ . However in the experimental studies the one-sided auto- and cross-spectral density functions are mainly used in order to consider only positive frequencies, ranging from 0 to  $+\infty$ . These functions can be written as follows:

$$G_{xx}(f) = 2S_{xx}(f) = 2 \lim_{T \rightarrow \infty} \frac{1}{T} E [|X_k(f, T)|^2] \quad (1.31)$$

$$G_{yy}(f) = 2S_{yy}(f) = 2 \lim_{T \rightarrow \infty} \frac{1}{T} E [|Y_k(f, T)|^2] \quad (1.32)$$

$$G_{xy}(f) = 2S_{xy}(f) = 2 \lim_{T \rightarrow \infty} \frac{1}{T} E [X_k^*(f, T) Y_k(f, T)] \quad (1.33)$$

Furthermore, assuming that the mean values have been removed from the sample records and that the integrals of the absolute values of the correlation functions are finite (this condition is always satisfied for finite record lengths):

$$\int_{-\infty}^{\infty} |R(\tau)| d\tau < \infty \quad (1.34)$$

it results that two-sided spectral densities represent also the Fourier transforms of the correlation functions as shown by the Wiener-Khinchin equations:

$$S_{xx}(f) = \int_{-\infty}^{\infty} R_{xx}(\tau) e^{-i\omega\tau} d\tau \quad (1.35)$$

$$S_{yy}(f) = \int_{-\infty}^{\infty} R_{yy}(\tau) e^{-i\omega\tau} d\tau \quad (1.36)$$

$$S_{xy}(f) = \int_{-\infty}^{\infty} R_{xy}(\tau) e^{-i\omega\tau} d\tau \quad (1.37)$$

and one-sided power spectral densities can be written in the following form:

$$G_{xx}(f) = 4 \int_0^{\infty} R_{xx}(\tau) \cos(2\pi f\tau) d\tau \quad (1.38)$$

$$G_{yy}(f) = 4 \int_0^{\infty} R_{yy}(\tau) \cos(2\pi f\tau) d\tau \quad (1.39)$$

$$G_{xy}(f) = 4 \int_0^{\infty} R_{xy}(\tau) e^{-i2\pi f\tau} d\tau = C_{xy}(f) - iQ_{xy}(f) \quad (1.40)$$

where  $C_{xy}(f)$  is the Coincident Spectral Density Function (or *co-spectrum*) and  $Q_{xy}(f)$  is the Quadrature Spectral Density Function (also called *quad-spectrum*). By using the polar complex notation the one-sided power spectral density can be written as:

$$G_{xy}(f) = |G_{xy}(f)|e^{-i\angle G_{xy}} \quad (1.41)$$

where magnitude (module) and phase can be expressed by the following relationships:

$$|G_{xy}(f)| = \sqrt{C_{xy}^2(f) + Q_{xy}^2(f)} \quad (1.42)$$

$$\angle G_{xy}(f) = \arctan \frac{Q_{xy}(f)}{C_{xy}(f)} \quad (1.43)$$

Finally, taking into account the following inequality:

$$|G_{xy}(f)|^2 \leq G_{xx}(f) \cdot G_{yy}(f) \quad (1.44)$$

it can be introduced the ordinary coherence function which is a scalar function of frequency that can be determined knowing one-sided or two-sided power spectral densities of both input  $x(t)$  and output  $y(t)$  signals. Its expression is usually written in the following form:

$$\gamma_{xy}^2(f) = \frac{|G_{xy}(f)|^2}{G_{xx}(f) \cdot G_{yy}(f)} = \frac{|S_{xy}(f)|^2}{S_{xx}(f) \cdot S_{yy}(f)} \quad (1.45)$$

Therefore it results that the codomain of the coherence function is:  $0 \leq \gamma_{xy}^2(f) \leq 1 \quad \forall f$

Observing the formula (1.44) it is notable that when the signals are characterised by not zero average values, they should be removed in order to eliminate the delta function behaviour at zero frequency.

More extensive information and detailed exploitations of the statistical frame at the base of the modal identification procedures of structures can be found in Bendat and Piersol (1993, 2000) and in a recently published work of Rainieri and Fabbrocino (2014).

### 1.3 TRANSFER FUNCTION

The main features of the dynamic behaviour of a mechanical system are provided by its transfer function usually called Frequency Response Function (FRF). This function is defined in frequency domain and allows us to identify the response of a stationary linear system respect to a generic input excitation. The response of the system is the input signal filtered by means of the FRF. Therefore the FRF  $H(f)$  plays a fundamental role in the dynamic identification methods aimed at derive the modal parameters of the system in order to evaluate its mechanical behaviour. In other works a correct definition of the experimental modal properties can be used to calibrate and to enhance finite element models that are usually considered to study the dynamic response of the system. Thus the model updating procedures are founded on experimental studies which provide the measured values of the physical properties to constrain the model parameters used for the numerical simulations.

### 1.3.1 Impulse response function

In Figure 1.2 the simplest Single-Input/Single-Output system (SISO) is depicted. In this kind of systems an output signal  $y(t)$  may be computed filtering the input signal  $x(t)$  with the FRF that characterises the system.  $h(t)$  indicates the function that identifies the response of the system in time domain.

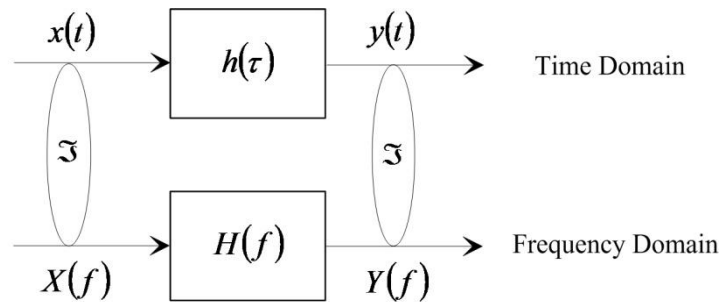


Figure 1.2: Single-Input/Single-Output ideal system.

However some assumptions must be taken into account at the base of this approach:

1. Linearity: the response of the system respect to a given combination of input signals is equal to the combination of the corresponding outputs;
2. Stationarity: the properties of the system (as modal parameters for dynamic mechanical systems) don't change over time, so that the coefficients of the differential equations governing the dynamic response of the system are independent of time;
3. Stability: the response of the system is not illimited when finite energy input excites the system. This condition may be written in this way:

$$\int_{-\infty}^{\infty} |h(t)| dt < \infty \quad (1.46)$$

4. The system is physically realizable. In other works the output of the system cannot anticipate the input. Thus it can be summarised as  $h(\tau) = 0$  for  $\tau < t_0$ .

In the case of the analysys of dynamic systems there is also another consideration about the observability of the output signals. In fact the geometric layout of the sensors used to perform the experiments needs to be properly designed in order to measure the outputs. For example, in order to measure the natural modes of a mechanical system, nodal points should be avoided because in these points the contribution of some modes is negligible or totally absent.

For ideal systems, the response respect to a generic input may be calculated using the Impulse Response Function  $h(t)$  which is the response of the system when it is excited by the Dirac's function  $\delta(t)$ :

$h(t) = y(t)$  when  $x(t) = \delta(t-t_0)$

Under these conditions the output of the system is given by the following integral:

$$y(t) = \int_{-\infty}^{\infty} h(\tau)x(t - \tau) d\tau \quad (1.47)$$

When the system is physically realizable (i.e.  $h(\tau) = 0$  for  $\tau < 0$ ) it possible to write the equation (1.47) as:

$$y(t) = \int_0^{\infty} h(\tau)x(t - \tau) d\tau \quad (1.48)$$

Looking at the frequency domain the corresponding equation of the (1.47) is based on the Fourier transforms of  $x(t)$  and  $y(t)$ :

$$Y(f) = X(f) \cdot H(f) \quad (1.49)$$

where:

$$H(f) = \int_0^{\infty} h(\tau)e^{-i2\pi f\tau} d\tau \quad (1.50)$$

The equation (1.50) indicates that the FRF together with the Impulse Response functions represent a Fourier pair. Furthermore it can be seen that:

$$X(f) = |X(f)|e^{i\angle X(f)} \quad \text{and} \quad Y(f) = |Y(f)|e^{i\angle Y(f)}$$

$$H(f) = \frac{|Y(f)|}{|X(f)|} e^{i(\angle Y(f) - \angle X(f))}$$

Starting from the equation (1.49) we can consider the complex conjugate  $X^*(f)$ :

$$X^*(f)Y(f) = H(f)X^*(f)X(f) \quad (1.51)$$

and it can be written as

$$G_{xy}(f) = H(f) \cdot G_{xx}(f) \quad (1.52)$$

In this way the FRF function is given by the complex ratio and it is usually indicated  $H_1(f)$ :

$$H(f) = \frac{Y(f)}{X(f)} \equiv \frac{G_{xy}(f)}{G_{xx}(f)} = H_1(f) \quad (1.53)$$

Conversely, if the complex conjugate of  $Y(f)$  is introduced in the above relationships (1.49), the transfer function  $H_2(f)$  may be found:

$$H(f) = \frac{Y(f)}{X(f)} \equiv \frac{G_{yy}(f)}{G_{xy}(f)} = H_2(f) \quad (1.54)$$



Because the autopower spectra are scalar functions both  $H_1(f)$  and  $H_2(f)$  have the same phase factor:

$$H_1(f) = \frac{1}{|X(f)|^2} |Y(f)||X(f)| e^{i(\angle Y(f) - \angle X(f))} \quad (1.55)$$

$$H_2(f) = \frac{|Y(f)|^2}{|X(f)||Y(f)| e^{-i(\angle Y(f) - \angle X(f))}} = \frac{|Y(f)|^2}{|X(f)||Y(f)|} e^{i(\angle Y(f) - \angle X(f))} \quad (1.55)$$

Furthermore the FRF functions  $H_1(f)$  and  $H_2(f)$  are linked between them by the following equation:

$$\frac{H_1(f)}{H_2(f)} = \frac{G_{xy}(f)G_{yx}(f)}{G_{xx}(f)G_{yy}(f)} = \gamma_{xy}^2(f) \quad (1.57)$$

where  $\gamma_{xy}^2(f)$  is the Coherence Function that assumes values close to unity under ideal conditions (linearity of the system, input and output signal are not contaminated by noise, absence of leakage effects, etc.).

Finally, by considering the equation (1.48) it possible to calculate the complex conjugate of each term of this formula:

$$Y^*(f)Y(f) = H^*(f)H(f)X^*(f)X(f) \quad (1.58)$$

Thus:

$$G_{yy}(f) = |H(f)|^2 G_{xx}(f) \quad (1.59)$$

therefore, the transfer function  $H_a(f)$  can be defined as:

$$|H(f)|^2 = \frac{Y(f)}{X(f)} \equiv \frac{G_{yy}(f)}{G_{xx}(f)} = |H_a(f)|^2 \quad (1.60)$$

When an ideal system is analysed, i.e. the above hypotheses are satisfied and both input and output signals are not influenced by noise effects and the measurements have been done without errors, for each record results that:

$$H_1(f) = H_2(f) = H_a(f) = H(f) \quad (1.61)$$

$$\gamma_{xy}^2(f) = \frac{|G_{xy}(f)|^2}{G_{xx}(f) \cdot G_{yy}(f)} = 1 \quad (1.62)$$

In real cases, the measurements of the input signal and the response of the system may be strongly affected by noise and any sources of excitation are not measured. For example, in the case of vibration measurements performed on civil structures (bridges, buildings) in addition to an external excitation signal used as input signal, usually generated by a shaker, also the contribution of other excitations could be measured, such that due to road traffic or to aerodynamic forcing. In this case it is

noteworthy that the  $H_1(f)$  function provides the best estimation of the FRF when the response of the system is influenced by the noise (output signal). Conversely, the function  $H_2(f)$  may effectively be used if the noise mainly affects the input signals.

#### 1.4 DETERMINATION OF THE NORMAL MODE SHAPES BY MEANS OF OUTPUT-ONLY MEASUREMENTS

One-sided cross power spectral density functions can be used to estimate the shapes of the structural modes of vibration of a mechanical system excited by white random noise. When the measurements are carried out using a sufficient number of sensors, if one wants to obtain the  $i^{\text{th}}$  mode shape, the following relationship may be applied:

$$\phi_i(y_i) = \sqrt{G_{y_i y_i}(f_i)} \quad i = 1, 2, 3 \dots \quad j = 1, 2, \dots r \quad (1.63)$$

However this equation is valid only when damping values are lower than 0.05 (Bendat and Pearsol, 1993).

The equivalent viscous damping can be calculated with the half-band amplitude method. This technique uses the auto-power spectra and the cross-power spectra derived by the measurements where the frequency peaks related to the dynamic response of the building are clearly identified due to the small noise contaminations. Thus the modal damping associated with each natural mode is given by the following equation:

$$\xi_i = \frac{f_b - f_a}{2f_i} \quad (1.64)$$

where  $f_a$  and  $f_b$  indicate the lower frequency and the upper frequency close the  $i^{\text{th}}$  natural resonance where:

$$G(f_b) = G(f_a) = \frac{G(f_i)}{2} \quad (1.65)$$

Both modal parameters may be estimated by means of the above approach only when the input spectrum has a uniform amplitude distribution closely to the structural resonances of the system and the damping values are low. Finally many authors observe that this method is effective to identify the dynamic response of the structures when the vibration modes are well separated. Whereas more advanced procedures must be implemented to overcome these limitations (time domain methods and frequency domain methods).

#### 1.5 ANALYSIS METHODS

The main purpose of the experimental modal analysis is to derive the response of a structure using a particular excitation signal. This response can be evaluated also in operational conditions or by means of modal testings performed in a controlled test environment. The identification of the modal

parameters of the structure from the measured data may be done with a wide range of numerical methods described by numerous authors. The different techniques can be applied taking into account the knowledge degree of the excitation features. In this way we can consider the Experimental Modal Analysis techniques if the excitation signal is artificially imposed and its features are analytically determined. Conversely, the Operational Modal Analysis methods may be used to derive the response of the structure under a random distribution of ambient noise sources. Furthermore it is important to establish the suitable experimental method if the natural modes of the structure are clearly separated or there are close modes in frequency domain. Finally low damping condition is assumed to apply some techniques. The first classification about the modal analysis methods is based on Single-Degree-of-Freedom (SDoF) and Multi-Degree-of-Freedom (MDoF) methods (He and Fu, 2001). Phase Resonance Methods are called the processing techniques based on the excitation of a single natural mode. Conversely, Phase Separation Methods are chosen when the contribution of several modes is recorded. However, it is usually possible to distinguish between Frequency Domain methods and Time Domain methods. The first category includes the following techniques:

- 1) Peak-picking method;
- 2) Circle-fit method;
- 3) Inverse FRF method;
- 4) Least-squares method;
- 5) Dobson's method;
- 6) Rational Fraction Polynomials;
- 7) Lightly Damped Structures;
- 8) Frequency Domain Decomposition.

Time domain methods include many numerical procedures as:

- 1) Least-squares time domain method;
- 2) Ibrahim time domain (ITD) method;
- 3) Random Decrement (RD) method;
- 4) ARMA Time Series method;
- 5) Least-squares Complex Exponential (LSCE) method.

The methods that will be examined in this thesis are the Peak-picking method and Frequency Domain Decomposition for the frequency domain methods and Random Decrement method as example of procedure operating in time domain.

### **1.5.1 Basic Peak-Picking method**

The Peak-Picking method (known also as Basic Frequency Domain method) is based on the auto- and cross-spectra observation in order to identify the frequency components related to the structural

response. This technique can effectively be used when the response of the structure is similar to the SDoF model around each natural resonance. In other words, the behaviour of the structure may be described as the superposition of several SDoF responses clearly separated in frequency domain. Under this assumption the response of each single vibration mode should be prevalent around each resonance. One or more reference sensors have to be chosen in order to calculate the Power Spectral Density functions, in fact, the reference channel used to identify a determined vibration mode could be inadequate to detect other natural modes. For instance, if we consider the response of a structure characterised by two bending natural modes, oriented in longitudinal and transversal direction, respectively, and by a torsional mode (third mode), it could be necessary to select a reference channel in both directions. By considering this kind of building, the analysis of the coherence function allows to identify bending and rotational modes in relationship to the reciprocal orientation of the channels considered for the computation of the coherence spectrum. When the coherence is close to the unity for both perpendicular and parallel configurations of the sensors it is probably that the frequency peak is related to a rotational mode. Conversely, bending modes are usually characterised by higher coherence values when the sensors are oriented in parallel direction. Differential behaviour can be observed for structures characterised by more complicated shapes and load distributions. Therefore, by analysing spectra and coherence functions more information about several vibration modes can be extracted. However, this procedure of modal identification may be affected by noisy measurements that can partially hide the frequency peaks related to the structure response.

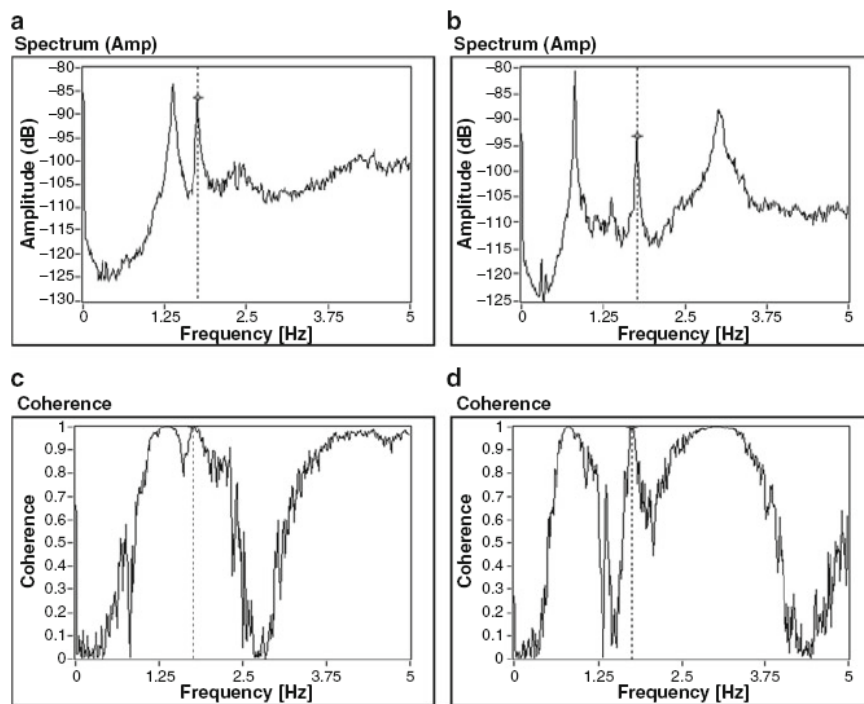


Figure 1.3: Identification of a torsional mode by means of the analysis of the auto-power spectra of two reference channels oriented in parallel (a) and orthogonal (b) direction and their coherence

functions calculated with channels arranged in parallel (c) and orthogonal (d) operational mode (by Rainieri and Frabbrocino, 2014).

### 1.5.2 Frequency Domain Decomposition method

This method has been proposed by Brincker et al. (2001) in order to improve the modal identification data processing, especially when closely spaced modes characterise the dynamic behaviour of the structures. FDD method is based on Singular Values Decomposition of the spectral density matrix. By considering the displacement vector  $s(t)$  measured above a structure, it can be obtained by the superposition of  $N$  amplitude normal modes, as follows:

$$\vec{s}(t) = \phi_1 \cdot q_1(t) + \phi_2 \cdot q_2(t) + \dots + \phi_N \cdot q_N(t) = \vec{\phi} \cdot \vec{q}(t) \quad (1.66)$$

Thus the correlation matrix of the responses can be written as:

$$\vec{R}_{ss}(\tau) = E[\vec{s}(t+\tau) \cdot \vec{s}(t)^T] \quad (1.67)$$

$$\vec{R}_{ss}(\tau) = E[\vec{\phi} \cdot \vec{q}(t+\tau) \cdot \vec{q}(t)^H \cdot \vec{\phi}^H] = \vec{\phi} \cdot \vec{C}_{qq}(\tau) \cdot \vec{\phi}^H \quad (1.68)$$

where the symbol <sup>H</sup> identifies the Hermitian operator. The corresponding equation in frequency domain assumes the following expression:

$$\vec{S}_{ss}(\omega) = \vec{\phi} \cdot \vec{S}_{qq}(\omega) \cdot \vec{\phi}^H \quad (1.69)$$

By considering the case where the modal coordinates  $q_n$  are uncorrelated, it can be demonstrated that the power spectral density (PSD) matrix  $S_{qq}(\omega)$  is a diagonal matrix. Furthermore, when the normal mode shapes are orthogonal, the equation (1.69) becomes the Singular Value Decomposition (SVD) of the response matrix  $S_{ss}(\omega)$  and it is usually written as:

$$\vec{S}_{ss}(\omega) = \vec{U}(\omega) \cdot [s_i] \cdot \vec{\phi}(\omega)^H \quad (1.70)$$

The matrix  $U(\omega)$  is the matrix of singular vectors and the matrix  $[s_i]$  is a diagonal matrix of singular values. As it appears from this explanation, plotting the singular values of the spectral density matrix will provide an overlaid plot of the auto-spectral densities of the modal coordinates. Note that here the singular matrix  $U(\omega)$  is a function of frequency because of the sorting process that is taking place as a part of the SVD algorithm (see Figure 1.4 for more details).

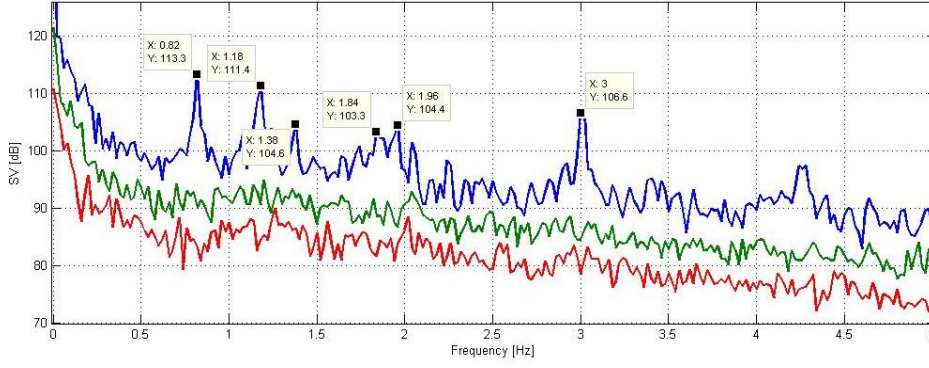


Figure 1.4: Example of singular value plots derived for the Bridge of Chains (Bagni di Lucca, Italy): natural frequencies of the bridge correspond to the peaks of the first Singular Value (blue line).

### 1.5.3 Random Decrement Technique

The Random Decrement Technique (Cole 1968, 1973) is a widely used OMA method operating in time domain aimed at estimating the free decay functions and that also provides an alternative method to evaluate the correlation functions. For this reason it is often used in combination with other identification methods. This technique was developed in order to analyse random time series and was successively applied to modal identification procedures of structures (Ibrahim, 1977; Vandiver et al., 1982; Asmussen et al., 1997, 1999). By considering a couple of ergodic stationary random processes indicated as  $x(t)$  and  $y(t)$  the following *RD signature functions* may be calculated:

$$\hat{D}_{xx}(\tau) = \frac{1}{N} \sum_{i=1}^N x(t_i + \tau) T_{x(t_i)} \quad (1.71a)$$

$$\hat{D}_{yx}(\tau) = \frac{1}{N} \sum_{i=1}^N y(t_i + \tau) T_{x(t_i)} \quad (1.71b)$$

$$\hat{D}_{xy}(\tau) = \frac{1}{N} \sum_{i=1}^N x(t_i + \tau) T_{y(t_i)} \quad (1.71c)$$

$$\hat{D}_{yy}(\tau) = \frac{1}{N} \sum_{i=1}^N y(t_i + \tau) T_{y(t_i)} \quad (1.71d)$$

In the experimental cases,  $x(t)$  and  $y(t)$  are the measurements and  $N$  indicates the number of triggering time instants collected when determined triggering conditions are satisfied. These conditions are referred to the initial conditions of the time segments in the averaging process and at zero time lag. There are more triggering conditions used in the experimental studies and they represent several particular cases of the following general condition:

$$T_{x(t)}^{G_A} = \{a_1 \leq x(t) < a_2; b_1 \leq \dot{x}(t) < b_2\} \quad (1.72)$$

The equation (1.72) establishes the initial conditions for the function and for its derivative. In other words it considers both displacement and velocity data time series. Other triggering conditions are:

$$T_{x(t)}^L = \{x(t) = a\} \text{ Level crossing} \quad (1.73a)$$

$$T_{x(t)}^P = \{a_1 \leq x(t) < a_2\} \text{ Positive point} \quad (1.73b)$$

$$T_{x(t)}^E = \{a_1 \leq x(t) < a_2; \dot{x}(t) = 0\} \text{ Local extremum} \quad (1.73c)$$

$$T_{x(t)}^Z = \{x(t) = a; \dot{x}(t) > 0\} \text{ Zero crossing} \quad (1.73d)$$

The number of triggering points may be modified by considering several triggering conditions or different triggering levels.

## **REFERENCES**

- Asmussen J.C. (1997) Modal analysis based on the Random Decrement Technique – Application to Civil Engineering structures, Ph.D. Thesis, Aalborg University, Denmark, August 1997.
- Asmussen J.C., Brincker R., Ibrahim S.R. (1999). Statistical theory of the vector random decrement technique, *Journal of Sound and Vibration*, 226, 2, 329-344.
- Bendat J.S., Piersol A. G. (1993). *Engineering Applications of Correlation and Spectral Analysis*, Wiley, New York, USA.
- Bendat J.S., Piersol A.G. (2000). *Random data: analysis and measurement procedures*, 3<sup>rd</sup> edn. Wiley, New York, NY.
- Brincker R., Zhang L., Andersen P. (2001). Modal identification of output-only systems using Frequency Domain Decomposition, *Smart Materials Structures*, 10, 441–445.
- Cole H.A. (1968). On-the-Line analysis of random vibrations, *Proceedings of AIAA/ASME 9<sup>th</sup> structures, structural dynamics and materials Conference*, April 1–3, 1968, Palm Springs, CA.
- Cole H.A. (1973). On-line failure detection and damping measurement of aerospace structures by random decrement signatures. NASA contractor report CR22-05.
- Ibrahim S.R. (1977). Random decrement technique for modal identification of structures, *J Spacecraft Rockets*, 14, 11, 696–700.
- He J., Fu Z.F. (2001). *Modal analysis*, Butterworth-Heinemann, 2001.
- Rainieri C. and Fabbrocino G. (2014). *Operational modal analysis of civil engineering structures. An introduction and guide for applications*, Springer, New York, USA.
- Vandiver J.K., Dunwoody A.B., Campbell R.B., Cook M.F. (1982). A mathematical basis for the random decrement vibration signature analysis technique, *J Mech Des*, 104, 2, 307–313.



## ***CHAPTER 2***



## GROUND-BASED RADAR INTERFEROMETRY AND REMOTE SENSING FOR STRUCTURAL MONITORING

---

### Abstract

*Natural and artificial vibrations can contribute to the degradation of the structures. Despite they are characterised by low amplitude, the dynamic actions at opportune frequencies can bring to failure of parts or entire of structures. Often the presence of dynamic actions, agents outside or inside of buildings is a cause of several problems such as the formation of cracks and the progressive deterioration of the mechanical resistance of the construction materials. These arguments become topical when involving the problem of the architectural heritage and historical buildings preservation. Most susceptible structures are slender structures, generally more disposed to instability conditions and to resonance effects. Dynamic monitoring is an effective method to estimate dynamic capabilities of existing structures and their strength to rare potentially strong actions like earthquakes, but also to detect their instantaneous response to commonly present dynamic actions like wind but also operating actions due to fruition of the buildings or coming from near neighbours. The remote sensing technology called ground-based radar interferometry has recently been introduced also to measure displacements of structures. By means of this technique it is possible to record the instantaneous displacements of even small magnitude and high frequency. Therefore the basic working principles of this method are here presented and described with special attention focused on the operating procedures.*

## 1.1 INTRODUCTION TO THE GROUND-BASED RADAR INTERFEROMETRY

Radar interferometry is a rather new technology originally developed for satellite applications in order to retrieve ground displacements related to natural hazards and other physical phenomena such as land subsidence induced by oil, gas and water extraction, with a millimetric accuracy over wide areas (Henderson and Lewis, 1998). In the last years, the same technology has been successfully implemented by using ground-based systems in order to overcome some of the limitations related to the satellite platform (e.g. low revisiting time of the available satellites and consequent temporal decorrelation of the radar signal and unwrapping problems, geometrical distortions induced by the almost vertical line of sight, etc.). Recent advances in ground-based radar techniques and systems have led to the development of microwave interferometers, suitable for non-contact monitoring of large structures, allowing the illumination of a specific scenario with a very high resolution which reaches less than one metre (Kaito et al., 2005; Pieraccini et al., 2005, 2008a; Gentile and Bernardini, 2008; Marchisio et al., 2008, 2009; Gentile and Saisi, 2011; Luzi et al., 2012a; Pieraccini, 2013). Differential Interferometric Synthetic Aperture Radar (DinSAR) is used to monitor slow movements and will not be used to study the vibrations of structures due to the low acquisition rate respect to the vibration frequencies (Farrar et al., 1999; Taylor, 2001; Crosetto et al., 2006).

The new ground-based interferometric radar system, IBIS system (Image By Interferometry Survey of Structures), allows us to measure in real time very small displacements of targets, along the radar Line Of Sight LOS, at several tens or hundred metres away from the observation point. Displacement information is taken from the phase shift contained in the back-scattered signal from the different points of the illuminated surfaces (Pieraccini et al., 2003). Since the first scientific applications dated back to the early 2000, ground-based radar interferometry has been extensively exploited for geological applications, such as monitoring of landslides (Antonello et al., 2004; Bozzano et al., 2008) and slope movements within open-pit mines (Harries et al., 2006) but also for the accurate measurement of static or dynamic deflection on civil engineering structures, such as bridges (Gentile and Bernardino, 2008; Gentile and Gallino, 2008), array of stay-cables (Gentile, 2010a, 2010b), historic towers (Atzeni et al., 2010; Pieraccini et al., 2009, 2014), wind towers (Pieraccini et al., 2008b), dams (Alba et al., 2008) and chimneys (Rödelsperger et al., 2010). The most significant advantages of ground-based radar interferometry are related to the high accuracy of the measurements, the long-range capabilities of the technology, the limited impact of atmospheric artefacts on the measurement performances, the opportunistic character of the measurement (in most of the cases, the natural reflections backscattered by the scenario are the measurement points) and the possibility to acquire simultaneously the response over a large number of points (especially for the Synthetic Aperture version of ground-based radar sensor).

## 2.2 INSTRUMENTAL FEATURES AND CAPABILITIES OF THE RADAR INTERFEROMETER IBIS-S

The main function of the IBIS-S radar interferometer is the simultaneous measurement of the displacements of different targets placed at different distances from the sensor. The sensor employs a coherent radar able to acquire consecutive images of the observed scenario, consisting of distance map of the backscattered signal coming from the reflecting targets, illuminated by the radar beam. For each target characterised by a good backscattered signal, the system is able to compute the displacement between consecutive acquisitions by comparing the phase information of the backscattered electromagnetic signal, collected at different times.

The radar system is based on the combination of two well-known radar techniques:

1. the Stepped Frequency Continuous Wave (SF CW) (Taylor, 2001) technique, employed to generate high-resolution waveforms (Wehner, 1995);
2. the interferometric technique (Henderson and Lewis, 1998), implemented to compute the displacement of each target through the phase information of the backscattered electromagnetic waves collected at different times.

### 2.2.1 Interferometry: working principles

Microwave interferometry has recently emerged as a new technology, specifically suitable to remotely measuring the vibration response of structures. Several authors observe that the interferometric technique has proven to be a useful remote sensing tool for vibration measurements of structures. This technique is implemented to compute the displacement of each object through the phase difference of the back-scattered microwave signals collected at different time intervals. When one single vibrating object is included inside a determined radar bin which is placed at a distance  $R$  from the radar, the radar response can be obtained by considering the electromagnetic field  $E$  that can be expressed by means of the following equation (Luzi et al., 2012b):

$$E = KSe^{-j\frac{4\pi}{\lambda}\left(R+\frac{\bar{R}\cdot\bar{d}(t)}{R}+R_{inst}\right)} \quad (2.1)$$

where  $\lambda$  is the wavelength of the signal;  $K$  and  $R_{inst}$  indicate both instrumental terms;  $S$  is a coefficient which takes into account the scattering of the target; finally,  $j$  is the imaginary unit. It is noteworthy that the phase term of the wave equation is linearly depending on the variation of the distance between the radar sensor and the reflective object. Both constant terms  $R_{inst}$  and  $R$  don't affect the phase variation calculus over the time for a specific radar bin. Conversely, the other term is directly depending on the vibration displacement along the LOS direction of the object. Taking into account the previous considerations, the displacement along the radar Line Of Sight  $d_{LOS}(t)$  is derived from the phase-shift  $\Delta\phi(t)$  by means of the following well known equation (2.2):

$$d_{LOS}(t) = \frac{\lambda}{4\pi} \Delta\varphi(t) \quad (2.2)$$

Basic principle of interferometry technique is represented in Figure 2.1.

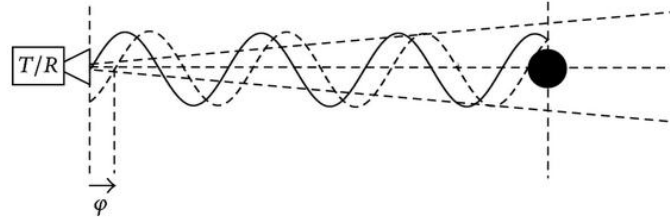


Figure 2.1: Basic principle of the interferometric analysis founded on the phase relationships (by Pieraccini, 2013).

This technique allows to measure in a short time the projection of displacement of different points of the observed structures in the range direction having the main care to distinguish which points are located at a certain range bin belonging to the wanted target and which ones belong to the surrounding environment (as sketched in Figure 2.2). The main advantages of the interferometric radar for structural health monitoring of civil infrastructures are high accuracy of measurements (0.01 mm) and high spatial resolution, simultaneous monitoring of several targets within the sensor applicable distance, independence from daylight and weather conditions for short recordings, portability, and quick set-up time.

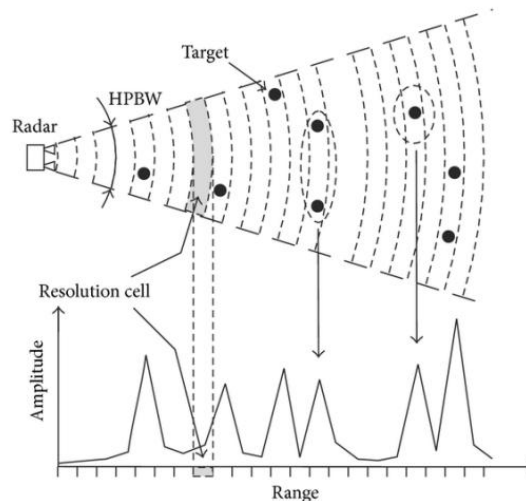


Figure 2.2: Radar Half-Power Beamwidth and one-dimensional Radar Power Profile (by Pieraccini, 2013).

For the aforementioned reasons, the acquired time history collects the displacement of the target projected along the sensor-target Line Of Sight (LOS). The LOS displacement  $d_{LOS}(t)$  is linked to the

displacements component  $v(t)$  and  $h(t)$ , in vertical and in horizontal plane, respectively, by means of the following equation (2.3):

$$d_{Los}(t) = v(t)\sin \beta + h(t)\cos \beta \quad (2.3)$$

where  $\beta$  indicates the LOS angle computed from the horizontal axis, as depicted in Figure 2.3.

### 2.2.2 Radar resolution

The resolution can be defined as the capability of the radar system to identify two closely objects. When a radar system with single-sided bandwidth (SSB) that transmits a single pulse and receives the signals reflected by two objects is examined, two adjacent targets can separately be resolved when the signals coming from each reflectors are delayed by at least  $1/B$  in time domain. Therefore the range resolution limit can be written as:

$$\delta R = \frac{c}{2B} \quad (2.4)$$

where  $c$  denotes the speed of the light. The  $1/2$  factor derives from the pulse traveling through the radar channel twice. This resolution limit criterion is usually indicated as *Rayleigh criterion* due to the analogous optical definition considered to resolve two closely spaced fringes.

### 2.2.3 Stepped Frequency-Continuous Waves Radar technique

Stepped Frequency Continuous Waves (SF CW) radar is a technique consisting of a discretised version of the Frequency Modulated CW technique where the frequency of the signal doesn't vary over the time following a linear relationship (similar to a sweep signal) but it varies through stepped intervals comprised within a bandwidth  $B$  (as shown in Figure 2.4). For example, by considering one swept period, a generic stepped-frequency continuous-wave signal may be expressed in the following way (Kong et al., 2009):

$$x(t_F) = \sum_{k=0}^{N-1} \left\{ \cos[2\pi(f_0 + k\Delta f)t_F] \right\} \cdot \text{rect}\left(\frac{t_F - kT - T/2}{T}\right) \quad (2.5)$$

where  $N$  is the number of frequencies;  $f_0$  indicates the initial frequency;  $\Delta f$  is the step of frequency;  $T$  is the time interval; and  $t_F \in [0, NT]$  is the fast time which means the time within one swept period. For one swept period, it can be considered that the echo signal shows a constant time delay  $\tau$  and taking into account the complex reflection coefficient, the reflected signal can be expressed as:

$$x_R(t_F) = |\Gamma| e^{j\phi} \sum_{k=0}^{N-1} \left\{ \cos[2\pi(f_0 + k\Delta f)(t_F - \tau)] \right\} \cdot \text{rect}\left(\frac{t_F - kT - T/2}{T}\right) \quad (2.6)$$

In most cases the time  $T \gg \tau$ , then the signal can be obtained by down converting and lowpass filtering:

$$y(t_F) = |\Gamma| e^{j\phi} \sum_{k=0}^{N-1} \left\{ \cos[2\pi(f_0 + k\Delta f)\tau] \right\} \cdot \text{rect}\left(\frac{t_F - kT - T/2}{T}\right) \quad (2.7)$$

$y(t_F)$  can be sampled with a rate  $1/T$  and it can be rewritten in the following form:

$$Y(k) = |\Gamma| e^{j\phi} \cos[2\pi(f_0 + k\Delta f)\tau] \quad (2.8)$$

with  $k=0, 1, 2, \dots, N-1$ . Whereas  $Y(k)$  can also be expressed in frequency domain as:

$$D(f) = |\Gamma| e^{j\phi} \text{rect}\left[\frac{f - f_c}{B}\right] \cos(2\pi f \tau) \quad (2.9)$$

where  $f=f_0, f_0+\Delta f, \dots, f_0+(N-1)\Delta f$ ,  $B=N\Delta f$ , and  $f_c$  denotes the central frequency. The equation (2.9) indicates the Stepped-Frequency Continuous-Wave baseband signal model of one swept period.

The distance between the radar receiver and the reflective target (simplified as a simple SDoF vibrating system) can be considered as the following time function:

$$r(t_s) = r_0 + A_M \sin(\omega_M t_s + \varphi_S) \quad (2.10)$$

where  $t_s=0, NT, 2NT, \dots$  is called *slow time* which means the time of the swept period,  $r_0$  is the average distance and  $A_M, \omega_M, \varphi_M$ , are amplitude, angular frequency and initial phase of the vibration motion that characterises the object. In the two way travel time can be written as:

$$\tau(t_s) = \frac{2r(t_s)}{c} = \frac{2[r_0 + A_M \sin(\omega_M t_s + \varphi_S)]}{c} = \frac{2r_0}{c} + \frac{2A_M \sin(\omega_M t_s + \varphi_S)}{c} = \tau_0 + \tau(t_s) \quad (2.11)$$

In the last equation the first term indicates the time delay of the average distance and the second one is related to the vibration of the reflective object.



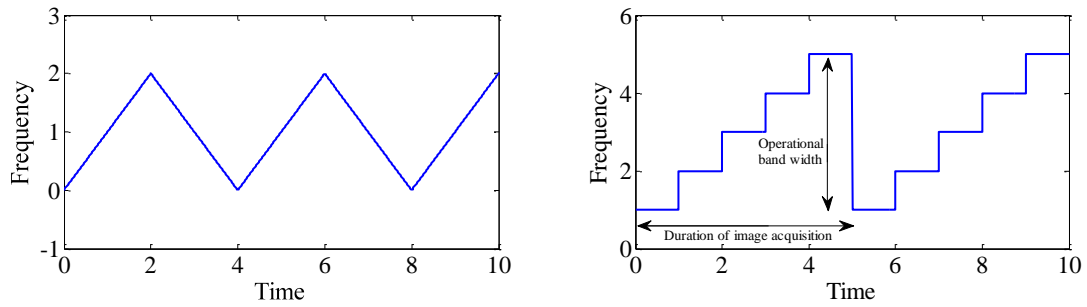


Figure 2.4: Comparison between transmitted signals: Modulated Frequency CW (left) and Stepped-Frequency CW (right) over time.

### 2.2.4 Radar beam

The sensor module of the IBIS-S sensor is provided with two horn antennas characterised by a maximum gain of 19dBi. It transmits the electromagnetic signals in Ku frequency band from 17.1 to 17.3 GHz, receiving the echoes from several targets placed inside the radar scenario. The most of the power of the signal is concentrated within the main beam of the radar antenna. The main lobe of the radiation pattern can be represented as a truncated cone characterised by elliptic base with the vertex corresponding to the antenna position. Thus different amplitudes characterise the main emission lobe, corresponding to the major and minor semiaxis of the ellipse, oriented along the vertical and the horizontal planes, respectively (-3dB beamwidth of  $17^\circ$  and  $15^\circ$  in the horizontal and vertical plane). These features have to be considered during the experimental tests in order to install the equipment in the most suitable position in respect to the objectives of the survey.

## **REFERENCES**

- Alba M., Bernardini G., Giussani A., Ricci P.P., Roncoroni F., Scaioni M., Valgoi P. and Zhang K. (2008). Measurement of dam deformations by terrestrial interferometric techniques, *Int Arch Photogramm Remote Sens Spat Inf Sci*, 37, 133-139.
- Antonello G., Casagli N., Farina P., Leva D., Nico G., Sieber A.J. and Tarchi D. (2004). Ground-based SAR interferometry for monitoring mass movements, *Landslides*, 1, 1, 21-28.
- Atzeni C., Bicci A., Dei D., Fratini M. and Pieraccini M. (2010). Remote Survey of the Leaning Tower of Pisa by Interferometric Sensing, *IEEE Geoscience and Remote Sensing Letters*, 7, 185-189.
- Bozzano F., Mazzanti P. and Prestinzi A. (2008). A radar platform for continuous monitoring of a landslide interacting with a under-construction infrastructure, *Italian J. of Engineering Geology and Environment*, 2, 35-50.
- Crosetto M., Casas A., Ranieri G., Loddo F., Atzori I. and Manunta M. (2006). First results from spaceborne radar interferometry for the study of ground displacements in urban areas, *Proceedings of the 12<sup>th</sup> European Meeting of Environmental and Engineering Geophysics*, Helsinki, September 4-6, EAGE, pp. 1-4.
- Farrar C.R., Darling T.W., Migliori A. and Baker W.E. (1999). Microwave interferometers for non-contact vibration measurements on large structures, *Mech. Syst. Signal Process.*, 13, 2, 241-253.
- Gentile C. and Bernardini G. (2008). Output-only modal identification of a reinforced concrete bridge from radar-based measurements, *NDT & E International*, 41, 544-553.
- Gentile C. and Gallino N. (2008). Ambient vibration testing and structural evaluation of an historic suspension footbridge, *Advances in Engineering Software*, 39, 4, 356-366.
- Gentile C. (2010a). Application of microwave remote sensing to dynamic testing of stay-cables, *Remote Sensing*, 2, 36-51.
- Gentile C. (2010b). Deflection measurement on vibrating stay cables by non-contact microwave interferometer, *NDT & E International*, 43, 3, 231-240.
- Gentile C. and Saisi A. (2011). Ambient vibration testing and condition assessment of the Paderno iron arch bridge (1889), *Construction and Building Materials*, 25, 9, 3709-3720.
- Harries N., Noon D. and Rowley K. (2006). Case studies of slope stability radar used in open cut mines, In *Stability of Rock Slopes in Open Pit Mining and Civil Engineering Situations*. SAIMM, Johannesburg, pp. 335-342.
- Henderson F.M. and Lewis A.J. (1998). *Manual of remote sensing. Principles and applications of imaging radar*. 3<sup>rd</sup> Ed., John Wiley and sons, New York, USA, 1998.
- Kaito K., Abe M. and Fujino Y. (2005). Development of a non-contact scanning vibration measurement system for real-scale structures, *Structure & Infrastructure Engng.*, 1, 3, 189-205.
- Kong L., Zhou Y., Cui G., Yang J. (2009). Micro-motion target sensing by stepped-frequency continuous-wave radar, *Journal of Electronics (China)* 26, 6, 782-787.

- Luzi G., Monserrat O. and Crosetto M. (2012a). The Potential of Coherent Radar to Support the Monitoring of the Health State of Buildings, *Research in Nondestructive Evaluation*, 23, 3, 125-145.
- Luzi G., Monserrat O. and Crosetto M. (2012b). Real aperture radar interferometry as a tool for buildings vibration monitoring: limits and potentials from an experimental study, *Proceedings of the 10<sup>th</sup> International Conference on Vibration Measurements by Laser and Non-contact Techniques (AIVELA '12)*, pp. 309–317, Ancona, Italy, 2012.
- Marchisio M., Ranieri G., Bernardini G., D'Onofrio L., Farina P., Manunta M. and Piroddi L. (2008). Applications of new technologies of ground-based interferometric radar to the study of cultural heritage buildings, *Proceedings of the 14<sup>th</sup> European Meeting of Environmental and Engineering Geophysics*, Krakov, Poland, 15-17 sept. 2008.
- Marchisio M., Ranieri G., Bernardini G., D'Onofrio L., Farina P., Manunta M. and Piroddi L. (2009). Applications of new technologies of ground-based interferometric radar to the study of cultural heritage buildings, *Proceedings of the 22<sup>nd</sup> EEGS Symposium on the Application of Geophysics to Engineering and Environmental Problems*, Fort Worth, 29 March - 2 April, SAGEEP, Volume 1, pp. 126-129.
- Pieraccini M., Luzi G., Mecatti D., Noferini L., Atzeni C. (2003). A microwave radar technique for dynamic testing of large structure, *IEEE Transactions on Microwave Theory and Technique*, 51, 5, 1603-1609.
- Pieraccini M., Fratini M., Parrini F., Pinelli G. and Atzeni C. (2005). Dynamic survey of architectural heritage by high speed-microwave interferometry, *IEEE Geoscience and Remote Sensing Letters*, 2, 28-30.
- Pieraccini M., Fratini M., Parrini F., Atzeni C. and Bartoli G. (2008a). Interferometric radar vs. accelerometer for dynamic monitoring of large structures: An experimental comparison, *NDT & International*, 41, 4, 258-264.
- Pieraccini M., Parrini F., Fratini M., Atzeni C. and Spinelli P. (2008b). In-service testing of wind turbine towers using a microwave sensor, *Renewable Energy*, 33, 1, 13-21.
- Pieraccini M., Fratini M., Dei D. and Atzeni C. (2009). Structural testing of historical heritage site towers by microwave remote sensing, *Journal of Cultural Heritage*, 10, 2, 174-182.
- Pieraccini M., Dei D., Betti M., Bartoli G., Tucci G. and Guardini N. (2014). Dynamic identification of historic masonry towers through an expeditious and no-contact approach: application to the "Torre del Mangia" in Siena (Italy), *Journal of Cultural Heritage*, 15, 275-282.
- Pieraccini M. (2013). Monitoring of Civil Infrastructures by Interferometric Radar: A Review, *The Scientific World Journal* 2013 1-8 <http://dx.doi.org/10.1155/2013/786961>
- Rödelsperger S., Läufer G., Gerstenecker C. and Becker M. (2010). Monitoring of displacements with ground-based microwave interferometry: IBIS-S and IBIS-L, *Journal of Applied Geodesy*, 4, 1, 41-54.
- Taylor J.D. (2001). *Ultra-Wideband Radar Technology*, Boca Raton, CRC Press, USA, 2001.
- Wehner D.R. (1995). *High-resolution radar*, 2<sup>nd</sup> Ed. Artech House, Boston, London, 1995.



## ***CHAPTER 3***



# DYNAMIC CONTROL OF HISTORICAL BUILDINGS THROUGH INTERFEROMETRIC RADAR TECHNIQUES: A USEFUL APPROACH FOR STRUCTURAL HEALTH MONITORING ON EARTHQUAKE DAMAGED STRUCTURES

---

## **Abstract**

*The structures damage conditions assessment requires numerous precautions to ensure the safety of people during site visits and inspections. Among several methods providing useful information about the conservation status of the structures, dynamic monitoring techniques are suitable to retrieve the global behaviour of the buildings. The diagnosis of anomalous features of the structural dynamic response is an index of alterations of the material state and, in the worst cases, is related to the presence of damaged structural elements. This chapter is aimed to assess the capability of remote sensing systems for the structural evaluation of the damage state of buildings and describes the results achieved in an interesting case study: the experimental dynamic analysis carried out on the inaccessible damaged bell tower of the Church of Santi Giacomo and Filippo in Mirandola (Italy). The study is based on observations performed using the IBIS-S ground-based radar interferometer to remotely measure the displacements of several elements of the building above 0.01mm amplitude. This totally noninvasive and nondestructive approach has proved to be reliably implemented as a suitable method to structural health monitoring procedures and especially for extensive and fast inspection analyses aiming at the first evaluation of the damage level and the soundness of slender buildings after earthquakes.*

### 3.1 INTRODUCTION

Structural damage identification is a fundamental element following an earthquake. A correct definition of the damage state of buildings allows us to establish technical procedures and operational standards for safeguarding the structures, aimed at restoring their original conditions. Structural Health Monitoring dynamic techniques can make possible to deduce the presence of lesions and estimate the severity of the damages to the structures by measuring the mode of vibration of the buildings. This is possible because the dynamic response of the structures is strongly affected by the conservation state of the materials and by possible cracks (Ivorra et al., 2011). The scientific literature includes many methods of structural dynamic response evaluation and algorithms for the extraction of main modal parameters (Ivanovic et al., 2000; Sohn et al., 2004). Several experimental configurations are classified in relationship to the number of measured output signals (number of sensors) and of the type of sources used to energize the structures. In this context, there are several experimental layouts to modal parameters identification. Specifically, it is possible to differentiate between forced vibration tests (i.e., using mechanical shaker or vibrodines), free vibration tests (i.e., using impulsive signals generated by means of falling objects inside or outside the buildings), and ambient vibration tests (i.e., using random sources as wind and man-made noise) (Maia et al., 1997). The last methods are very useful for assessing the structural dynamic behaviour and to quickly evaluate the conditions of existing damaged structures after an earthquake excitation. However, the most common data acquisition techniques use contact sensors. Velocimeters or accelerometers arrays are usually placed inside the building and are used to record time series of ambient vibration. In this context, many studies have been performed in order to evaluate the effects related to the damage state of structures through non-destructive vibration tests.

In particular, Bongiovanni et al. (1998, 2000) have analysed the dynamic behaviour of two earthquake damaged bell towers by means of both ambient vibration measurements and ground motion recordings. Sixty-seven aftershocks have been recorded by using fixed monitoring devices in order to study the seismic response of the structures under seismic ground motion. Many researchers have observed significant changes in dynamic properties of structures. Natural frequencies changes on masonry structures have been highlighted by Clemente et al. (1999). Pandey et al. (1991) proposed to analyse the structural mode shapes in order to extract useful information for structural damage localization. Furthermore new methodologies for Non-destructive Damage Evaluation (NDE) based on the variation of the dynamic behaviour of structures under seismic loads are studied by numerous authors (Ponzo et al., 2010; Dinh et al., 2012; Omrani et al., 2012a, 2012b; Bisht and Singh, 2012, Ditommaso et al., 2014) and different levels of NDE methods can be considered taking into account the information degree provided by each method (Rytter, 1993).



In the last decade, advances in the field of Ground-based Remote Sensing assured remote data acquisition and real-time monitoring of vibrations in critical conditions, as well as the dynamic control of severely damaged structures after earthquakes. In this chapter, a procedure aimed at evaluate the damage state of structures built in areas affected by earthquakes is proposed. This approach is based on remote monitoring techniques of mechanical vibrations by means of interferometric radar surveys. This method allows us to perform the monitoring of potentially damaged structures with maximum safety conditions. In fact, the assessment of the structural damages during the next phase of an earthquake, is an extremely delicate procedure due to precarious stability conditions of structures and due to possible further aftershocks during the technical inspections carried out by specialists. For this reason, a case study where we have applied this operative approach will be discussed here. It deals with the stability control of the bell tower of San Giacomo Roncole (damaged by the Emilia earthquake, Italy) using the dynamic surveys performed with the ground-based microwave interferometer IBIS-S.

### **3.2 DESCRIPTION OF THE STUDY AND METHOD**

The test site was chosen in order to analyse a strongly damaged but not totally crushed bell tower, for which the remote sensing approach was the only compatible one with safety conditions. The experimental settings were designed with the task to have comparable results from two main acquisition distances from the target and two different direction projections of measured displacement.

#### **3.2.1 The tower: a brief historical overview and description of the damage**

The Emilia earthquake has caused numerous damages to the structures. The buildings most affected by the earthquake are industrial structures (factories and warehouses) and cultural heritage buildings (churches, bell towers, civic and clock towers, etc.), whose geometric and constructive features have contributed to increasing their vulnerability in case of earthquakes. In this work, we present the study performed for the bell tower of San Giacomo Roncole. The actual structure was built from 1771 to 1774 with the same materials of the previous Carmelite Convent of Santa Maria delle Grazie della Galeazza (Andreoli, 1987). The building is located few metres away from the singular nave of the church. The structure replaced an earlier tower, adjacent to the body of the church, and demolished by the damage caused by the vibrations of the bells. The new tower is a masonry structure located at southwest of the church. The tower reaches a height of about 36 metres with a square base (5 metres per side). After the earthquakes of the 20<sup>th</sup> and 29<sup>th</sup> May, 2012, (magnitude  $M_I=5.9$  and  $M_I=5.8$ , resp.) the building sustained serious damage to the base, highlighted by displacements of about 2 cm toward the southwest side and of 1 cm on the southeast side. In other words, after the earthquake, the structure was shifted at the base, assuming an eccentric position. Also there are various fractures on the first section of the tower horizontally and diagonally crossing its perimeter walls, where a rigid

motion on the order of centimetres was measured. The top of the structure collapsed at about 9 metres from the base toward the southwest side (see Figure 3.1).

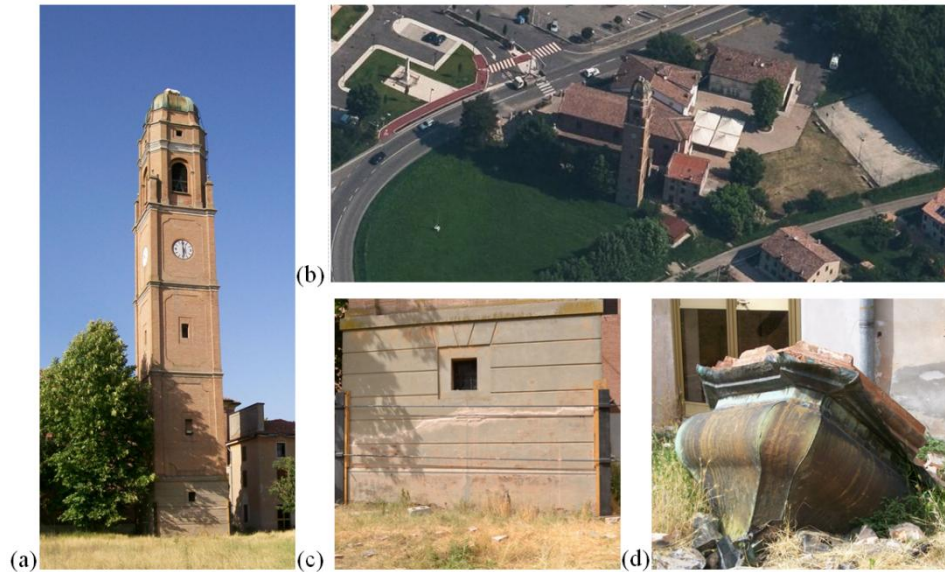


Figure 3.1: Some images of the damaged bell tower: (a) southwest side of the building; (b) panoramic view; (c) cracks at the base of the tower; (d) collapsed top.

### 3.2.2 Sensor installation and data processing

The tower of San Giacomo Roncole is a slim structure with a shape characterized by several natural corners (see Figure 3.2). Consequently, the measurements are performed without artificial corner reflectors installed on the body surface of the structure. This is an essential condition because the structure is seriously damaged. Dynamic surveys are carried out using three different configurations. In the first one, the IBIS-S system was placed in front of the tower in the South-East direction in order to monitor the dynamic behaviour of the full body of the structure with  $30^\circ$  LOS angle, computed for the emitting cone axis of the radar sensor. The second radar station was placed in the southwest direction ( $30^\circ$  LOS angle). The last acquisition was performed with the IBIS-S system located under the tower ( $70^\circ$  LOS angle). The acquisition geometry was selected in order to reduce the effects of all possible noise sources, such as suspended cables and other metal structures or trees and vegetation inside the radar profile. Each acquisition had a duration of about 10 minute with a sampling frequency of 200 Hz. The vibrations of the building were measured in real time during the field operations. The Fourier spectra of signals were provided by processing the acquired data with IBIS Dataviewer and Matlab software in order to assess the main frequencies of the structure. Before of the spectral analysis, the displacement data were detrended and tapered with Hamming function to reduce leakage effects. We have applied the Frequency Domain Decomposition technique (Brincker et al., 2001) based on singular values decomposition of the power spectral density matrix to identify the structural

dynamic response of the tower. By using this decomposition method, main modal parameters can be identified with high accuracy even in the case of strong noise contamination of the signals.

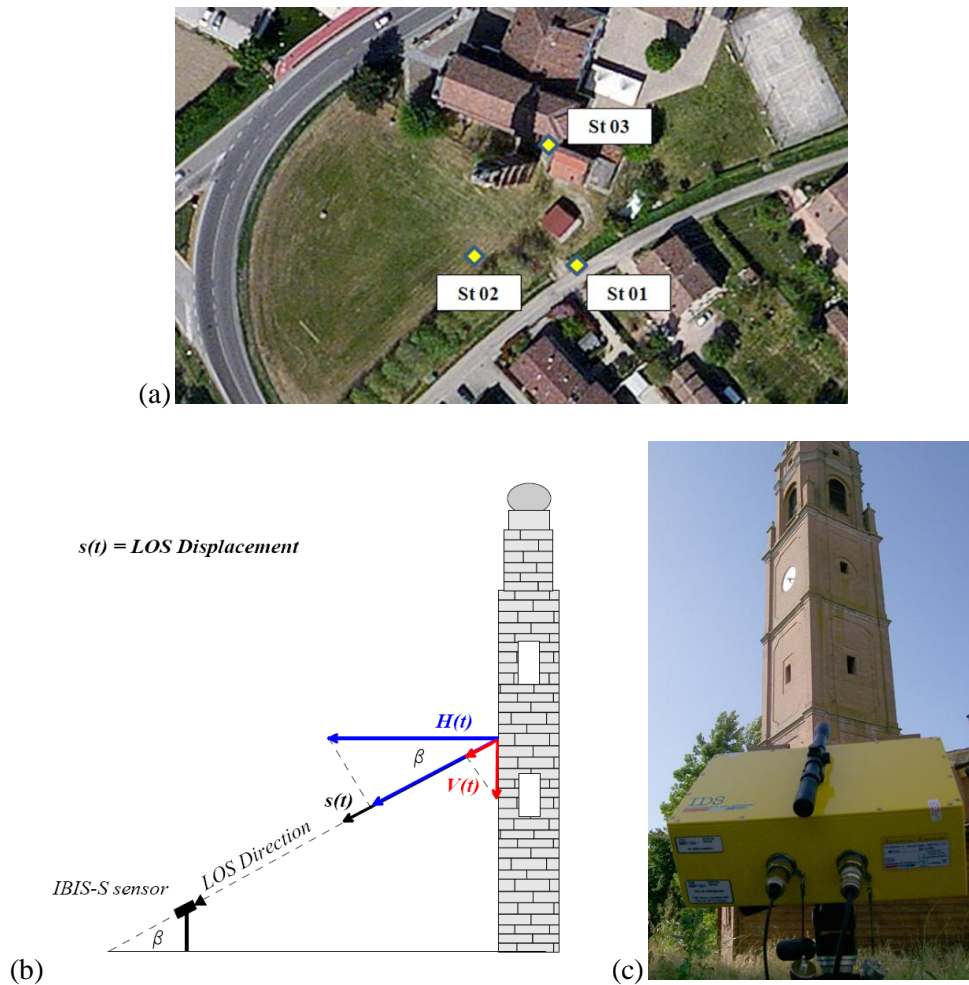


Figure 3.2: (a) Installation of the IBIS-S system in several acquisition stations placed at 25 m (St 01) and 23 m (St 02) from the base of the tower with inclination of  $30^\circ$  and at 8 m (St 03) with inclination of  $70^\circ$ . (b) Radar line of sight displacement and true displacement vector. (c) Image of the IBIS-S system used during the experiments.

### 3.3 RESULTS AND DISCUSSION

The range bins with high signal-to-noise ratio (SNR) along the radar power profile are associated with different natural back-scatterers located inside the radar scenario. However, the Signal-to-Noise Ratio of the radar response from this structure is high and the structure is isolated inside the radar scenario. Thus several range bins may be selected to be analyzed. Five range bins of the radar power profile are selected to estimate fundamental vibration properties of the structure by means of the FDD decomposition technique (Brincker et al., 2001). The radar bins are selected in function of the distance along the radar line of sight between each radar-bin and the IBIS-S sensor. These range bins correspond to five reflective points placed on the bell tower facade. This operation is easily performed knowing the geometric characteristics of the tower (the height of several architectonic elements such

as windows and other ledges), the horizontal distance of the radar station, and the inclination of the IBIS-S head. The displacements retrieved from radar data are shown in Figure 3.3.

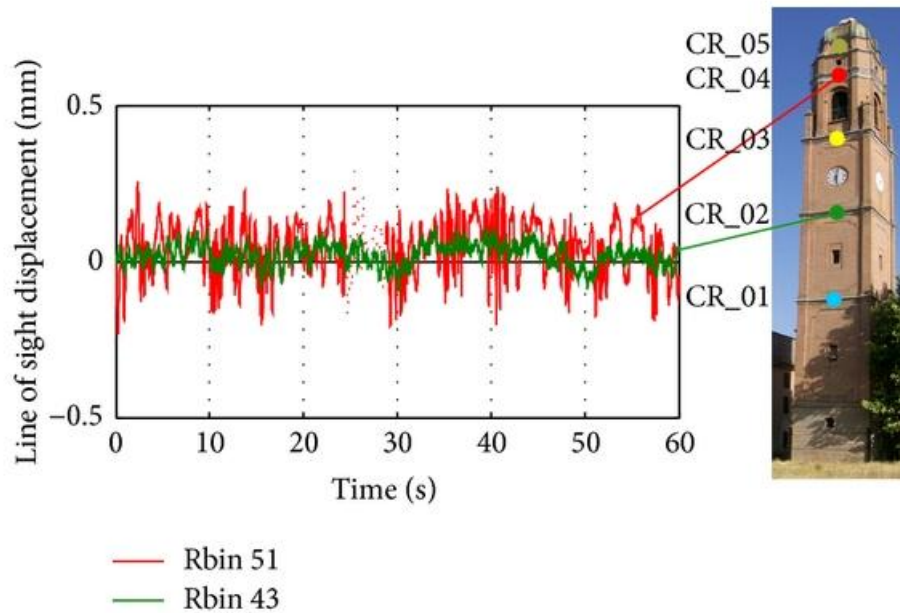


Figure 3.3: One-minute record acquired with the second configuration: LOS displacement over the time. The time series are related to two range bins selected from the radar power profile and correspond to different heights of the tower.

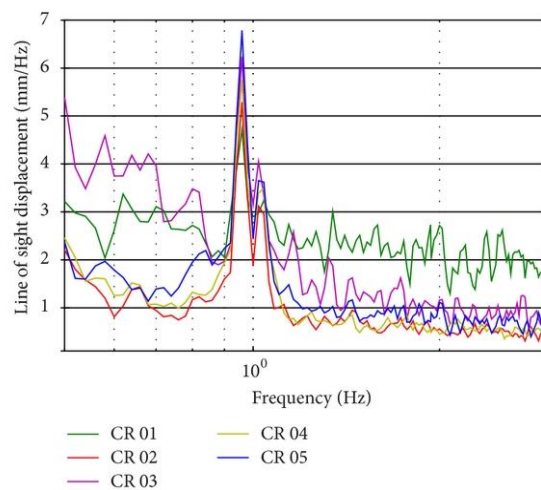


Figure 3.4: Displacement spectra calculated using the entire 10-minute record, for five different radar-bins with variable SNR achieved from data acquisition with configuration ST01.

These time series have been obtained observing the tower from a position to the base of the tower, at a distance of 23 metres (configuration 2). During all measurements, a regular wind with moderate speed of 5.5 m/s blew. The calculated displacement spectra, obtained over the whole recorded ten minutes signal, are shown in Figure 3.4. A band-pass filter (0.3 Hz–10 Hz) was applied to reduce the presence

of disturbances linked to atmospheric effects and to vibration of the sensor itself. The influence of the first effect is prevalent on the measured phases and, as a consequence, on the estimated displacements with long period (0.1–0.2 Hz). Another effect is caused by the vibration of the measurement tool. Luzi et al. (2012) observe that the measured resonant frequency of the system ranges within  $10\text{Hz} \pm 2\text{Hz}$  for typical working conditions. Then a low-pass filtering may be applied in order to assure that the measured vibrations are not imputable to the natural response of the tripod-head sensor system. All amplitude spectra are characterized by a clear harmonic components at 0.96 Hz (corresponding period of 1.04 s) whose amplitude increases with the height of the analysed range bin. This behavior agrees with the expected amplitude variation associated at the first natural mode (simple bending). This periodicity cannot be directly retrieved from all displacement time series but only for the 50<sup>th</sup> range bin corresponding to the reflection from the height of 30 metres on the tower (see Figure 3.5). The obtained value of 0.96 Hz could be influenced by the presence of structural damage caused by the earthquake. Several empirical relationships available for masonry structures, like those proposed by the Italian Building Code NTC-2008, the Spanish National Code NSCE-02, and by literature studies (Rainieri and Fabbrocino, 2012), are used to assess the fundamental frequency of vibration. The obtained results range between 1.4 and 1.5 Hz. The significant difference (31%–36%) between the experimental value and the estimated values could be imputed to the damage caused by the earthquake. It is generally recognised that the period of vibration grows while increasing the mass of the vibrating system and while reducing the stiffness. The radar measurements allow to estimate the main features of the dynamic behaviour (amplitude of vibration) of several parts of the building located at different heights. In this case we have monitored the structure from different perspectives and we have compared the experimental mode shapes obtained for both ST1 and ST2 radar configurations. The mode shape retrieved by the configuration 3 was not used for this analysis because the displacements measured in LOS direction are not comparable with the others. In fact, in this configuration, the microwave sensor is more inclined ( $70^\circ$ ) and is installed at short distance from the tower (8 metres). Measured displacements along two directions are projected along the horizontal plane. The experimental mode shapes show a similar trend, as we can see in Figure 3.6. We observe that the maximum values are measured from St-02 IBIS-S station and are characterized by amplitude ranges from 0.05 to 0.2 mm. The fundamental mode of vibration is a bending mode with the same frequency of 0.96 Hz in both directions of measurement. Possible anomalous behaviour has been detected at the point placed at about 17 metres. In fact, a significant increasing in the amplitude of the measured displacement is shown by the modal shape at this level of the structure, especially with respect to the lower level (located at 11 metres height above the ground surface). There is an increase of 100% (acquisition station 1), moving from 0.04 mm to 0.08 mm of maximum amplitude at the first structural vibration frequency and an increase of 80 % (acquisition station 2), from 0.05 mm to 0.09 mm, which are unlikely attributable to geometric differences in the two building levels or to largely variable construction features of the elevating structure. Therefore, this trend could be reliably related

to the structural damages of the building observed at the middle level. Moreover, the larger displacements obtained in the second acquisition are justified by the major shift recorded in this direction (about 2 cm) due to seismic action.

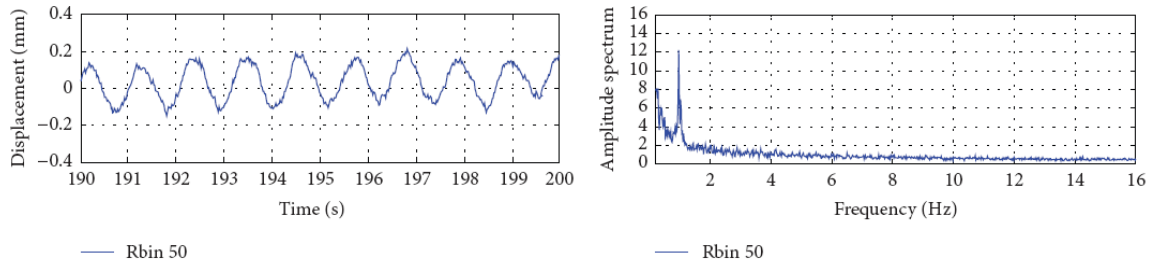


Figure 3.5: Sinusoidal trend of the displacements recorded at the 50<sup>th</sup> range bin (30 metres height) shown in both Time (left) and Frequency domain (right).

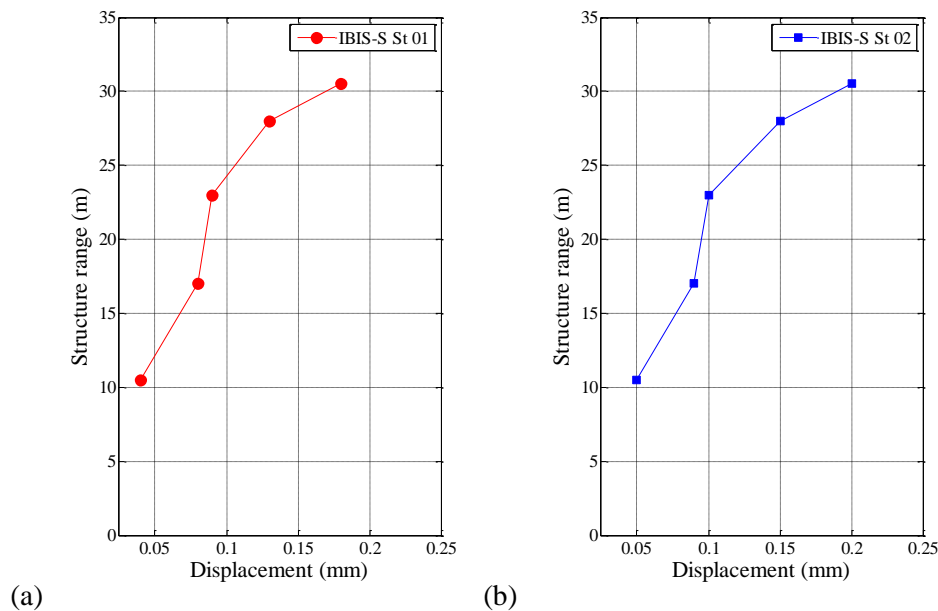


Figure 3.6: Comparison between the experimental modal shapes retrieved from two points of view of the IBIS-S system: (a) station St01; (b) station St02.

### 3.4 DISCRETE MODEL OF THE TOWER

In order to evaluate possible changes of the modal parameters of the structure occurred due to the seismic-induced damages, the first experimental natural frequency of the tower has been compared with the theoretical one achieved through a numerical simulation. The numerical analysis has been done by means of a Finite Element model of the structure which has been characterised assuming elastic modulus, Poisson ratio and density values for masonry materials in agreement with the reference values proposed by technical guidelines (table C8A.2.1 of the Italian technical code NTC 2008 – CM 2009) to evaluate the linear elastic behaviour of the structure. This approach is based on very low magnitude deformations and can be considered in order to study the behaviour of the

undamaged structure under ambient vibration induced loads (wind forces, microseisms, cultural or man-made noise).

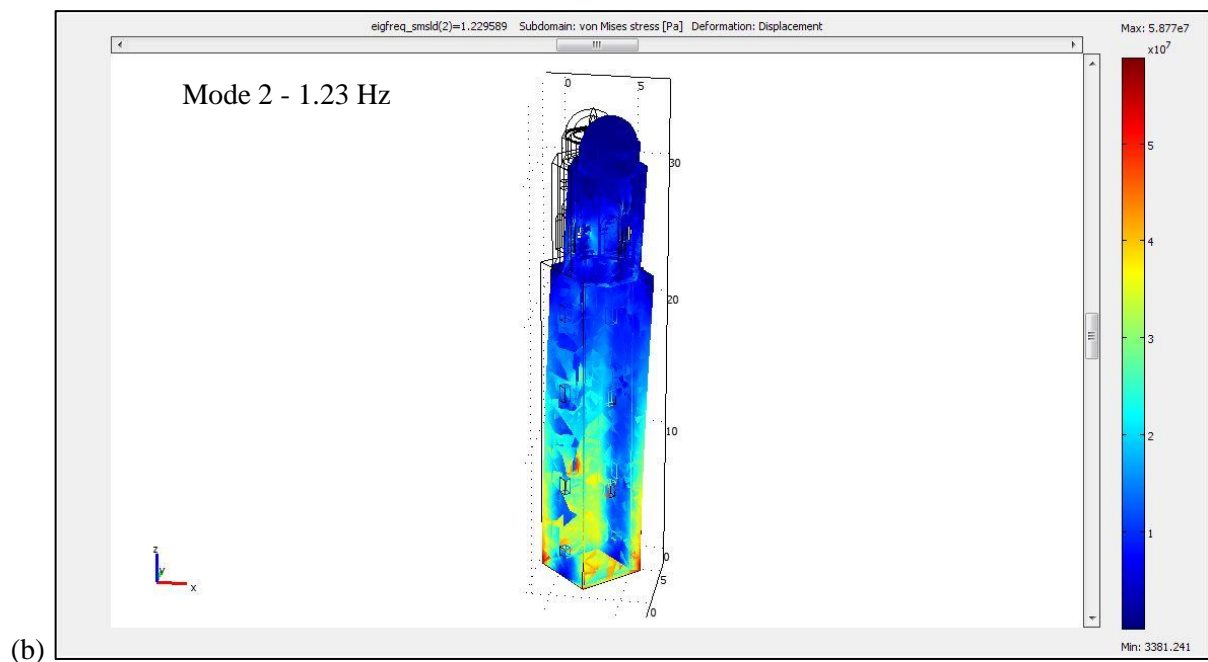
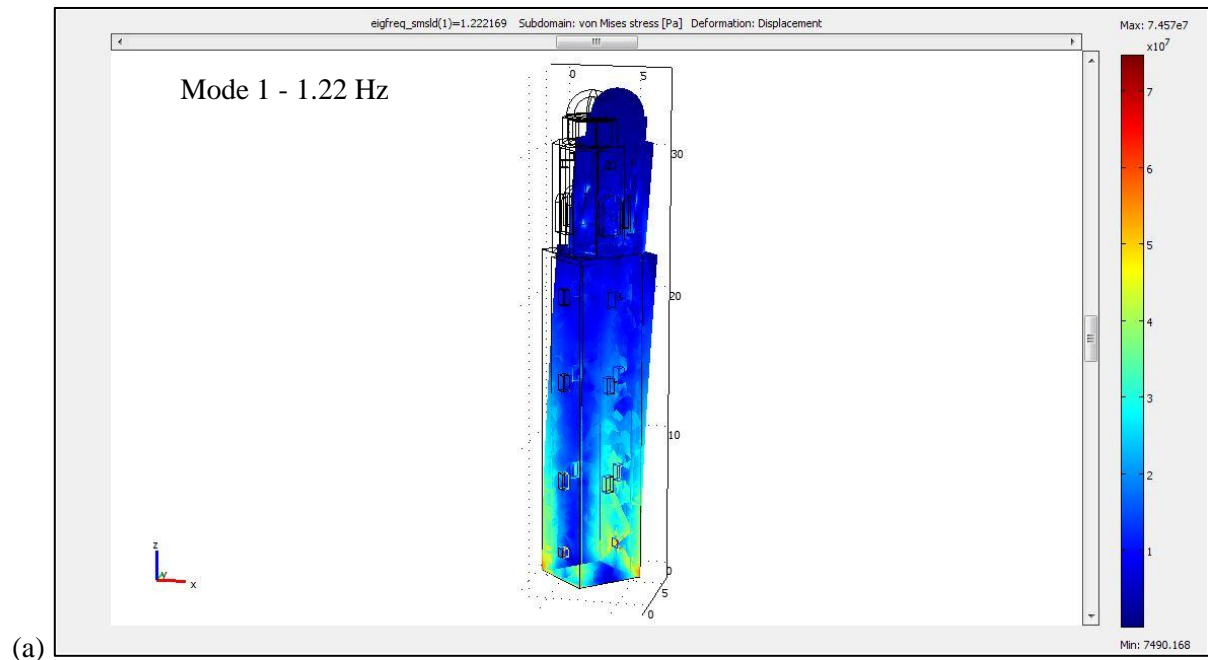


Figure 3.7: Modal shapes of the Finite Element model corresponding to the natural frequencies of 1.22 Hz and 1.23 Hz.

Although the material properties used to perform the numerical analysis should be derived through in situ measurements using both direct and non-destructive methods (e.g. direct shear tests on masonry walls, rebound hammer, ultrasonic and sonic tests, etc.) in this case it has not been possible to use data achieved by these surveys due to the absence of pre-existing studies and the actual state of damage of

the building. Thus the most probable physical properties have been considered and partially reduced. The values assigned to the materials have been stored in Table 3.1. External geometric features have been derived by the work of Pesci et al. (2013). The thickness of the perimetral wall is about 0.98 metres at the square base of the structure. Finite Element Comsol Multiphysics software has been used to perform the eigenfrequency analysis of the discrete model. Fixed node boundary conditions have been chosen at the nodes placed at the base of the model to constrain the building. Numerical results are shown in Figure 3.7 where it is possible to see that the first mode is a flexural mode that includes main deformations along the X axis at the frequency of 1.22 Hz. The second mode is close to the first one at the frequency of 1.23 Hz but involves displacements of the model oriented along the Y axis. The higher vibration modes cannot to be taken into account due to the high uncertainties that affect the model and for this reason are not discussed in this context. As it can be observed the natural modes of the model, derived by means of the linear dynamic analysis, are characterised by higher frequency values than those experimentally measured. This result could confirm that the measure of the modal parameters can be used to evaluate post-earthquake damage conditions of the buildings.

Material properties		
Density (kg/m <sup>3</sup> )	Poisson ratio	Young's modulus (N/mm <sup>2</sup> )
1,800	0.2	3,000

Table 3.1: Physical properties of the model.

### 3.5 CONCLUSIONS

This work proposes the use of the ground-based microwave interferometry for remote sensing of vibrations of structures aimed at providing useful information for specialists about the damage state of structures in areas affected by earthquakes. For this reason, the first application of the ground-based radar interferometry to study the dynamic response of an inaccessible damaged building has been described. The results have been obtained by means of experimental dynamic tests aimed at evaluating main modal parameters of an ancient masonry bell tower in an urban environment. The measurements were performed through ambient vibration recordings. The experimental data used to derive the vibration features of the structure have been critically discussed to identify possible effects related to the structural damages. In general, this method can be used to estimate displacements ranging from a few microns up to several millimetres for large structures, as thin and tall structures or other types of buildings (towers, skyscrapers and bridges). The possibility of remotely working makes this approach suitable for the dynamic control of buildings that have reported structural damages after an earthquake, especially for cultural heritage buildings and for civil structures of strategic interest during the emergency interventions.



## **REFERENCES**

- Andreoli E. (1987). San Giacomo Roncole: raccolta di notizie storiografiche popolari”, Mirandola edizioni, Mirandola, Italy.
- Bongiovanni G., Buffarini G. and Clemente P. (1998). Dynamic characterisation of two earthquake damaged bell towers, Proceedings of the 11<sup>th</sup> European Conference on Earthquake Engineering (Paris, September), Balkema, Rotterdam.
- Bongiovanni G., Clemente P. and Guffarini G. (2000). Analysis of the seismic response of a damaged masonry bell tower, in the Proceedings of the 12<sup>th</sup> World Conference on Earthquake Engineering WCEE, New Zealand, 2000.
- Brincker R., Zhang L. and Andersen P. (2001). Modal identification of output-only systems using frequency domain decomposition, *Smart Materials and Structures*, 10, 441-445.
- Clemente P., Baratta A., Buffarini G. and Rinaldis D. (1999). Changes in the dynamic characteristics of a masonry arch subjected to seismic actions. In Frýba L. & Náprstek J. (Editors), *Structural Dynamics – Eurodyn’99*, A.A. Balkema (for E.A.S.D.), Rotterdam, Vol. 2, 1185-1190.
- Ditommaso R., Ponzo F.C., Auletta G. and Iacovino C. (2014). Testing a new procedure for damage detection on framed structures subjected to strong motion earthquakes, Proceedings of the Second European Conference on Earthquake Engineering and Seismology, Istanbul, Aug. 25-29, 2014.
- Bisht Saurabh S., Singh Mahendra P. (2012). Detecting sudden changes in stiffness using high-pass filters, *Struct. Control Health Monit.* 19, 319–331. DOI: 10.1002/stc.433
- Dinh H.M., Nagayamaz T. and Fujinoy Y. (2012). Structural parameter identification by use of additional known masses and its experimental application, *Struct. Control Health Monit.* 19, 436–450. DOI: 10.1002/stc.444
- Ivanovic S.S., Trifunac M.D. and Todorovska M.I. (2000). Ambient vibration tests of structures – A review, *Bulletin of Indian Society of Earthquake Technology: Special Issue on experimental methods*, pp. 1-49, 2000.
- Ivorra S. Pallarés F.J. and Adam J.M. (2011). Masonry bell towers: dynamic considerations, Proceedings of the Institution of Civil Engineers, Structures and Buildings, 164, February 2011, Issue SB1, 3–12. Paper 900030 doi: 10.1680/stbu.9.00030
- Luzi G., Monserrat O. and Crosetto M. (2012). Real Aperture Radar interferometry as a tool for buildings vibration monitoring: limits and potentials from an experimental study, Proceedings of the 10<sup>th</sup> International Conference on Vibration Measurements by Laser and Non-contact Techniques — AIVELA 2012, pp. 309-317, Ancona, Italy.
- Maia N.M.M., Silva J.M.M., He J., Lieven N.A., Lin R.M., Skingle G.W. and To W.M. (1997). *Theoretical and Experimental Modal Analysis*, Research Studies Press: New York, USA.
- Mainstone RJ (1974) “Supplementary note on the stiffness and strength of infilled frames”, Current paper CP13/74, Build. Res. Establishment, London.

Omrani R., Hudson R. E. and Taciroglu E. (2012a). Story-by-story estimation of the stiffness parameters of laterally-torsionally coupled buildings using forced or ambient vibration data: I. Formulation and verification. *Earthquake Engng. Struct. Dyn.*, 41, 12, 1609–1634.  
Doi: 10.1002/eqe.1192

Omrani R., Hudson R. E. and Taciroglu E. (2012b). Story-by-story estimation of the stiffness parameters of laterally-torsionally coupled buildings using forced or ambient vibration data: II. Application to experimental data, *Earthquake Engng. Struct. Dyn.*, 41, 12, 1635–1649.  
Doi: 10.1002/eqe.1193

Pandey A.K., Biswas M., Samman M.M. (1991). Damage detection from changes in curvature mode shapes”, *Journal of Sound and Vibration*, Vol. 145: Issue 2, pp. 321-332.

Pesci A., Teza G., Bonali E., Casula G., Boschi E. (2013). A laser scanning-based method for fast estimation of seismic-induced building deformations, *ISPRS Journal of Photogrammetry and Remote Sensing*, 79, 185–198.

Ponzo F. C., Ditommaso R., Auletta G., Mossucca A. (2010). A Fast Method for Structural Health Monitoring of Italian Strategic Reinforced Concrete Buildings, *Bulletin of Earthquake Engineering*, 8, 6, 1421-1434. DOI: 10.1007/s10518-010-9194-6

Rainieri C. and Fabbrocino G. (2012). Estimating the elastic period of masonry towers, *Proceedings of the SEM IMAC 30<sup>th</sup> Conference*, Jan. 30-Feb. 2, 2012, Society for Experimental Mechanics Inc., Jacksonville, FL, USA.

Rytter A. (1993). *Vibrational based inspection of Civil Engineering Structures*, Ph.D. Thesis, University of Aalborg, Denmark.

Sohn H., Farrar C.R., Hemez F.M., Shunk D.D., Stinemates D.W., Nadler B.R. and Czarnecki J.J. (2004). A Review of structural health monitoring literature: 1996–2001,” *Los Alamos National Laboratory Report*, LA-13976-MS, USA.

## ***CHAPTER 4***



## COMPARISON OF NATURAL AND ARTIFICIAL FORCING TO STUDY THE DYNAMIC BEHAVIOUR OF BELL TOWERS IN LOW WIND CONTEXT BY MEANS OF GROUND-BASED RADAR INTERFEROMETRY: THE CASE OF THE LEANING TOWER OF PISA

---

### Abstract

*The study of Cultural Heritage assets needs the application of non-destructive and non-invasive monitoring techniques. In particular, monuments and historical buildings which are open to the visitors and/or subject to important stress must be studied for their dynamic response. Thus, this chapter is focused on the application of ground-based interferometry on one very important historical building, the Leaning Tower of Pisa in Italy. The analysis of these kind of structures is important to catch their dynamic response to natural actions in general, and also to assess the effects due to pedestrian and users, and consequently to define functional capabilities and levels of acceptable dynamic stress. The studied structure was subject to artificial loading by synchronous movement of about twenty people. Artificial forcing led the structure to a resonance condition with the same frequency of the one due to the natural noise excitation, which was separately measured, and with an oscillation amplitude more than thirty times greater than the natural one (in conditions of weak wind). During the passive stages of the survey the recorded structural vibrations were very closed to the instrumental sensitivity, making difficult to distinguish vibration amplitudes amplifications of various segments at various heights. Through the spectral analysis of the acquired data it was possible to estimate the vibration frequencies of the first modal shapes of the structure along two orthogonal directions. The power spectra of the passive survey data have the same maximum frequency of the active but contain more noise at low frequency.*

## **4.1 INTRODUCTION**

The estimation of the vulnerability of historical buildings and the monitoring of their dynamic response under the functional fruition conditions are a primary goal of cultural management and preservation actions. The historical buildings that are most sensible to dynamic loadings are relatively slender linear structures, such as towers and bridges, for which it is fundamental to know the natural frequencies and to prevent the resonance effect of variable natural (e.g. winds) or other loads. It is possible to evaluate the natural frequencies of the entire structure by observing the simultaneous movements of different points of the studied structure. For valuable buildings in seismic active areas the dynamic behaviour can be compared with the soil characteristics and with the expected seismic actions allowing the implementation of possible preventive operations. The evaluation of the dynamic behaviour of historical buildings allows furthermore to plan the fruition activities which are compatible with the cultural asset preservation both inside and through the structure or for activities in the immediate neighbours (e.g. more or less heavy traffic, metropolitan lines, machines and construction sites). The most traditional way to measure the oscillations of architectural structures is to use accelerometers networks directly installed on them (Abdel-Ghaffar and Scanlan, 1985; Samman and Biswas, 1994; Salawu and Williams, 1995; Cunha et al., 2001; Li et al., 2006; Gentile and Saisi, 2007; Gentile and Gallino, 2008). More recently laser doppler instruments have been developed which are able to measure only one point at a time (Cunha and Caetano, 1999; Towers et al., 1995; Cunha et al., 2001; Nassif et al., 2005; Lee and Shinozuka, 2006; Castellini et al., 2006). The survey of vibrations of structures allows to detect the buildings natural frequencies without invasive actions. These are fundamental parameters for structural analysis and tests, allowing to take into account the effects of dynamic solicitations such as traffic, general anthropic actions, strong winds or earthquakes. In particular the knowledge of the dynamic responses of cultural heritage buildings is an important tool to plan their use and to determine the compatibility of activities inside the structure or close to it. The survey carried out can be an effective, quick and simple method to verify the acceptable levels of usability of cultural heritage slim buildings. Furthermore human artificial solicitation proved to significantly enhance Signal to Noise Ratio (SNR) in interferometric monitoring of vibrations, obtaining the same spectral results of natural solicitation, and can be specifically useful in case of structures with low exposition to winds like in urban environments or in conditions of extremely weak winds.

## **4.2 APPLICATIONS AND RESULTS**

The case study object of the survey has been one of the most known Italian monument in the world, the Leaning Tower of Pisa. The tower was built during about 200 years starting from 1173 in the site of the actual Square of Miracles (Figure 4.1 (a)), which is inserted in the UNESCO World Heritage List from 1987. It is a circular bell tower of a height of about 56 meters (ranging from 55.86 to 56.70

meters due to its inclination) and an inclination driven to 3.97 degrees from previous 5.5 degrees measured before restoration and soil consolidation (Figure 4.1 (b)).



Figure 4.1: Aerial view (a), from North location, of the Piazza dei Miracoli (Miracles Square) in Pisa, Italy, with a shot of the Monumental Cemetery, the Baptistery of San Giovanni, the Cathedral of Santa Maria Assunta and the Leaning Tower; West ground view (b) of the Leaning Tower with the right transept of the Cathedral on the left of the picture.

The tower has the original Pisan Romanic style. The external diameter of the tower is 15.5 meters at the ground level with an inner well of 7.4 meters diameter (measured at ground level). In the cylindrical wall between outside and the well a spiral staircase is built and conducts to the upper levels. The tower is composed of eight levels, the upper one of which being back from the facade edge contains the belfry. The lower level is walled with projecting pilasters surmounted by arches. Levels from the second to the seventh one have a backward thinner wall to make room for an open gallery bounded by columns and arches. The construction works started in August 1173 under the probable design of architect Bonanno Pisano, continued till 1178 for five years reaching the half of the fourth level for economical and political problems of the municipality. The works stopped for about one hundred for various reasons. In 1272 the construction resumed, but during the building the tower began to incline more and more due to differential soil subsidence (recently it was discovered that unfortunately it was exactly over the bank of an ancient riverbed) (Marchisio et al., 1998). The architect Giovanni di Simone tried to correct the constructive problem by modifying the inclination of the highest part and giving to the tower the curved axis that it has today. Interrupted in 1278 at the end of the seventh level, the construction again resumed after almost a century in 1360. The tower was concluded in 1370 under the direction of architect Tommaso di Andrea with the final level of the belfry. Over time, the inclination of the tower was aggravated and various restoration workshops were opened. More recently, it was proceeded to consolidation works which conduct to the actual inclination and to the subsequent reopening of sightseeing (Croci, 2000; Settis et al., 2005). The Leaning Tower of Pisa has been investigated by means of interferometric radar technologies. Every level of the tower has decorations and mouldings which constituted good natural reflectors for the

radar signal. Data were acquired from four different points located at ground level in the direction of the four cardinal points at distances of about 20-30 metres from the tower (Figure 4.2 and Table 4.1).

<b>ACQUISITION LAYOUTS</b>				
	<b>A</b>	<b>B</b>	<b>C</b>	<b>D</b>
DISTANCE FROM THE TOWER [M]	30.3	25.3	26.3	27.3
RADAR ELEVATION FROM THE GROUND [m]	0.60	0.60	0.62	0.61
WIND	Weak, from N-E	Weak, from N-E	Weak, from N-E	Weak, from N-E
ENFORCEMENT ACTION	YES	NO	NO	NO
FREQUENCY OF SAMPLING [Hz]	30	30	30	30
RESOLUTION IN RANGE [m]	0.75	0.75	0.75	0.75
MAXIMUM RANGE [m]	200	200	200	200

Table 4.1: Operative conditions and configuration of IBIS-S for the four acquisitions.



Figure 4.2: Plan view of the area with the four positions of measure.

The main reflection points in the power range profile for the acquisition point A, (Figure 4.4), correspond with the visible levels of the tower (points 4-7, 11 of Figure 4.3) and with the metal scaffolding scatterers positioned in the upper part (points 8-10) and in the lower part of the tower (points 2-3) for maintenance tasks. First peaks of the SNR instantaneous curve (points 1-3 of Figure 4.3) are also influenced by the people crossing in the line of sight of the interferometer. This discrimination is based on the distance between the antenna and the potential targets in the direction



of the radar line of sight and also on the spectral content of each time series displacement. The displacements are measured along the line of sight of the instrument and they can be subsequently projected along the direction orthogonal to the main axis of the structure (horizontally).

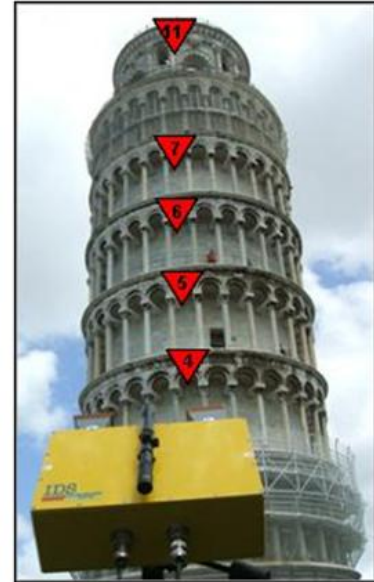
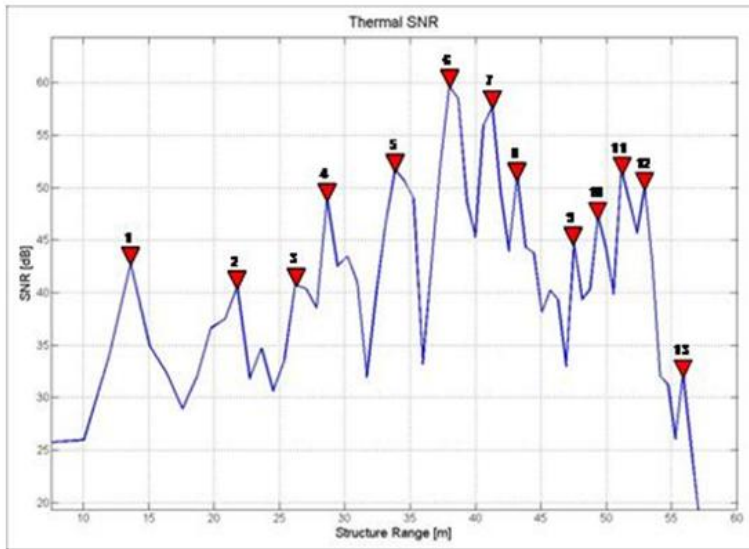


Figure 4.3: Power profile and selection of measuring points: it is important to distinguish between peaks power on metal scaffolding and those really belonging to the structure

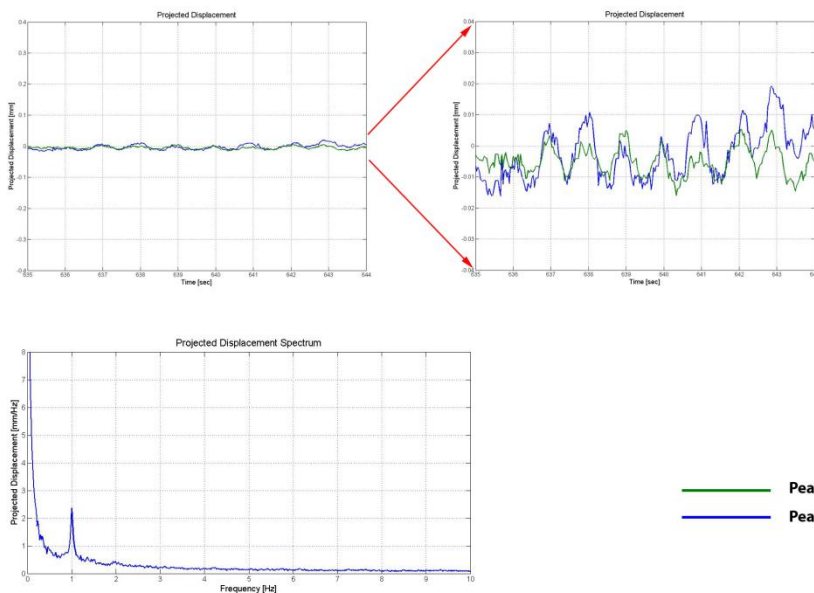


Figure 4.4: Analysis of the results: position A, points 5, 11. Natural vibration induced by the wind. Results obtained in the time and frequency domain show the dominant frequency of 1Hz for both the two point.

The observations from acquisition point A (Figure 4.2 and Table 4.1) were first made in presence of weak wind (Figures 4.4) and later in conjunction with a simultaneous and coordinated movement of about 20 people in the upper part of the tower (Figure 4.5).

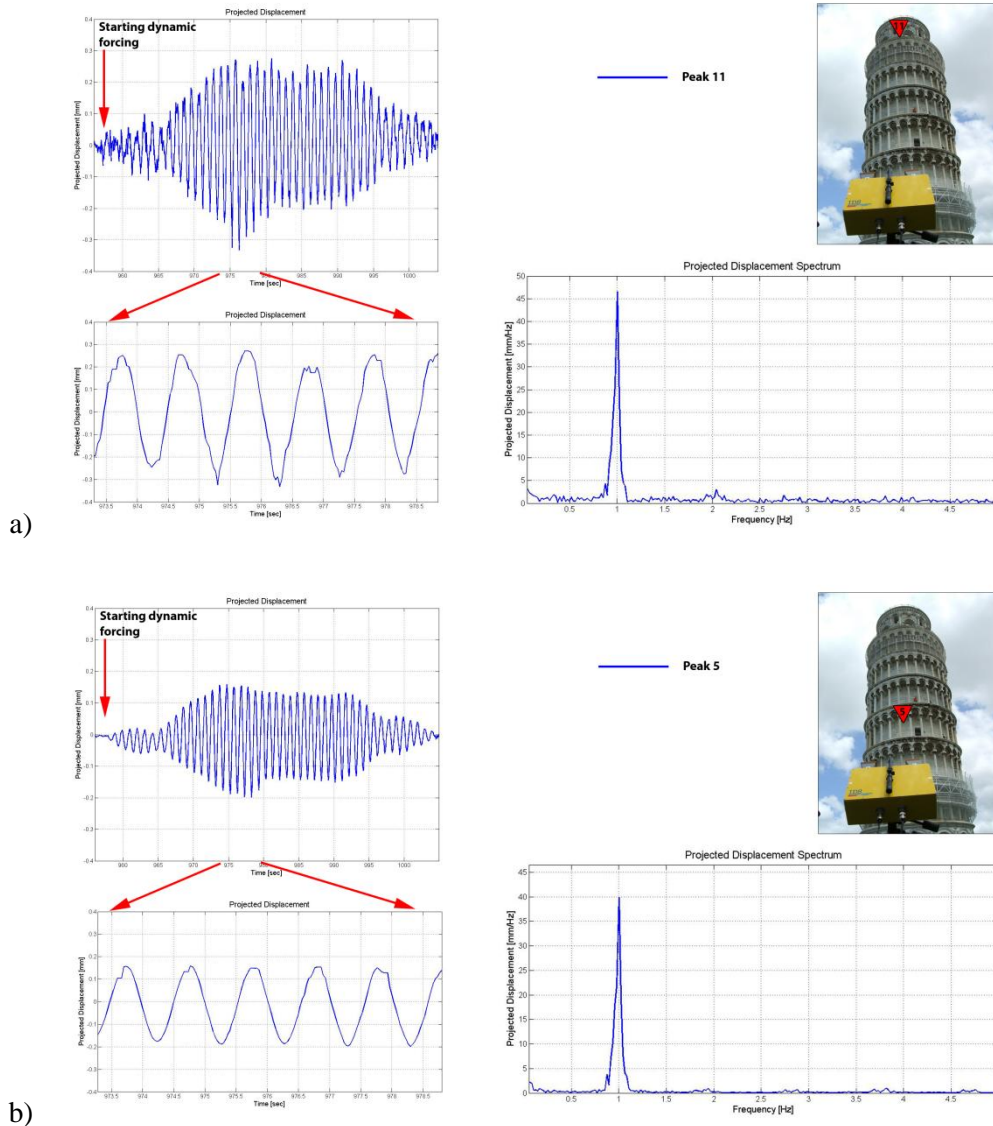
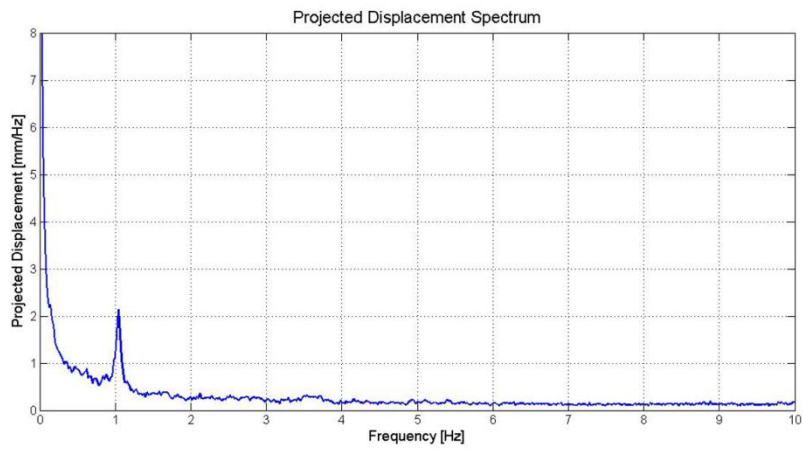


Figure 4.5: Vibration induced by the coordinated movement of about twenty people placed on top of the tower (results obtained in time and frequency domain). (a) Signal reflected from point 11 on the top of the tower: during stress forced the displacement component orthogonal structure takes a sinusoidal with fundamental frequency  $f_0 = 1\text{Hz}$  and maximum amplitude peak-peak equal to 0.60 mm; (b) Signal reflected from point 5 at middle of the tower height: during stress forced the displacement component orthogonal structure takes a sinusoidal with fundamental frequency  $f_0 = 1\text{Hz}$  and maximum amplitude peak-peak equal to 0.34 mm.

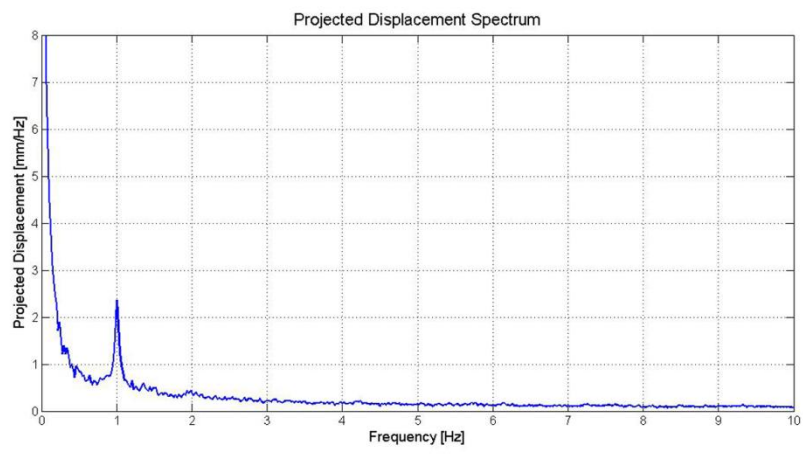
It is important to note that SNR peaks in radar profile curve are referred to all the respective peaks, and that in the same range bin (0.75 m width) more than one main reflecting point can be present, so that identified points are indicative of potentially more than one architectural element inside the range bin but we can consider these solidly joint to the near and central one. For both passive and artificially

forced dynamic surveys the sampling rate used to acquire vibration data was set to 100 samples per second. Each measurement was performed using 300 s time windows. The structural response of the tower was derived by means of the analysis of all time series of displacement measured from the radar system and related to natural back-scatterers of the building. The signals were detrended and padded with zero samples. The frequency analysis of each recorded trace was done via 50 s time windows with 10 % of overlapping sub-samples tapered with the Hanning function. The observations from the acquisition points B (West), C (North) and D (East) of map in figure 3 and table 1 (Figures 4.7 B-C-D) were made only in presence of weak wind. The analysis of the spectral composition of the signals recorded from four separate locations and coming from different height levels makes possible to identify the first fundamental frequency of oscillation of the structure. In Figure 4.4, two different time series are analyzed from back-scattered signals coming from the top and at middle height of the tower and recorded from the first acquisition point (point A in plan of Figure 4.2). The loading condition is a weak wind. Signals shown in the time domain graphs are little noisy sinusoids with the same frequency and coherent phase, and the spectral content evaluation in the frequency domain graph show a peak at 1 Hz. The displacement magnitude is in the order of IBIS system accuracy. This spectral component is highlighted for the resonance condition with the structure response with respect to the natural trend of the wind-induced vibrations which are characterised by progressively decreasing amplitudes with higher frequencies. In Figure 4.5, two different time series are analyzed from back-scatterers located at the top and at middle height of the tower and recorded from the same acquisition point of Figure 4.4. Loading condition is produced in this case by the simultaneous and coordinated movement of the group of about 20 people on the top of the tower simulating a horizontal sinusoidal excitation. The time series of the entire experiment show a starting oscillation of low amplitude followed by a growing amplitude due to the reached resonance condition. The time domain plot of a window of these time series for both the two reflection points during the resonance condition shows a clear sinusoidal behaviour, with amplitude of 0.34 and 0.60 mm. The spectral analysis confirms that both the signals have a main component of 1 Hz during the resonance condition. In Figure 4.6, the spectra of the signals coming from about the same reflection level and recorded from the three remaining acquiring position is shown. The loading condition of Figure 4.6 is only a weak wind. The oscillation frequency of the tower in this condition and for all the acquisition positions and directions is equal to 1 Hz. The coordinated movement of the people on the upper part of the tower was able to solicit the structure resonance at a fundamental frequency of 1 Hz. Same frequency of 1 Hz has been obtained for only wind loading conditions and for four perpendicular acquiring directions and is substantially the same frequency reported in other scientific studies carried out using the radar interferometry (Atzeni et al., 2010) or by means of in-contact microtremor measurements (Nakamura et al., 1999). During the artificial and coordinated horizontal solicitation, displacement signals coming from the structure follow a trend of sinusoidal type with significantly greater amplitude than the ones

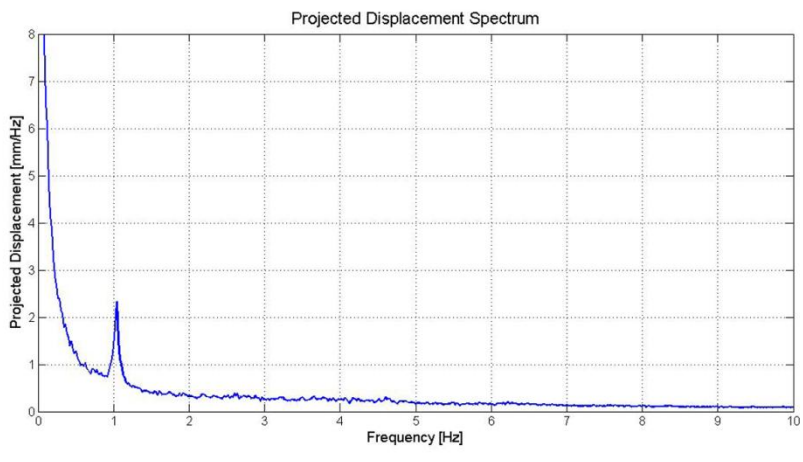
induced by only the weak wind and random vertical forces. Time domain traces were also more regular and smoothed in conditions of artificial solicitation than in natural condition.



**B**



**C**



**D**

Figure 4.6: Frequency composition of the signal reflected from the points at middle height of the tower for the measure positions B, C and D and their identification on pictures with the same viewpoints of the operating IBIS-S. All the measurements are collected with only wind energization.

Furthermore we have performed the experimental modal analysis for the first vibration mode of the tower in order to evaluate the effectiveness of the radar measurements in both experimental conditions. The analysis was done using the Frequency Domain Decomposition technique based on singular values decomposition method (Brincker et al., 2001). By means of this technique the main modal properties of the structure can be identified using only-output measurements also even in the case of strong noise contamination of the acquired signals. The fundamental frequency of the tower appears at 1 Hz for both surveys. The first flexural modal shapes are shown in Figure 4.7 where the displacement amplitudes were retrieved for each selected range bin identified along the structure profile.

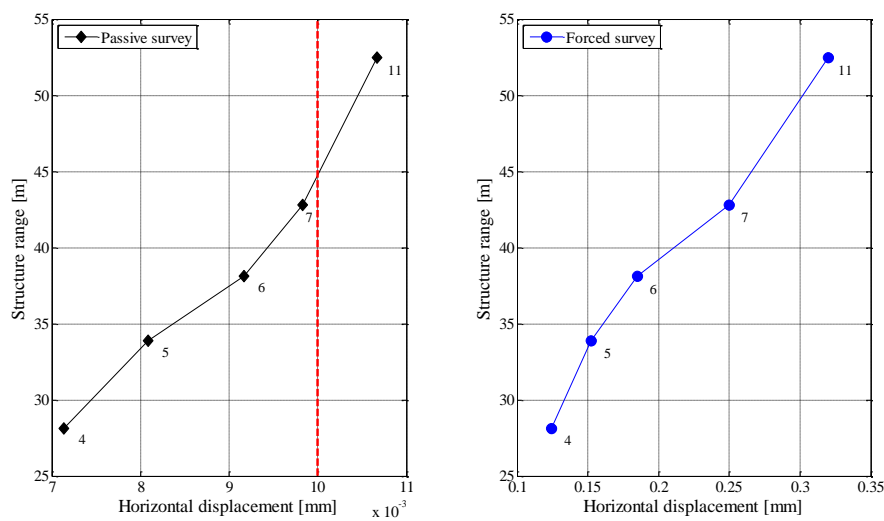


Figure 4.7: First experimental flexural modal shape: (a) passive survey and (b) artificially forced survey.

In these plots the maximum displacement for each selected point is not reported in term of absolute value but only its horizontal projection is shown. In fact, it can be reasonably assumed as the main component of the displacement of the tower considering the geometric features of this structure. Both mode shapes are characterised by amplitudes increasing with the height of each reflector. The red dashed line drawn in Figure 4.7(a) indicates the time domain radar accuracy (10  $\mu\text{m}$ ). We can see that during the passive survey the maximum displacements due to the solicitation done only by the weak wind directly acting on the structure, especially for the points 4, 5, 6 and 7, are lower than the system threshold and in the point 11 is comparable with it. However we have to note that system accuracy is given in the line of sight direction so that its horizontal projection must be considered a little smaller and also points 6 and 7 are in the order of bigness of system accuracy. Conversely, looking at the displacements related to the active survey (Figure 4.7(b)), they are characterised by significant increase of amplitude values for all reflector points with measured values of about thirty times greater than in the passive condition, recorded at the top floor of the structure. Therefore we can observe that

the weak artificial forcing contributes to significantly improve the reliability and the effectiveness of the radar measurements.

### 4.3 CONCLUSIONS

The ground based interferometry technology allowed to observe the behaviour of one important cultural heritage building under external actions made-up by low amplitude winds and people movements inside the structure. The monitored target, a slender structure, was the optimal application field of ground-based Real Aperture Radar interferometers allowing to refer the range distances to the structure singularities with a good back-scattering behaviour and to project the range displacements along the most probable oscillation directions.

The survey of structural vibrations allowed to detect the buildings natural frequencies without invasive actions. A fundamental parameter for structural test and monitoring has been obtained. It allows one to take into account the effects of dynamic solicitations such as using conditions, strong winds or earthquakes. The knowledge of the dynamic responses of cultural heritage buildings is of main importance for the plan of use and for the determination of compatible activities inside the structure or immediately close. Soliciting the Leaning Tower of Pisa with a dynamic forcing of few moving people we were able to reach resonance effects but anyway reasonably maintaining safety condition for the structure (only about 0.60 mm amplitude of oscillation on the top). This survey has proved to be an effective, quick and simple method to verify the acceptable levels of usability of cultural heritage slim buildings. Future insights could bring to define use capabilities of analyzed cultural heritage structures for various environmental conditions such as different wind conditions or with other vibration sources. Furthermore human artificial solicitation proved to significantly enhance Signal to Noise Ratio in interferometric monitoring of vibrations, substantially obtaining the same spectral results of natural solicitation, and can be specifically useful in case of structures with low exposition to winds like in urban environments or in conditions of extremely weak winds. The natural frequencies obtained are in good agreement with the results of other dynamic tests on the same tower present in literature. This result is not trivial because the artificial forcing action has proved to act as a white noise without introducing spurious frequencies in the displacements power spectra.

The interferometric radar has shown clear advantages confirmed also by existing literature, including:

1. the possibility of conducting surveys without direct access to the structure, performing a totally non-invasive survey;
2. the high speed of installation and acquisition (just 30 minutes)
3. the possibility to provide a virtually continuous mapping of movements, having real time results;

4. the precision, directly measuring the structural displacement with an accuracy of 1/100 mm;
5. the possibility to obtain, with standard data processing, the natural frequencies of observed structures, allowing to predict dynamic response to earthquakes, winds or working loads.

## **REFERENCES**

Abdel-Ghaffar A.M. and Scanlan R.H. (1985). Ambient vibration studies of Golden Gate Bridge: I. Suspended structure, *J. Eng. Mech.*, 111, 4, 463-482.

Atzeni C., Bicci A., Dei D., Fratini M. and Pieraccini M. (2010). Remote survey of the leaning tower of Pisa by interferometric sensing, *Geoscience and Remote Sensing Letters, IEEE*, 7, 1, 185-189.

Brincker R., Zhang L., and Andersen P. (2001). Modal identification of output-only systems using frequency domain decomposition, *Smart Materials and Structures*, 10, 3, 441-445.

Castellini P., Martarelli M. and Tomasini E.P. (2006). Laser Doppler Vibrometry: Development of advanced solutions answering to technology's needs, *Mechanical Systems and Signal Processing*, 20, 6, 1265-1285.

Croci G. (2000). General methodology for the structural restoration of historic buildings: the cases of the Tower of Pisa and the Basilica of Assisi, *Journal of Cultural Heritage*, 1, 1, 7-18.

Cunha A. and Caetano E. (1999). Dynamic measurements on stay cables of cable-stayed bridges using an interferometry laser system, *Experimental Techniques*, 23, 3, 38-43.

Cunha A., Caetano E. and Delgado R. (2001). Dynamic tests on a large cable-stayed bridge, *J. Bridge Engineering*, 6, 1, 54-62.

Gentile C. and Saisi A. (2007). Ambient vibration testing of historic masonry towers for structural identification and damage assessment, *Construction and Building Materials*, 21, 6, 1311-1321.

Gentile C. and Gallino N. (2008). Ambient vibration testing and structural evaluation of an historic suspension footbridge, *Advances in Engineering Software*, 39, 4, 356-366.

Henderson F.M. and Lewis A.J. (1998). *Manual of Remote Sensing. Principles and Applications of Imaging Radar*. 3<sup>rd</sup> Ed., John Wiley and sons.

Lee J.J. and Shinozuka M. (2006). Real-time displacement measurement of a flexible bridge using digital image processing techniques, *Experimental Mechanics*, 46, 1, 105-114.

Li X., Ge L., Ambikairajah E., Rizos C., Tamura Y. and Yoshida A. (2006). Full-scale structural monitoring using an integrated GPS and accelerometer system, *GPS Solut.*, 10, 4, 233-247.

Marchisio M., Cosci M., D'Onofrio L., Biagioni A. and Landucci N. (1998). A Geophysical Study of the Palaeo-beds of the Rivers in the Plain of Pisa, *Proceedings of IV Meeting of the Environmental*

and Engineering Geophysical Society (European Section), Barcelona, September 14-17, EEGS, 1998, pp. 441-444.

Nakamura Y., Gurler E.D. and Saita J. (1999). Dynamic characteristics of leaning tower of Pisa using microtremor - preliminary results, Proceedings of the 25<sup>th</sup> JSCE Earthquake Engineering Symposium, vol. 2, pp. 921-924, Tokyo, Japan, July 1999.

Nassif H.H., Gindy M. and Davis J. (2005). Comparison of laser Doppler vibrometer with contact sensors for monitoring bridge deflection and vibration, *NDT & International.*, 38, 3, 213-218.

Salawu O.S. and Williams C. (1995). Bridge assessment using forced-vibration testing, *J. Struct. Eng.*, 121, 2, 161-173.

Samman M.M. and Biswas M. (1994). Vibration testing for nondestructive evaluation of bridges. II: Results, *J. Struct. Eng.*, 120, 1, 290-30.

Settis S., D'Elia M., Jamiolkowski M., Macchi G., Veniale F., Viggiani C. (2005). *La Torre Restituita (Studies and Interventions That Have Allowed the Stabilization of the Pisa Tower)*, vol. 3, Istituto Poligrafico dello Stato.

Towers D.P., Buckberry C.H., Stockley B.C. and Jones M.P. (1995). Measurement of complex vibrational modes and surface form-a combined system, *Meas. Sci. Technol.*, 6, 9, 1242.



## ***CHAPTER 5***



# NON-DESTRUCTIVE EVALUATION OF THE DYNAMIC BEHAVIOUR OF HISTORIC BELL TOWERS BY INTEGRATING CONTACT AND REMOTE SENSING MEASUREMENTS

---

## **Abstract**

*In this chapter the dynamic behaviour of two slender structures with very similar geometry was investigated in order to evaluate the role played by the construction materials. The comparison was conducted on their vibration properties as resonance frequencies, damping coefficients and mode shapes. The studied structures are two bell towers of a church which were built in two different historical times, with an interval of about one century, using different construction techniques and materials. The experimental tests were carried out by means of output-only measurements of ambient vibration using both contact and non contact techniques. The signals were acquired using a tri-directional tromometer and two short period seismometers, both placed in prearranged station-points on the structures. Furthermore the vibrations of the structures were also measured with the IBIS-S microwave interferometer which is able to provide sub-millimetric displacements along the radar Line-Of-Sight (LOS) without need of any contact with the surface. Therefore the experimental dynamic response of the two towers was estimated by integrating both velocity and displacement data. Though the vibration of the structures had low magnitude, both surveys allowed us to identify the main linear dynamic properties of the structures. On the basis of these passive surveys a linear Finite Element Model was calibrated in order to confirm the relationship between materials and vibration properties.*

## 5.1 INTRODUCTION

For different reasons, in many cases it is not possible to excite structures with a known input signal or to measure the main features of the input. Especially for large structures or for high-rise buildings, only ambient vibration measurements can be effectively performed to study the dynamic response of the structures. In fact high energy input should be generated to provide useful results. These methods mainly use wind energy, but also microtremors, microseisms and other kinds of available random and periodic sources (Ivanovic et al., 2000). Furthermore the passive surveys represent a suitable method of the dynamic characterisation of cultural heritage structures due to their non-destructive and non-invasive features which prevent any possible causes of structural damage. In other words, the intensity of the input signal must be calibrated in order not to damage the studied structure during active or forced vibration tests. However this fact is not a trivial issue and the passive surveys allow one to overcome the previous mentioned limitations (Gentile and Saisi, 2007). These experiments are usually performed through many contact sensors installed on the structures by means of different geometric configurations (Bongiovanni et al., 1998, 2000; Cunha and Caetano, 2006; Buffarini et al., 2009; Ivorra et al., 2009). A more simple instrumental layout has been used by other authors to derive the experimental vibration properties of multi-story buildings (Gallipoli et al., 2004; Castellaro et al., 2010), bridges (Stabile et al., 2013) and Reinforced Concrete arch dams (Calcina et al., 2014). More recently innovative non-contact radar systems have been developed to measure displacement time series and many papers have been focused on the use of these microwave sensors to perform both static and dynamic surveys. The capability to measure sub-millimetric displacements has been tested by several works where this system was effectively applied to study the dynamic behaviour of a wide variety of structures such as bridges, tall buildings, wind turbine towers, stay cables, industrial chimneys, damaged and inaccessible slender structures, modern communications towers and ancient bell towers, in open and urban contexts (Pieraccini, 2013).

Many scientific articles have been focused on the relationship between geometric features and dynamic response of structures with the proposal of several empirical relationships (Lagomarsino, 1993; Rainieri and Fabbrocino, 2012). The effects produced by asymmetric geometries of a 21-story building on its structural dynamic response have been investigated by Bui et al. (2014) using in situ ambient vibration tests and numerical seismic analyses. Instead, the different dynamic response of two similar modern buildings has been studied by Castellaro et al. (2013) in order to understand the influence of both soil-structure and structure-structure interaction phenomena.

In this chapter we deal with the study of two almost twin bell towers in order to evaluate the influence of the construction materials on the dynamic properties of the structures. The examined structures were built by employing different materials and techniques but they are characterised by very similar geometries. The study has been performed using both ambient vibration records acquired with one digital tri-directional tromograph or two short period seismometers, and displacement time series

measured by means of a coherent radar system, called IBIS-S (Image by Interferometry Survey). The paper is organised as follows: in section two the main historical and architectural features of the analysed structure are briefly reported. In the third section, the ambient vibration surveys and main results are described for each method, considering both advantages and limitations. The fourth section describes the Finite Element Model calibrated and built in order to interpret and to confirm the observations performed through the experimental investigations. Finally theoretical and experimental results are compared and integrated in discussion and conclusions sections.

## 5.2 DESCRIPTION OF THE STRUCTURE

The church of Sant'Anna is located in the old historic district of Stampace in Cagliari town, in southern Sardinia (Italy). The construction of the actual structure was started on 27th May 1785 following the project of the architect Giuseppe Viana but works proceeded very slowly mainly due to lack of funds and construction was completed in about thirty-three years. However at the end of the first construction stage the church lacked the east tower which was included in the original project with two symmetrical towers. These second tower was built in 1938 with geometric features very similar to the older one. Different materials were used due to the complicated construction process. In particular, the ancient tower is a masonry structure, as the main structural parts of the church are, and the second tower is a Reinforced Concrete building. Figure 5.1 shows an overview of the main stages of construction. The church was built in Piedmontese Baroque style (Kirova et al., 1994) and is characterised by a single longitudinal nave surrounded by four side chapels. There are three domes aligned along the longitudinal axis of the structure with different shapes, heights and diameters.

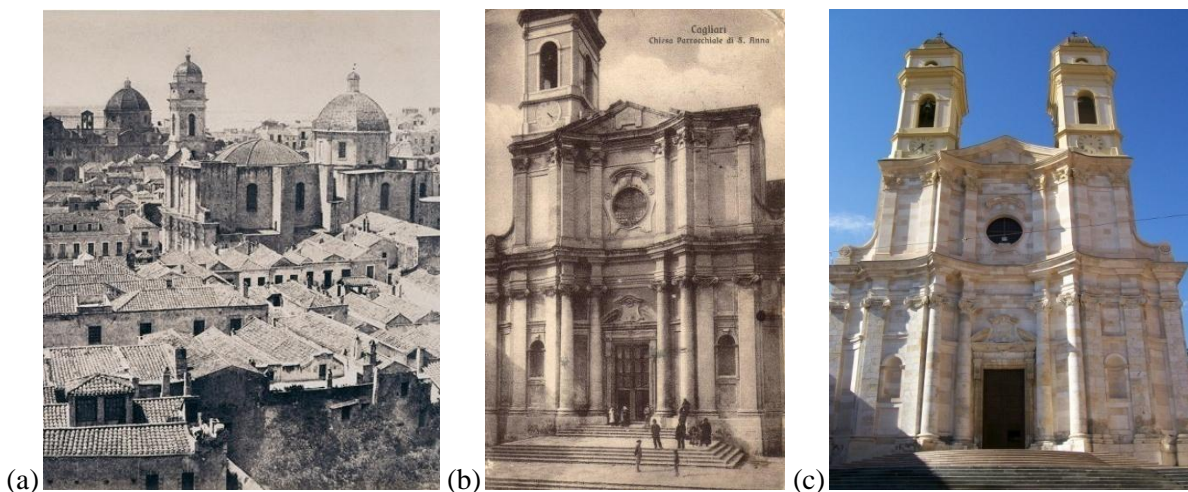


Figure 5.1: Main steps of construction of Sant'Anna church: (a) lateral view of the church in 1854; (b) the façade until to 1938 (image of 1920); (c) the church completed with the east tower in a recent image (2014).

The transept is crowned with the highest dome in the central body of the church. The church is about 66 m in length, 24 m in width, with an average height of 20 m. The transept is 25 m long and 14 m

wide. The lateral towers are merged with the body of the church façade until about 22 m, whereas the upper levels reach 42 m in height. Only the oldest tower is provided with four bells whereas the other one is totally empty inside and its main role is to complete the design symmetry. The original structure of the church was severely damaged and partially destroyed (especially the central dome and the transept) during the bombing of the Second World War and was later rebuilt. However, both towers were only slightly damaged on their external surfaces, struck by fragments from explosions. To simplify we will call tower A the old masonry structure and tower B the Reinforced Concrete structure.

### **5.3 DESCRIPTION OF THE EXPERIMENTAL VIBRATION TESTS AND RESULTS**

The experimental dynamic investigations carried out on the examined structure were performed only through passive surveys using ambient vibration tests. Vibration measurements were done by means of velocity transducers directly installed above the structures and through the coherent radar system IBIS-S which is capable of providing synchronous displacement time series related to more natural reflector points along the structure radar power profile. In general, the use of contact sensors, as seismometers or accelerometers, presents many advantages in terms of reliability of the results (Cappellini et al., 2014). This is mainly due to the lack of ambiguity of data which are clearly referred to their acquisition points, while in the radar surveys particular attention must be given to distinguish signals coming from points in the whole scenario but not belonging to the target structure. Another potential problem of the radar acquisitions could be due to the condition of two points with the same distance from the instrument, at the acquisition resolution, which time series displacements are recorded in the same range bin,. However the structures are not always accessible at all levels to install the measurement devices.

In this research we have integrated the data acquired by means of three different measurement tools in order to build a more detailed frame of the dynamic behaviour of the structures.

#### **5.3.1 Microtremor measurements**

Three kinds of measurements have been performed for the vibrational study of the two structures by means of different instrumental equipments (Figure 5.2).

The first survey was carried out using only a single triaxial tromometer Tromino (Micromed) which is composed by three high gain velocity transducers, three low gain velocity transducers and three accelerometers. Each set of sensors is oriented along orthogonal axes. By using this device, eighteen microtremor stations were positioned inside of the structures. All microtremor stations located on the structure are reported in Figure 5.2. In particular, the measurement points were located along the two vertical directions in order to compare the dynamic behaviour of the towers. Twenty-minute asynchronous measurements of vibration were acquired with 512 Hz sampling frequency. The stations

[TR18], at the base of tower A, and [TR14], at the base of tower B, were distinctly assumed as reference sites for the collected vibration data (see Figure 5.2(a, d)). However the recordings performed in these points highlighted the same frequency content and any significant difference was not observed by swapping the reference sites. The measurements inside the towers were acquired for short times and with similar environmental conditions, then were compared to the reference recordings. The microtremor traces were analysed in time and in frequency domain. Also, directional and Short Time Fourier analyses were done for each station. The spectral ratios of each channel have been computed in order to estimate the empirical dynamic response of the buildings. The starting resolution in frequency domain was 0.05 Hz due to the time length of the window used to perform the Fast Fourier Transform (FFT) analysis which was set to 20 seconds for all time series. A low smooth (1%) was also applied in frequency domain in order to preserve the narrow spectral peaks that could be related to the structural behaviour.

The second tests group was performed with two short period seismometers. These measurements were carried out with two geophones S13 (Geotech instrument) set in horizontal operational mode and connected to a seismograph Geode. The tests were conducted only in the upper levels of both towers, where they are totally external to the body of the church (Figure 5.2(a, e)). Seven configurations of measurement were performed using these devices. Each one was designed in order to provide specific information about the dynamic properties of the towers as the identification of their rotational modes by means of the phase relationship between different synchronous displacement time series acquired on several stations on the towers. The channels were always oriented in longitudinal or in transversal direction along the axis of the structure. The instrumental configurations may be classified in relation to the mutual position of the sensors because parallel and orthogonal setups were used in order to derive the relative displacements of the towers (opposite or in phase movements). The different acquisition setups are illustrated in Figure 5.3. Six measurements have been performed using both sensors arranged on the same structures: three on the concrete tower (tower B) and three on the masonry tower (tower A), respectively. In one case the sensors have been arranged in order to acquire simultaneously microtremor traces above the two towers. The initials TT, LL and LT in the name of each configuration indicate the orientation of the acquisition axis of the sensors (Transversal-Transversal, Longitudinal-Longitudinal, Longitudinal-Transversal). In the configurations [LL01] and [TL02] the sensors are installed on the tower B at the level B corresponding to the open windows (at about 26.4 m from the ground floor of the church). The configuration [LL03] was performed installing the first geophone, Ch01 in Figure 5.3(a), on the tower A and the second geophone, Ch02, on the tower B. The transducers were placed at the same level used for the previous acquisitions (level B). The acquisitions [LL04] and [LL05] were taken using the sensors on two different levels (A and B) of each tower, at 22 m and 26.4 m respectively, in the same station points used with the triaxial

tromometer. Finally, the acquisition layouts called [LL06] and [LT07] repeated the first and the second configurations for the structure A.

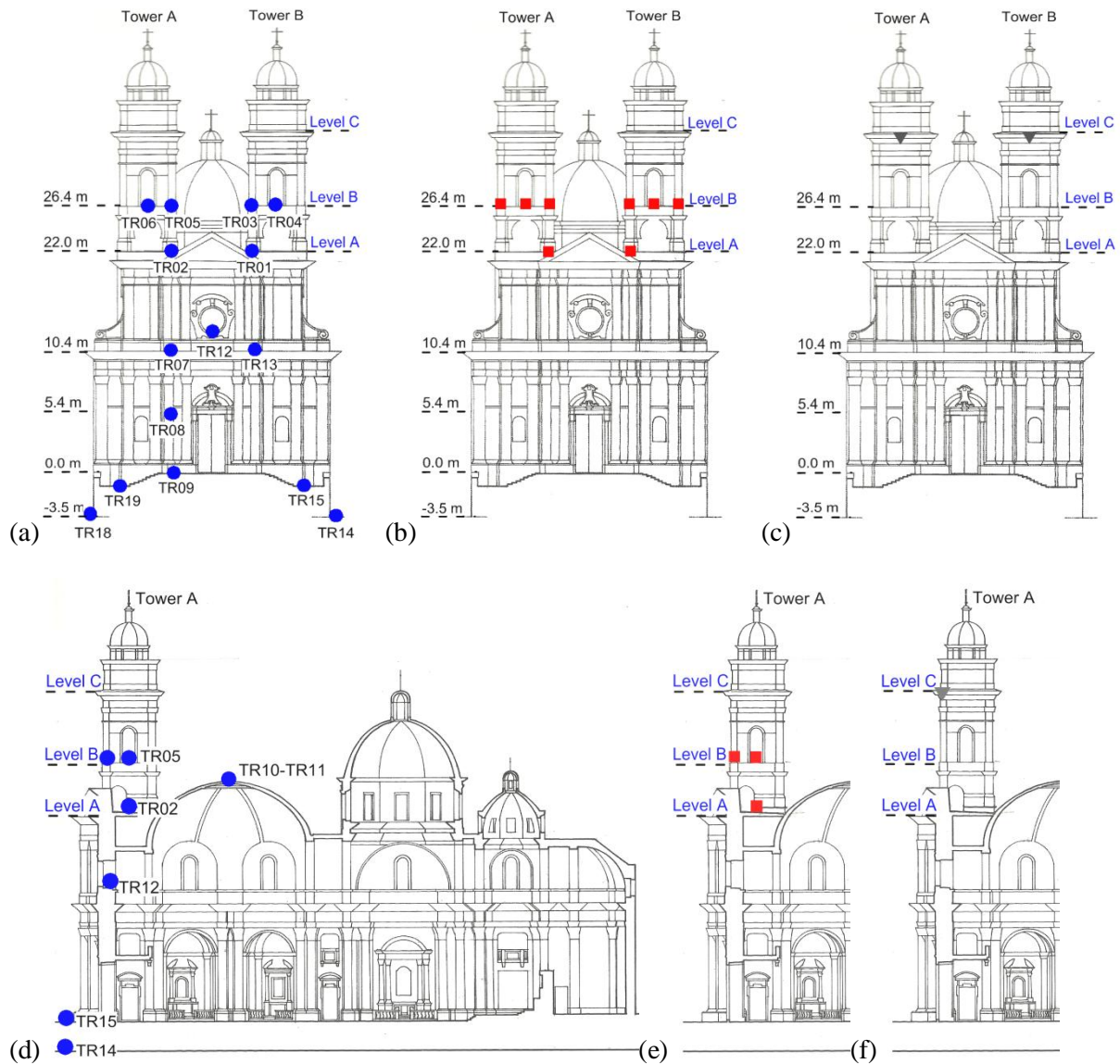


Figure 5.2: Instrumental geometric layout: (a, d) Single triaxial tromometer stations (blue circles); (b, e) Seismometers S13 stations (red squares); (c) Natural backscatterers identified from the interferometric survey (gray triangles).

Finally, the ground-based radar interferometer IBIS-S was used to measure the displacements of the top levels of the towers from two outdoor stations (Figure 5.2(c, f)). This was done in order to get the dynamic characteristics of the towers under environmental excitations mainly due to the wind action and secondly related to the vehicular traffic around the structure. The data collected using the remote measurement tool, were acquired with two different geometries. With this technology one can measure vibration time series related to inaccessible points such as the top segments of the two towers. The survey has been conducted by two different acquisition points. In the first radar



configuration, aimed to measure the displacements of the tower A, the system was located in front of the main façade of the church aligned to the tower with 60 degree of vertical inclination of its head.

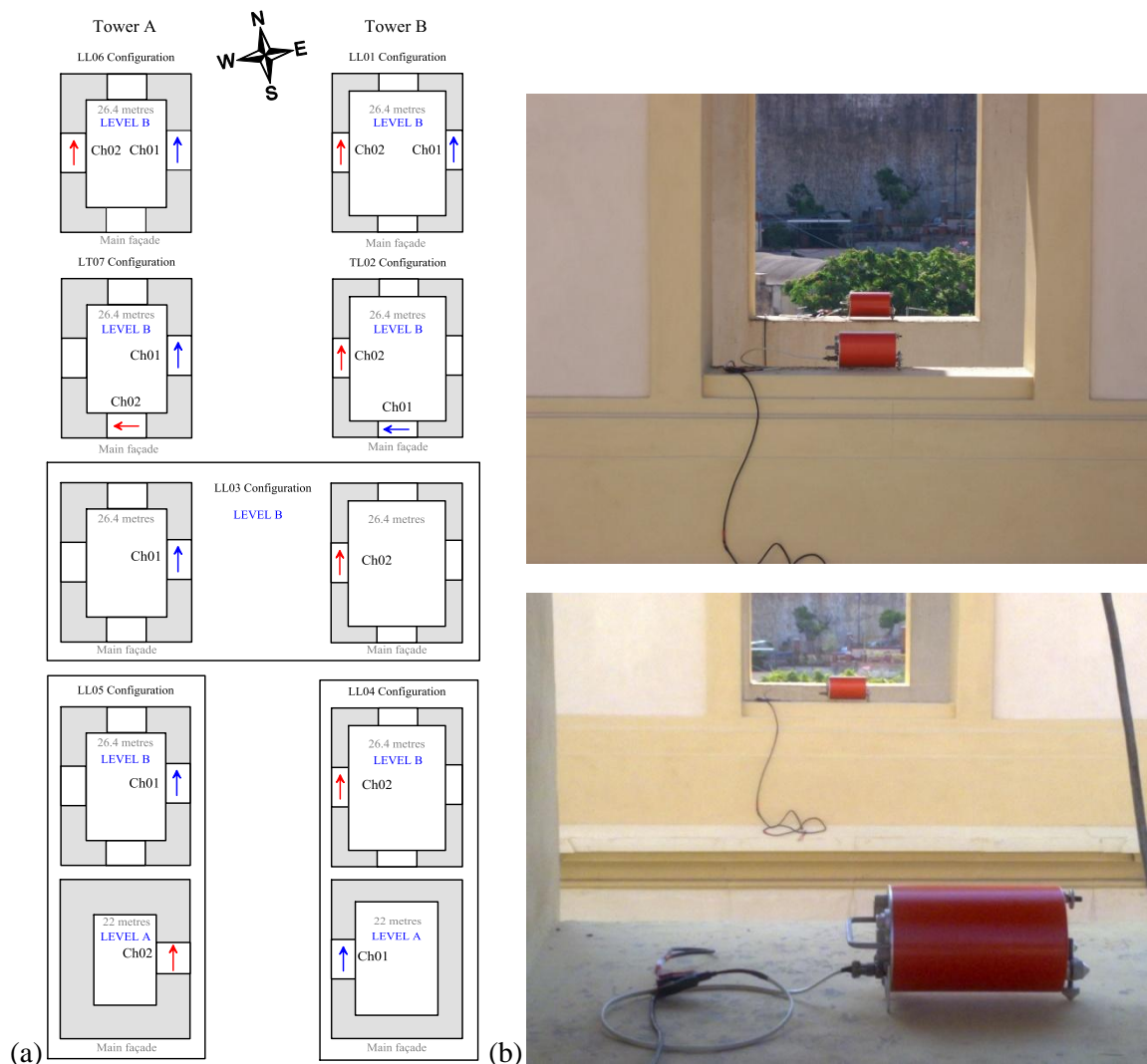


Figure 5.3: Single-channel seismometers layouts. (a) Scheme of the geometric features of the measurement configurations; (b) Some views of the sensors installed on the towers (LL01 above; LL03 below).

The observation angle has been selected in order to mainly illuminate the interesting part of the structure. In the second configuration the radar was installed symmetrically to the first acquisition point aligned and oriented towards the tower B (Figure 5.4). Both surveys have been done using 100 Hz sampling frequency and 100 metres of maximum range of acquisition. Each measurement provides the displacement traces along the radar Line Of Sight (LOS). These traces may be processed to achieve the natural resonances of the structures. The two bell towers are characterised by several natural back-scatterers such as cornices, arches and corbels which can provide significantly high reflected signals to the radar in relation to the background noise. Nevertheless both radar configurations were able to detect reliable measurable amplitudes of vibration only for two radar bins

(one for each tower) corresponding to the reflection points located at the topmost of the structures. Probably the displacements recorded in the other range bins didn't have significant magnitude of amplitude when projected in LOS direction. Further measurements were carried out installing the interferometer in the narrow lateral streets in order to detect also the transversal displacements. However these configurations have not provided any significant result probably due to the small component of displacement in LOS direction because of the high inclination of the sensor head.

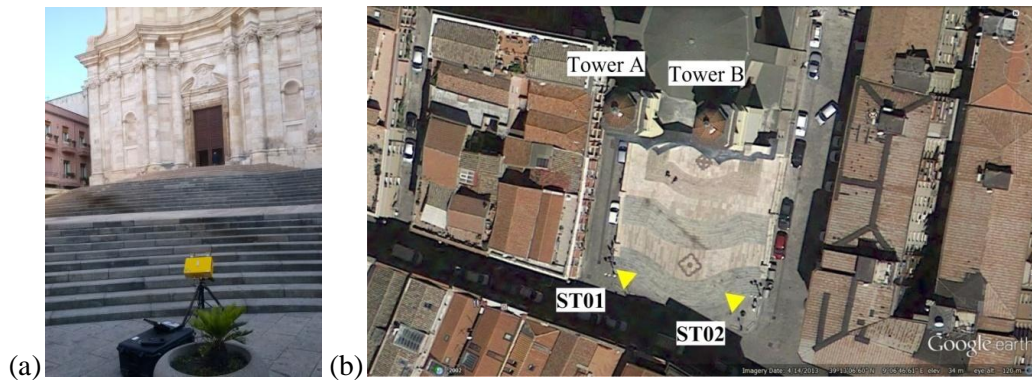


Figure 5.4: Radar measurements: (a) Image of the interferometer IBIS-S during the survey; (b) Sketch of the geometric configurations adopted for the radar survey.

### 5.3.2 Experimental results and discussion

#### *Triaxial single station survey*

Data acquired by Tromino sensor were processed with Standard-Spectral-Ratio technique (SSR, Borchardt, 1970), Horizontal-to-Vertical Spectral Ratio (HVSr, Nakamura, 1989), directional and transient spectral analyses.

Figure 5.5 and Figure 5.6 show the SSR spectral ratios for all stations normalised with respect to the reference sites, respectively: 5.5(a) longitudinal direction (S-N) signals on tower A normalised to [TR18]; 5.5(b) longitudinal direction signals on tower B normalised to [TR14]; 5.6(a) transversal direction (E-W) signals on tower A normalised to [TR18]; 5.6(b) transversal direction signals on tower B normalised to [TR14]. In these plots it is possible to observe that the natural frequencies clearly appear in both directions of measurement. The whole recorded spectra are characterised by many maxima, probably related to the structural response of the remaining parts of the church.

The spectra plotted in Figure 5.5(a) were calculated for seven microtremor stations on the tower A and they show two frequency peaks at about 2.3 Hz and 2.6 Hz in the longitudinal component with maximum amplitude recorded at the second spectral peak. The same components at 2.3 Hz and 2.6 Hz are measured in the transversal direction (Figure 5.6(a)) but in this case the amplitudes are greater for the first frequency peak. Furthermore, looking at the simple velocity spectra the frequency peak at 2.3 Hz is present in both components of the motion but it is more marked in the transversal direction.

Conversely the peak at 2.6 Hz highlights also important directional effects with larger amplitude recorded in the longitudinal direction as shown by the angular spectrum computed for this measurement. This is plotted in Figure 5.7 together with other spectra related to the stations located above the towers. Directional effects strongly affect the dynamic behaviour of the towers and clear anisotropic amplitude distributions are shown on both structures by the signals collected at the higher stations normalised respect to the lower ones.

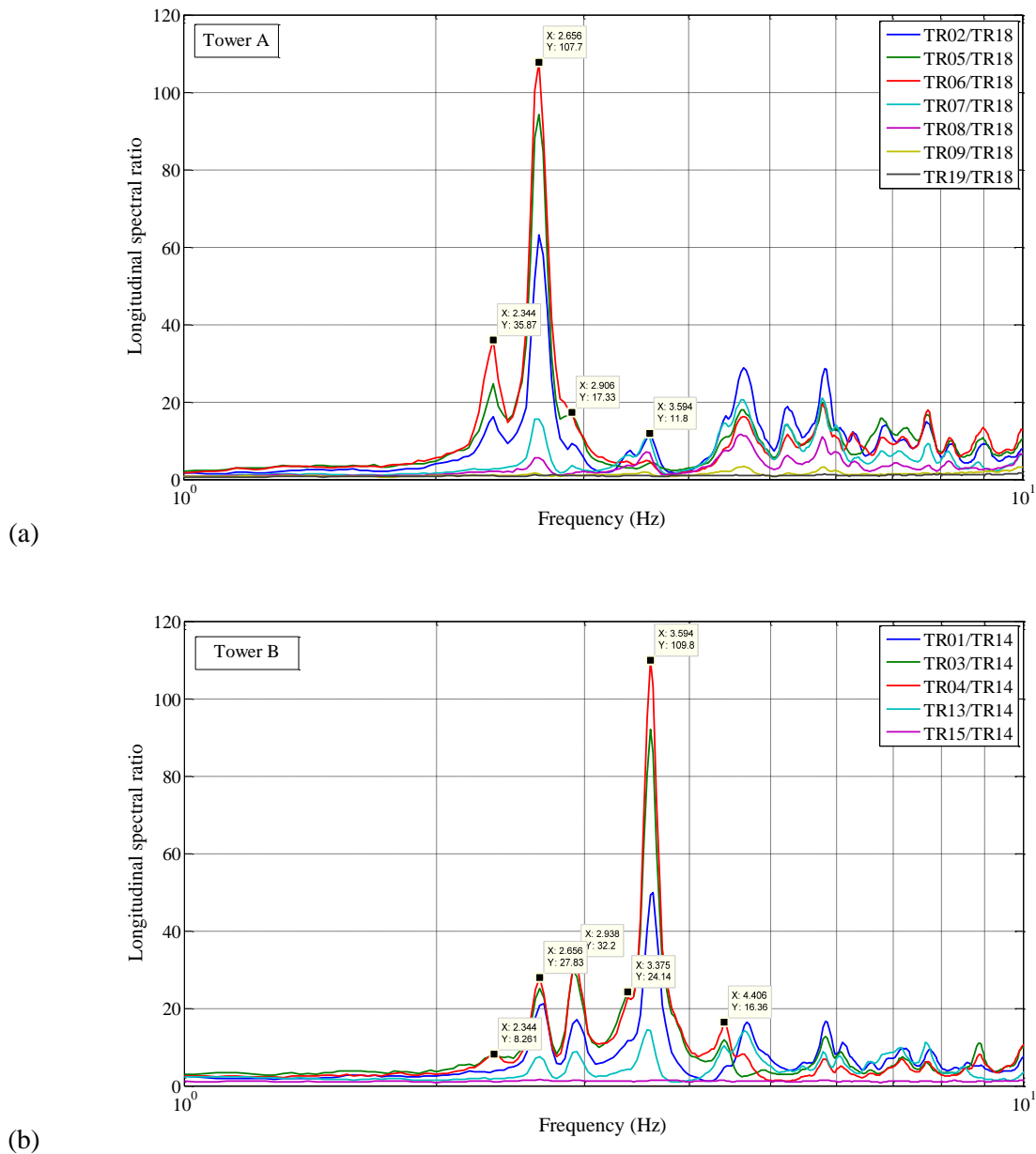
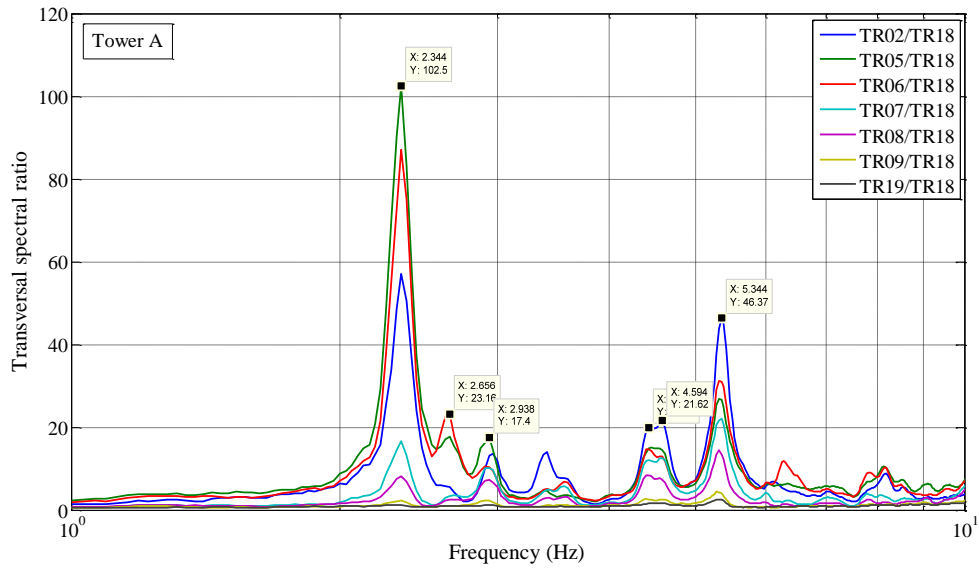
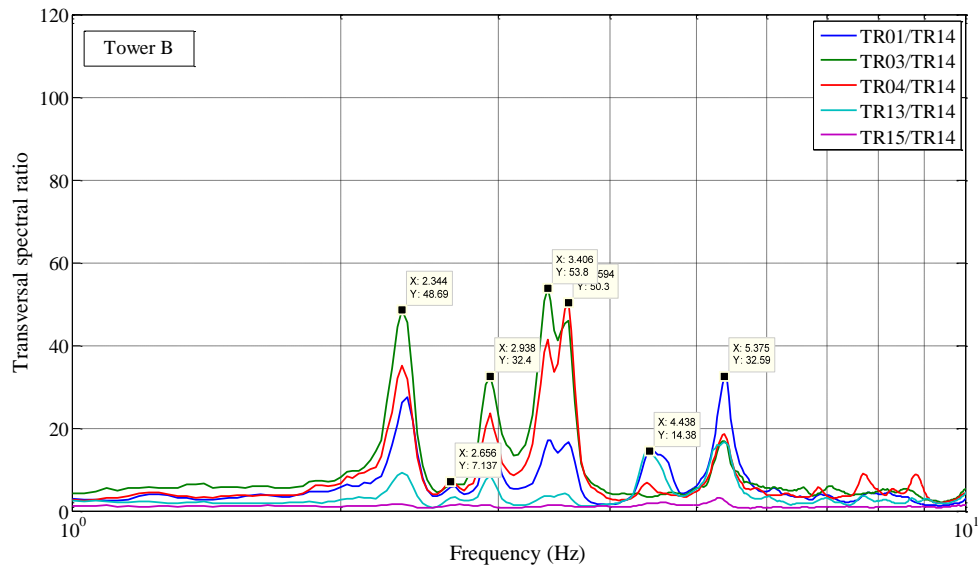


Figure 5.5: Standard Spectral Ratios computed for the longitudinal component of the motion.



(a)



(b)

Figure 5.6: Standard Spectral Ratios computed for the transversal component of the motion.

The experimental response of the structure derived by the measurements carried out on the tower B is shown in Figure 5.5(b) and Figure 5.6(b). In these graphs further frequency peaks are highlighted. In fact, looking at the longitudinal ratio several spectral peaks at 2.3 Hz, 2.6 Hz, 2.9 Hz, 3.4 Hz and 3.6 Hz were found. However here the maximum amplitudes are shown at the higher frequencies and this is more evident at 3.6 Hz. Especially in the measurements done in the stations [TR03] and [TR04] (level B) this component is sharply amplified. This could be related to the differential behaviour of the tower B probably due to its different features. The components highlighted by the transversal ratios show high amplification effects at 2.3 Hz, 2.9 Hz, 3.4 Hz and finally at 3.6 Hz. It is important to

observe that in transversal direction the frequency at 2.6 Hz is characterised by very weak amplification with growing height. The spectral component with maximum amplitude at 3.4 Hz is probably related to a normal vibration mode which shows important deformations along the transversal axis of the tower B.

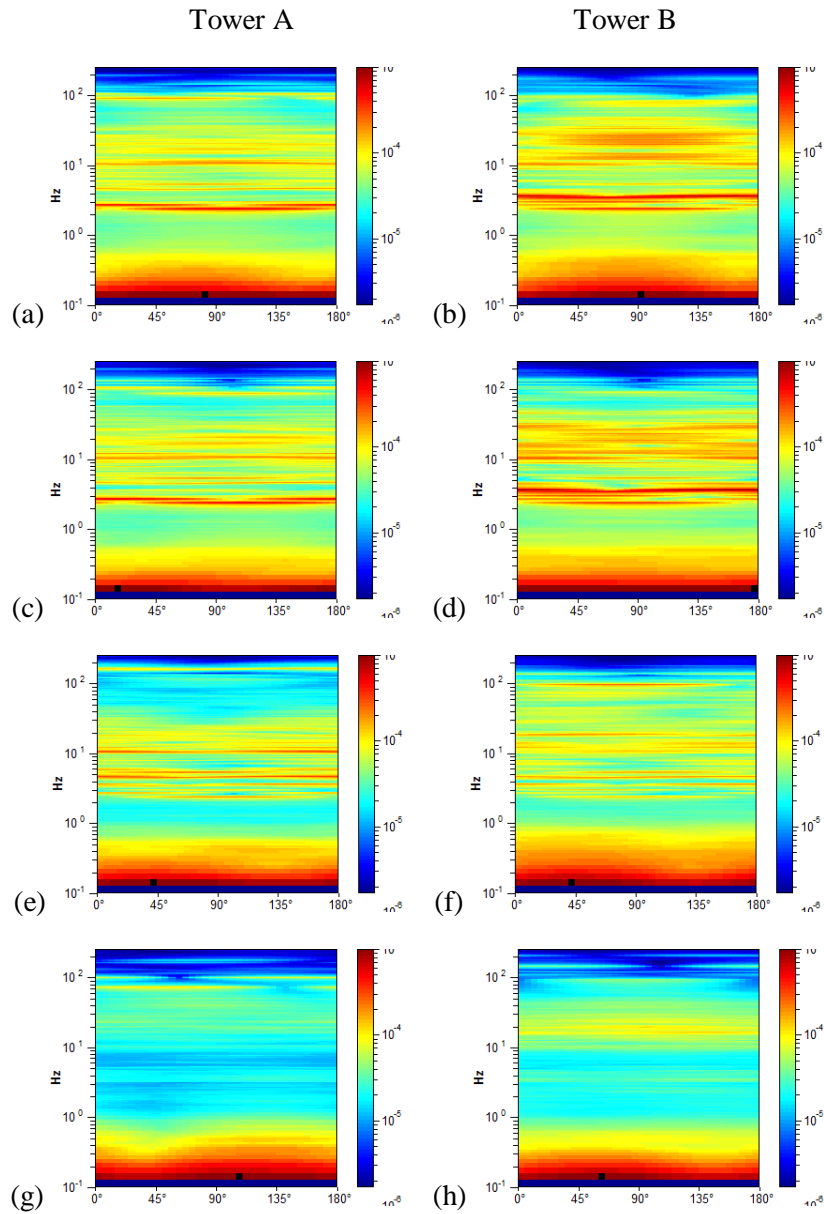


Figure 5.7: Directional spectra computed for several stations above the structures: (a) [TR05]; (c) [TR06]; (e) [TR07]; (g) [TR18]; (b) [TR03]; (d) [TR04]; (f) [TR13]; (h) [TR14].

Both these frequency components at 3.4 Hz and 3.6 Hz are not present in the spectra of the recordings acquired on the higher level of the structure A and this observation could confirm the previous hypothesis about the different linear dynamic behaviour of the two towers. Furthermore Figure 5.8 shows the specific spectral ratios calculated between traces [TR04] and [TR06] with the following equation:

$$SSR = \frac{|H_{TR04}(f)|}{|H_{TR06}(f)|} \quad (5.1)$$

where  $H_{TR04}(f)$  and  $H_{TR06}(f)$  are the spectra related to the measurements collected on tower B and tower A respectively (at level B), aimed to identify which frequencies are prevalently linked to the dynamic response of the tower B. These plots clearly show a strong peak at 3.6 Hz acquired by the longitudinal channel, with amplitude twenty-five times greater in the [TR04] station than in the [TR06] station. In the transversal ratio, the frequency of 3.4 Hz clearly appears amplified on the tower B (about eight times). Also for two peaks at 2.9 Hz and 3.6 Hz a low amplification effect may be observed.

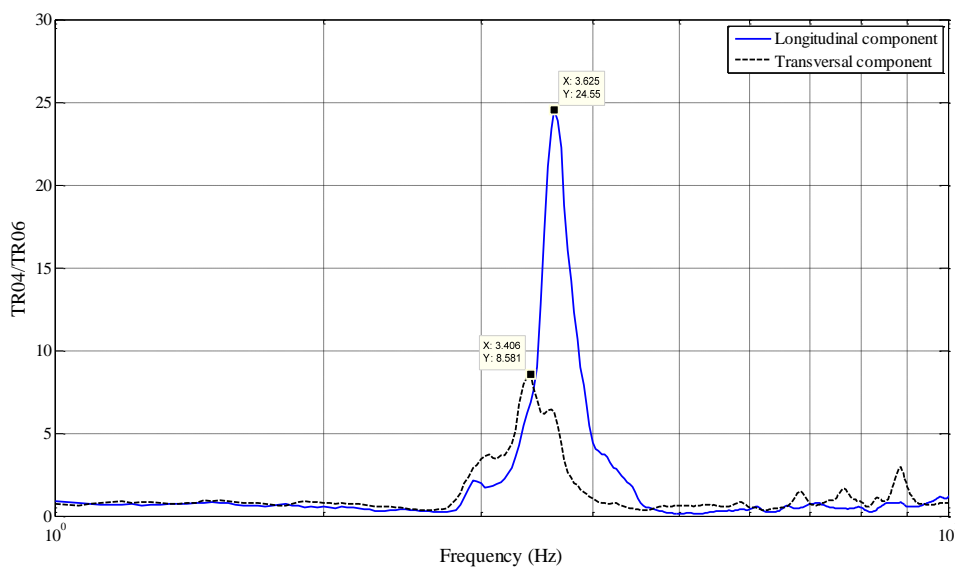


Figure 5.8: Spectral ratios computed between [TR04] and [TR06] stations located on the top levels of the towers in order to estimate the different amplification effects of the structures.

As observed by several authors (Gallipoli et al., 2004) also the microtremor Horizontal-to-Vertical-Spectral Ratio (HVSR) can be effectively used to identify the fundamental dynamic characteristics of the structures. Although this empirical method is usually able to provide only general information, in this case the H/V spectra shown in Figure 5.9 and Figure 5.10 appear suitable to highlight different frequency peaks related to the structural resonances of the building. However in both longitudinal and transversal spectral ratios we can observe that the amplitude at 3.6 Hz is small even for the time series acquired in the station [TR05] and [TR06] on the level B of tower A. Furthermore the amplification effect on HVSRs at 3.4 Hz and 3.6 Hz is lower than that observed on the standard ratios (SSR) computed using only homologous components. This effect indicates that both natural modes related to these frequencies are probably characterised also by significant vertical displacements which determine lower H/V spectral amplitudes.

The microtremor field was collected also on the dome bedecking the initial part of the single nave of the church (station [TR10] plotted in Figure 5.2(d)). In particular this measurement was performed installing the sensor in the upper part of the dome in order to acquire the displacements likely related to the first mode of vibration of this element, which may be presumed similar to the fundamental oscillation mode of a plate. The spectra computed here for the vertical component of the motion present significant frequency peaks at about 10 Hz and 22 Hz. Thus these components could characterise the main vertical displacements of the southern dome.

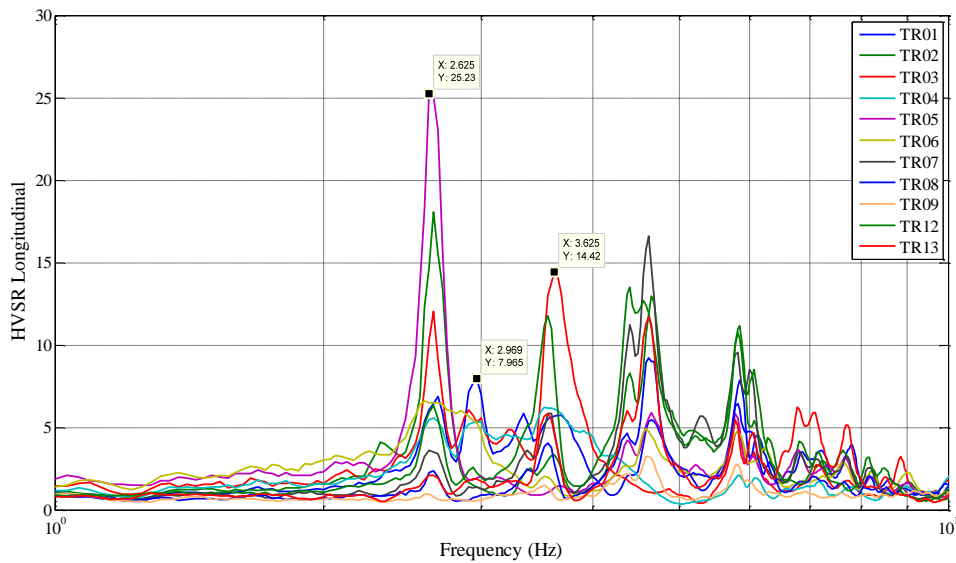


Figure 5.9: Horizontal-to-Vertical Spectral Ratios – longitudinal direction.

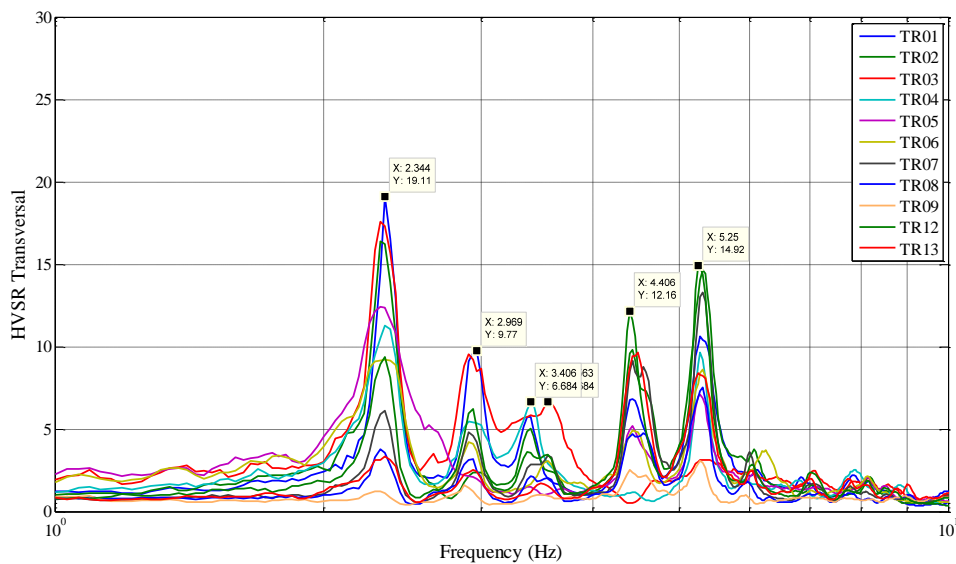


Figure 5.10: Horizontal-to-Vertical Spectral Ratios – transversal direction.

### *Synchronous coupled sensors survey*

Through the synchronous measurements of noise it was possible to estimate the main vibration frequencies of the structure by means of the Power Spectral Density (PSD) functions such as auto-power and cross-power spectra. This method is based on the frequency analysis of the auto-correlation and cross-correlation functions calculated for different pairs of signals acquired on the structure. This approach has been followed by many authors in the past years (Bongiovanni et al., 2000). Furthermore several authors highlight that the frequency peaks related to the structural natural resonances are in phase or 180 degree out of phase in different points of the same structure and in this way we can discriminate them by the other peaks related to the spectral content of the background microtremor field (Bendat and Piersol, 1993). However this criterion is valid only for low damping values (i.e. lower than 0.05). The amplitude spectra provide the resonance frequencies of the structures. Whereas the phase lag between several signals may be used to identify the approximated modal shapes or to discriminate between flexural and rotational modes. A further element that can usually be considered to evaluate the reliability of the measurements uses the coherence function. This function is computed for each pair of signals and assumes very close to unity values at the natural frequencies of vibration of the structure. This condition could be not satisfied for some masonry structures due to non linear behaviours even shown at very low magnitude excitation (Buffarini et al., 2009).

In the Figures 5.11-5.12 the cross-power spectra computed for each couple of sensors have been reported. As we can observe the amplitude power spectra of several configurations presented many frequency peaks characterised by significant magnitude. These frequencies could be related to the dynamic response of the structure if they are coupled with significant values of the phase factor and with high values of the coherence function. In the configuration [LL01] the frequency peak at 3.6 Hz showed greater amplitude than the other spectral peaks. Furthermore it was associated to high value of coherence and to 0 degree of phase delay. This condition is related to the presence of the structural flexural mode that mainly affects the measurement done on the tower B. In the measurement taken on the tower A using the configuration [LL06] this frequency peak at 3.6 Hz was not detected while it was observable under the configuration [LT07] with a small amplitude. This was in good agreement with the spectral ratios computed using the vibration data acquired with the digital tromograph Tromino. Furthermore, by analysing the phase relationships between the channels achieved by the different setups, it is been possible to summarise the following points:

- The spectral component at 2.3 Hz is the first vibration frequency of the structure, mainly acting in transversal direction. This consideration has been supported by the analysis of the transversal power spectral densities, where this frequency showed greater amplitude than in the other direction. Especially in the configuration [LL04] (on the tower B) this component was not



observed in neither records acquired by the longitudinal channels placed on two levels of the structure. Conversely it was clearly shown by the seventh configuration [LT07] with maximum amplitudes recorded along the transversal axis of the tower A;

- The spectral peak at about 2.6 Hz showed strong anisotropic effects including a flexural mode shape mainly characterised by displacement components in longitudinal direction. As we can see in the parallel configurations [LL05] and [LL06] the phase factor for this frequency showed significant values (0 degree) and was associated to high coherence (greater than 0.9);
- The frequency of 3.6 Hz is probably related to a mode of vibration that includes main, but not exclusive, displacements along the longitudinal direction of the Tower B. In fact, looking at the phase factor, it was 0 degree for the measurements performed with parallel channels (LL01) and 180 degree in the orthogonal configuration (LT02); this component was detected with very low amplitude also on the tower A and analogous considerations can be done. This natural mode has weakly affected the dynamic response of the masonry bell tower;
- Finally the parallel configuration called [LL03] has put in evidence that the displacements related to the frequencies of 2.3 Hz and 2.6 Hz were 180 degree out phase for the first component and in phase for the second one. Maximum value of coherence was observed at 2.6 Hz in the cross-power spectrum computed for the longitudinal position of the channels on the towers.

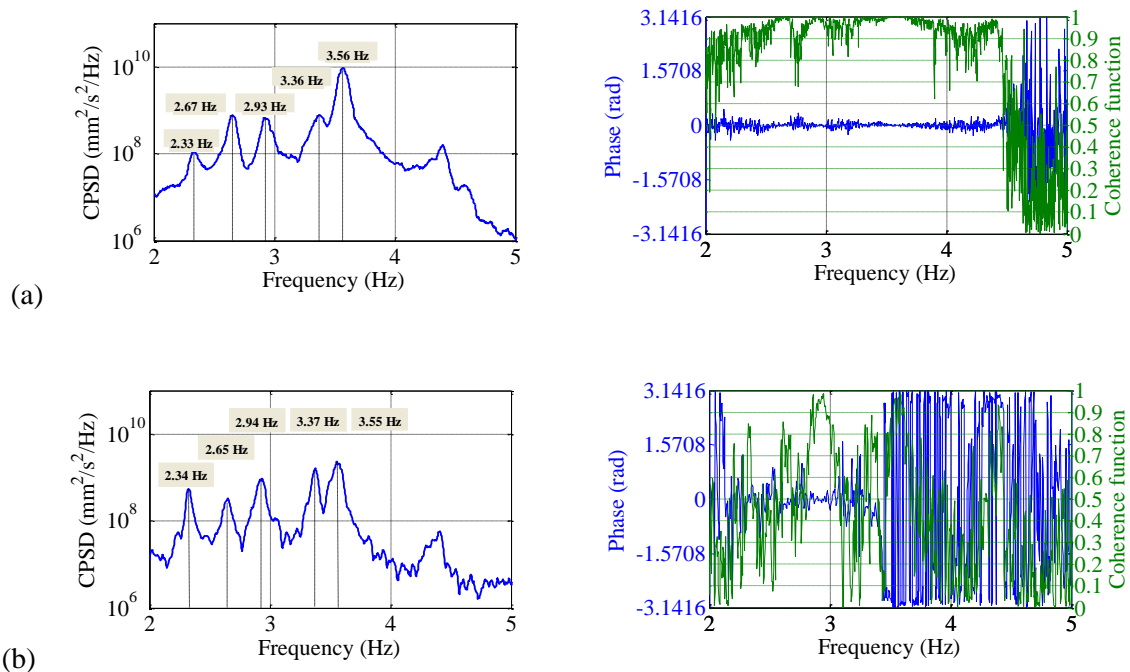


Figure 5.11: Cross-power spectral density functions: configurations (a) [LL01], (b) [TL02].

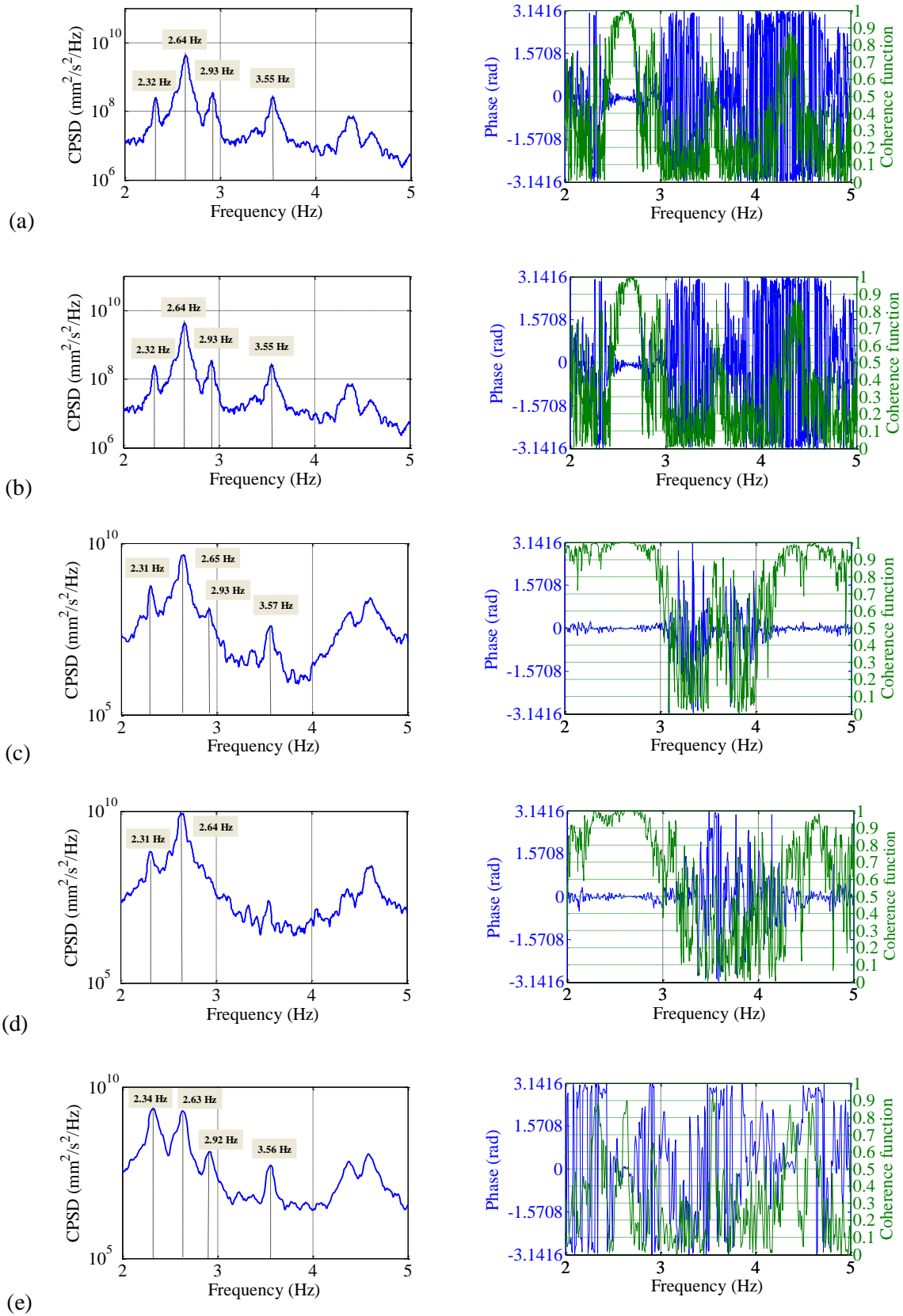


Figure 5.12: Cross-power spectral density functions: configurations (a) [LL03]; (b) [LL04]; (c) [LL05]; (d) [LL06]; (e) [LT07]. Amplitude spectra (left), phase spectra and coherence functions (right).

As discussed by Ivorra et al. (2011), a common feature that affects the dynamic behaviour of the masonry bell towers is their low damping coefficient. In fact, as observed by several experimental studies (Gentile and Saisi, 2007; Ramos et al., 2010; Benedetti and Gentile, 2007; Julio et al., 2008; Schmidt, 2007; Wilson and Selby, 1993), the damping ratio usually ranges between 1.5 % and 2.5 %. However higher values were sometimes estimated by other authors: Bayraktar et al. (2009) observe 3.616 % of modal damping for the first natural mode and 3.387 % for the second one of a masonry bell tower. These very low values can affect the significant amplification effect related to the resonance conditions which happen when the frequency of the dynamic forcing (e.g. forces generated by the ringing of the bells or by the ground motion excitations) is close to one of the natural frequencies of the structure.

In the case of Sant'Anna bell towers, the modal damping has been estimated following the NonPaDAn method (Non Parametric Damping Analysis (Mucciarelli and Gallipoli, 2007)) and using the half-band amplitude method for random vibration recordings. The results are compared in Table 5.1 where it is possible to see that the NonPaDan technique provides weakly higher values of equivalent viscous damping for the resonance frequencies at 2.3 Hz, 2.6 Hz and 2.9 Hz. However, taking into account the approximations at the base of both methodologies (Single Degree of Freedom model), the differences between the different estimation techniques are negligible.

Mode No.	Frequency $f$ (Hz)	NonPaDAn $\xi$ (%)	Half-band method $\xi$ (%)
1	2.3	2.1	1.8
2	2.6	1.5	1.3
3	2.9	1.4	1.3
4	3.4	0.7	0.8
5	3.6	1.6	1.6

Table 5.1: Experimental damping estimation.

### *Interferometric survey*

The radar power profiles measured from the stations ST01 and ST02 are plotted in Figure 5.13. In these images the amplitude of the microwave signal backscattered by the structure is plotted as function of the height for both radar stations. Several signals have been recorded by the microwave sensor along the structure range with high Signal-to-Noise ratio. The continuous vertical lines drawn on the radar images identify the range bins including the frequency peaks related to the dynamic response of the structure. The correspondence of these range bins with towers elements is reported in Figure 5.2 where the origin of the reflection is indicated as a point (symbol gray triangle) for a quick identification but the real reflector is the whole part of structure volume included in the range bin.

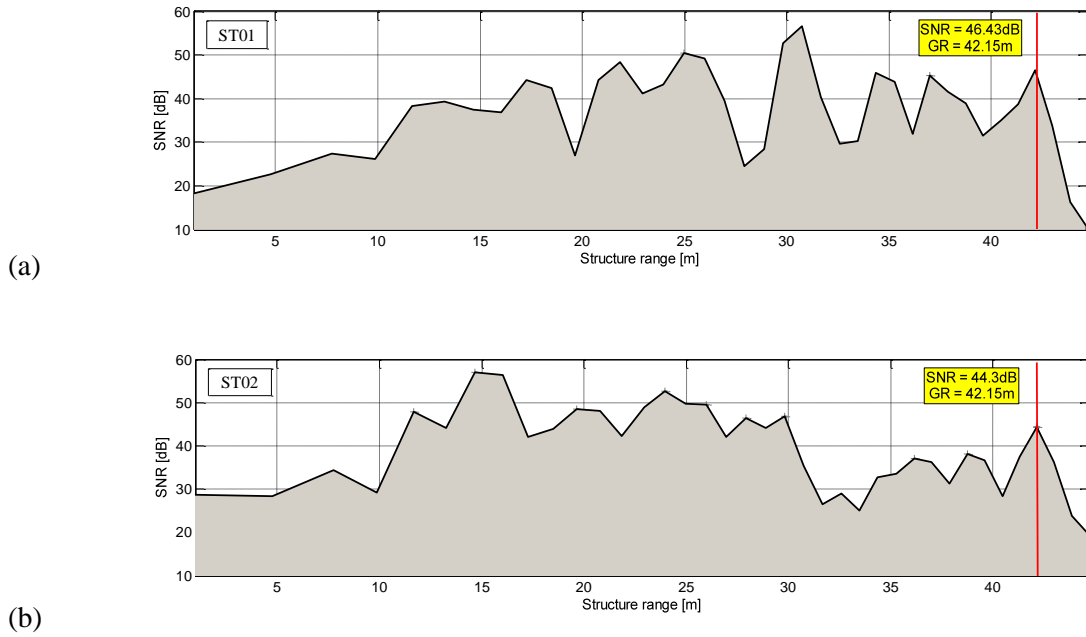


Figure 5.13: Structure Range Power profiles derived for the stations ST01 (a) and ST02 (b). The vertical lines drawn in the plots indicate the radar bins which show the frequency peaks related to the structure response.

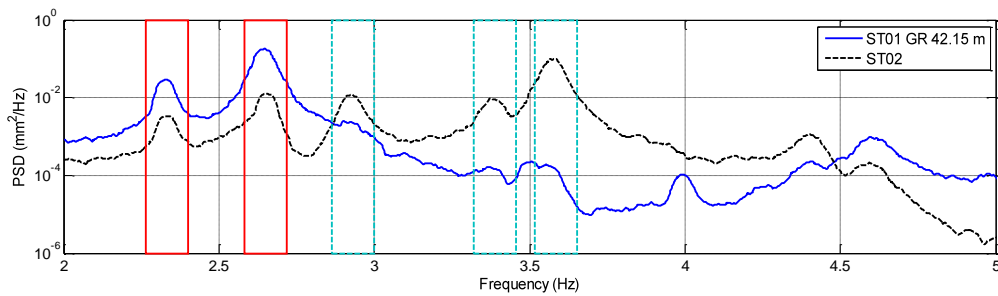


Figure 5.14: Power spectral densities vs frequency of the displacements measured at about 42 metres height from the radar stations: red boxes indicate the frequencies that are mainly amplified by the tower A; cyan dotted boxes include the peaks related to the resonances of the tower B.

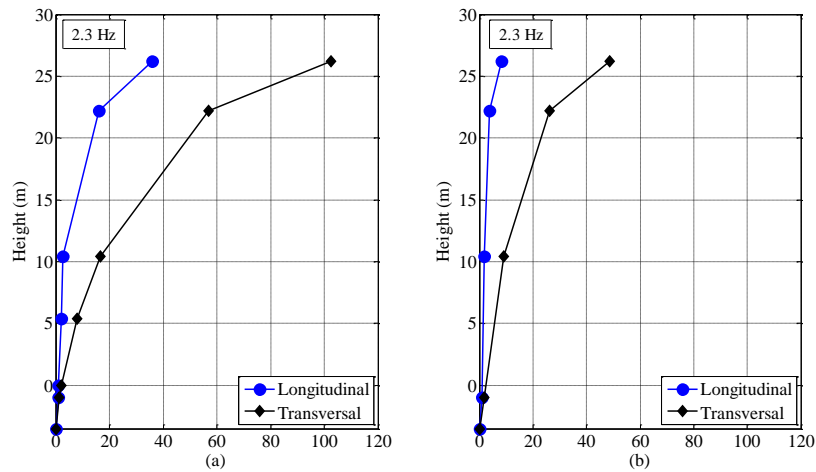
The spectral estimation of the time histories measured at the selected range bins (level C) was performed by means of the Welch's modified periodogram using 50 s of time length of the average window and 66% of overlapping window, obtaining 0.02 Hz spectral resolution. The power spectral densities were used to identify the natural resonances of the structures by the vibration data also for the interferometric survey as it was done for the seismometric measurements. In Figure 5.14 the PSD functions computed for the radar bins are reported where there is the reflected signal coming out from the towers A (configuration ST01) and B (configuration ST02). A Low-pass Butterworth filter has been applied in order to enhance the structural response of the towers. The PSD graph of the signals recorded from the position ST01 shows two resonant frequencies of the structure, corresponding to 2.3 Hz and 2.6 Hz. The measurements collected from position ST02 pointed out further resonance

frequencies at 2.9 Hz, 3.4 Hz and 3.6 Hz. No higher frequency components were detected. The structural frequencies with maximum amplitude which have been identified through the radar measurements, were mostly ones linked to the vibration modes with prevalent deformations along the longitudinal axis of the church because of the geometry of acquisition.

### 5.3.3 Experimental modal shapes

The normalised amplitudes related to each frequency peak have been compared for the measurements performed, by the two seismometric surveys, along the vertical directions corresponding to each tower of the church. The experimental mode shapes have been obtained for the fundamental mode (2.3 Hz, Figure 5.15) and for the second natural mode (2.6 Hz, Figure 5.15) that probably are both characterised by simple flexural shapes.

#### Mode I



#### Mode II

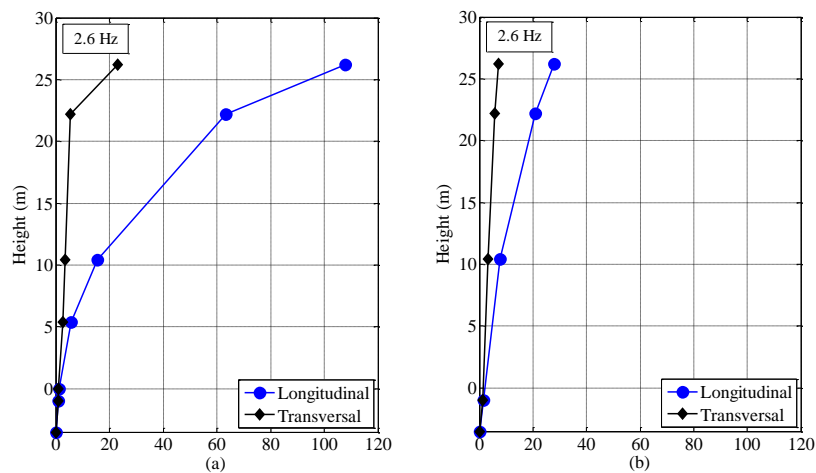


Figure 5.15: First and second flexural mode shapes (normalised respect to the reference levels) in the longitudinal and transversal directions: (a) tower A; (b) tower B.

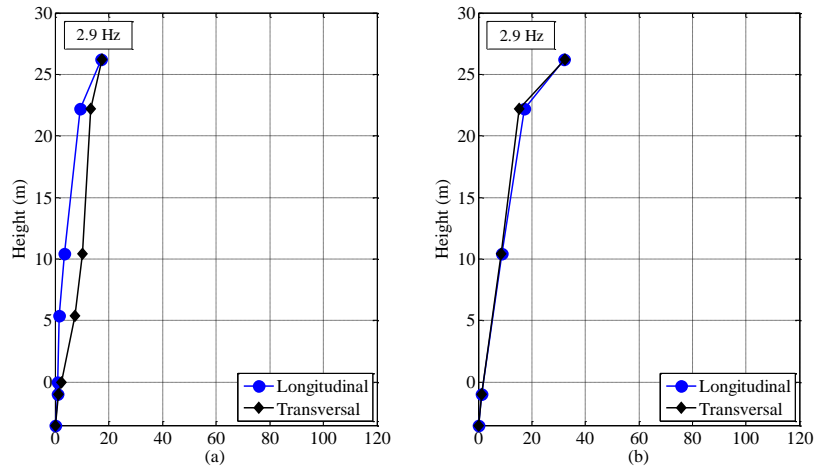


Figure 5.16: Normalised amplitude vs height for the vibration mode at 2.9 Hz: (a) tower A; (b) tower B.

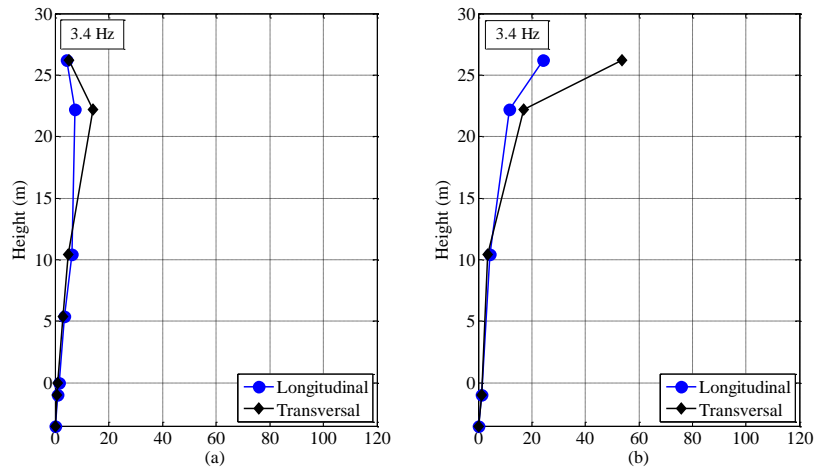


Figure 5.17: Normalised amplitude vs height for the mode at 3.4 Hz: (a) tower A; (b) tower B.

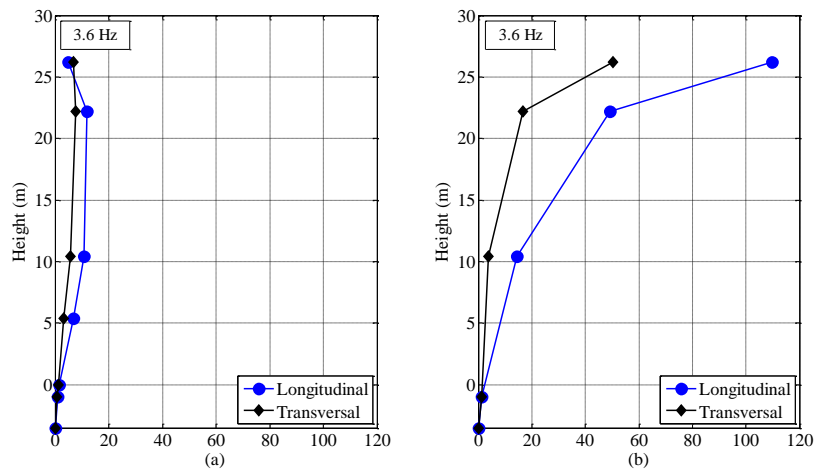


Figure 5.18: Normalised amplitude vs height for the mode at 3.6 Hz: (a) tower A; (b) tower B

Conversely, the other plots (Figures 5.16-5.18) could be considered as mode shapes only knowing the phase relationships between the signals acquired at several heights. However, these plots are also suitable to highlight what frequency components are related to greater amplification effects from the base to the top of the structures. Both longitudinal and transversal amplitudes were plotted for each frequency. As we can see the first vibration mode is mainly characterised by transversal displacements. This characteristic is more evident for the tower A where the maximum amplification effect is about 200 % greater than that observed in the longitudinal component. Conversely, the second natural mode of the structure includes prevalent longitudinal deformations with higher amplifications detected on the tower A. The next spectral peak shows significant amplitude values in the measurements performed along both axes of the towers. In particular, this spectral component appears at about 2.9 Hz and has maximum amplification values equal to about 30 for the tower B. This component was also measured in the station [TR10] placed on the elliptic dome with comparable amplitude. This fact allows us to consider that the frequency at 2.9 Hz could be related to a natural mode of vibration that significantly involved the whole structure of the church rather than to be linked to the response of only the towers. Finally, as previous discussed for the standard spectral ratios, both vibration modes at 3.4 Hz and 3.6 Hz mainly affected the dynamic behaviour of the tower B where they showed significantly higher amplitude values than in tower A. In this case it is clearly highlighted the differential behaviour of the two towers because these frequencies are only weakly transmitted and amplified to the top level of the stonemasonry structure. Furthermore, the maximum amplifications on the tower B were related to the longitudinal component of the mode at 3.6 Hz. Instead the tower A showed only small amplification effects in both directions of measurement for these natural modes.

## **5.4 FINITE ELEMENT ANALYSIS AND VALIDATION OF EXPERIMENTAL RESULTS**

The described experimental surveys allowed us to reconstruct the main features of the vibration modes of the structures. However in order to get a theoretical description of the structural dynamic behaviour aimed also to confirm the experimental results, a numerical dynamic analysis was implemented.

### **5.4.1 Finite Element Model**

The numerical simulation has been carried out using 3D Finite Element Analysis solver of Simulation Mechanical software (Autodesk package). In order to do a simplified model of the structure, the geometric data were obtained by using available bibliographic information (Kirova et al., 1994) and in situ inspections and measurements of the walls width. The geometry of the structure was imported as external CAD file, composed by five subdomains (see Figure 5.19 and Table 5.2): the first one composed of the main body of the structure (the single anterior nave of the church and the side chapels); the second part including the transept and the choir; finally, other three subdomains were

generated to include the two bell towers and the central octagonal dome, respectively. In this way it was possible to assign different physical properties to each subdomain in order to simulate the different materials used for the construction of the various parts of the building. Fixed constraints, corresponding to zero displacement and rotation at the boundary nodes of the mesh, have been imposed at the base of the structure. In other words, this kind of simplified hypothesis about the boundary conditions assumed at the base of the structure, neglect any possible effect related to the interaction between the foundation soil and the structure. This approach has been followed also by other authors (Pieraccini et al., 2014) and although it doesn't take into account any interaction phenomena can be adopted for large structures when the influence of the vibrations transmitted by the foundation soil is considered small or negligible. Especially when the soil resonances are well separated from the frequencies of the structure, these assumptions can be considered reliable. This condition was verified by the specific case study where the main resonance of the soil was found at about 15 Hz in various ground 3D microtremor stations around the church. The contact with neighbouring buildings at the northern side of the church was modelled using 1D linear elastic springs at the boundaries of the model acting in X (longitudinal) direction (see Figure 5.19). Stiffness value (k) was established to be 2,000 N/mm in order to enhance the calibration procedures. However it has been possible to observe that the boundary conditions imposed at the northern side of the church have very low influence on the modal behaviour of the towers which are located in the opposite side of the structure.

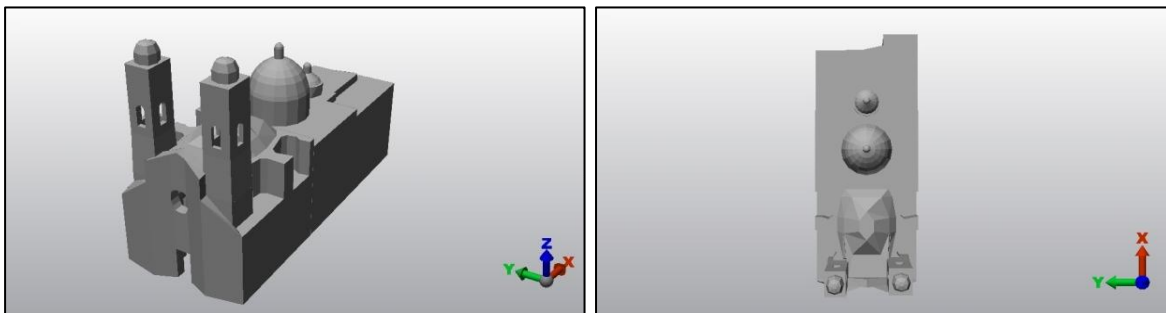


Figure 5.19: 3D Finite Element model of the church: perspective view (left) and top view (right).

Only the main features of the church were preserved in the model as the pillars, the perimetral stonemasonry walls and the domes. The mesh used for the final discrete model has 75,661 nodes corresponding to 150,141 solid brick elements. The mechanical properties assumed to start the numerical eigenfrequency analysis were elastic modulus, Poisson's ratio and density of the different materials.

However these values were fixed for each subdomain of the model assuming a homogeneous distribution inside each block (see Table 5.2). Young's modulus and density values equal to 2,100 N/mm<sup>2</sup> and 1,900 kg/m<sup>3</sup> have been assigned to the first and to the second subdomain, northern and



southern main parts of the church including masonry walls and roofs. Instead, the average values of elasticity modulus and density were taken equal to  $2,200 \text{ N/mm}^2$  and  $1,700 \text{ kg/m}^3$  for subdomain 3 of the model (tower A, masonry). In order to take into account the voids of the windows and the progressive reduction of thickness of the central octagonal main dome, the density value of the subdomain 4 has been imposed to be  $1,700 \text{ kg/m}^3$ . Finally, the parameters established for the subdomain 5 (tower B, reinforced concrete) have been chosen to be  $20,000 \text{ N/mm}^2$  and  $2,200 \text{ kg/m}^3$ . Furthermore, the Poisson's ratio was assumed equal to 0.2 for masonry and 0.25 for concrete blocks. However, several authors observe that the value assigned to the Poisson's ratio weakly affects the dynamic properties of a physical linear model (Ivorra et al., 2011; Pieraccini et al., 2014).

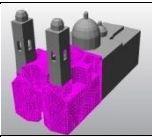
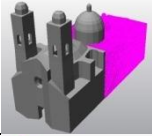
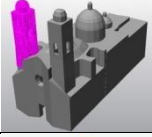
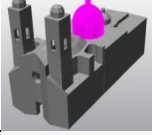
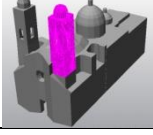
Subdomain No	Block identification	Young modulus ( $\text{N/mm}^2$ )	Density ( $\text{kg/m}^3$ )	Poisson ratio
Part 1		2,100	1,900	0.2
Part 2		2,100	1,900	0.2
Part 3		2,200	1,700	0.2
Part 4		2,000	1,700	0.2
Part 5		20,000	2,200	0.25

Table 5.2: Physical properties of the final model used for the numerical simulation.

It is noteworthy to stress that the dynamic model was built with large uncertainties affecting the physical parameters assigned to each material due to poorly-depth knowledge of them (especially in terms of their spatial distribution). Thus the numerical analysis here conducted was devoted to match the first experimental modal frequencies of the two bell towers. In other words the model parameters were modified following an iterative approach in order to obtain a good agreement with the experimentally observed natural frequencies. In particular, Young's modulus has been identified as the parameter that mainly affects the response of the linear model due to its wide range of variability, if compared to the values that can be assumed by the density and by the Poisson coefficient.

For this reason, several non-destructive sonic tests were performed in order to reduce the range of variation of the elasticity modulus assigned to each material composing the perimetric walls of the

bell towers. P-wave propagation velocity has been measured in direct transmission set-up in five points of each tower (above the roof level, at about 24 metres height). The source signal was generated using a simple hammer. Sampling frequency equal to  $20.833 \mu\text{s}$  and time duration have been chosen in order to effectively record the waveforms at the receiver and also to improve the first arrivals identification (see Figure 5.20). Considering the distance between both shot and receiver points and the travel time of the signal along the path inside the medium, it was possible to derive P-wave velocities for the tested sections of the walls. Results highlight that stonemasonry walls were characterised by P-wave velocity ranging from 980 m/s to 1,100 m/s. Conversely, sonic pulse velocity values estimated for the concrete elements result comprised between 2,600 m/s and 3,000 m/s. Therefore, on the basis of this additional information, the model has been constrained in order to reduce the residual differences between vibration data and finite element analysis. Obviously, the corresponding elasticity modulus has been calculated by using the most acceptable values of density and Poisson ratio, as previously described.

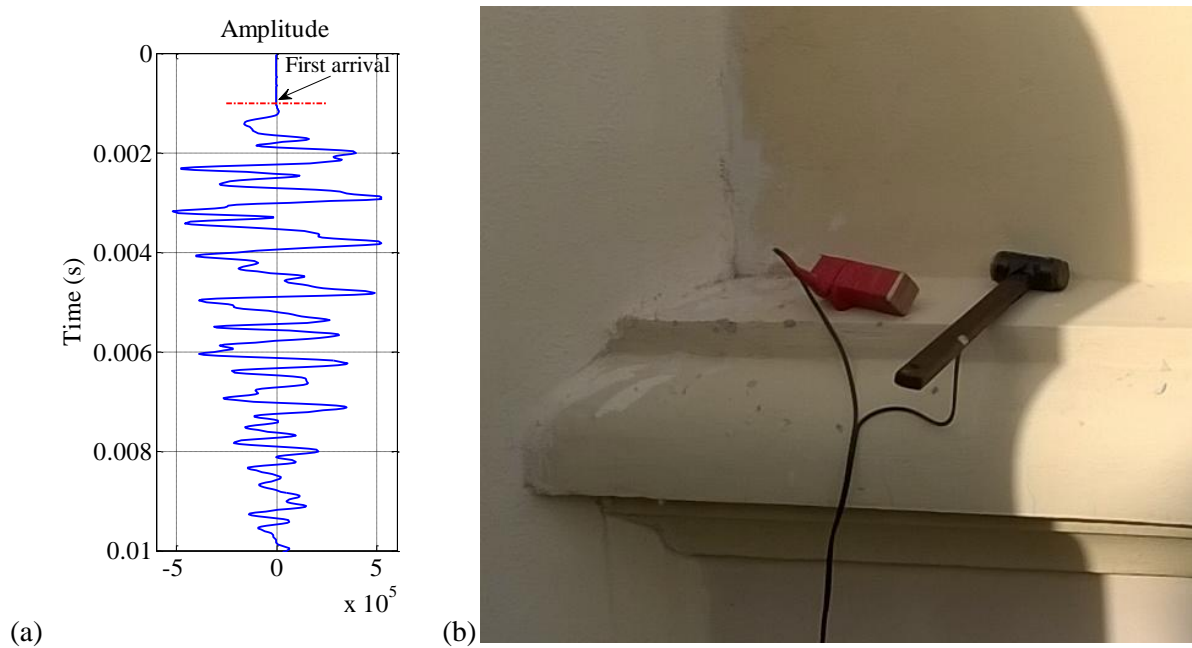


Figure 5.20: Sonic tests: (a) first arrival identification; (b) equipment used as source of elastic waves.

However, the bell towers of Sant'Anna church represent a really particular and difficult case for dynamic studies due to the boundary conditions imposed at the sides of the structures where both towers are connected and partially included into the adjacent church walls. This fact could explain higher frequencies of vibration than those measured in other structures with similar height. Analogous considerations have been done by other authors for bell towers connected to the church body (Foti et al., 2012) and for high modern buildings connected to other low-rise structures (Castellaro et al., 2013). By means of the Finite Element approach a linear dynamic analysis was developed for the structure by resolving a generalised eigenvalue problem.

### 5.4.2 Calibration and validation

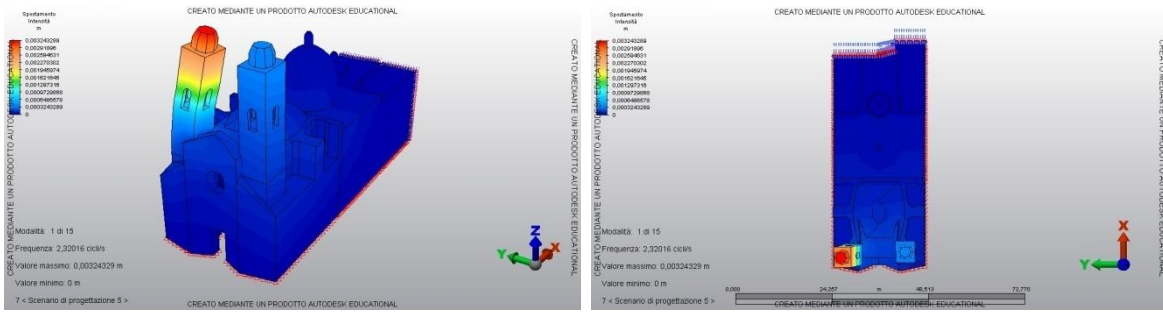
Figure 5.21 shows the four modal shapes of the structure model showing the displacements of the towers. The first mode is a bending mode which is mainly associated to transversal deformations of the church indicated as Y-direction in the relative plot. The second mode involves the translation motion along the X-direction (longitudinal mode) with a small component also in Y-direction. The natural frequencies obtained by means of the numerical analysis have been stored in Table 5.3 where it is possible to observe that the analytical results are close to the experimental eigenfrequencies. Also in the Finite Element Model, the modes at 3.25 Hz and at 3.65 Hz significantly affect the vibration of the tower B due to its different mechanical properties; these values correspond to two bending modes with maximum displacements achieved in transversal direction for the lower frequency and in longitudinal direction for the higher mode, respectively.

Frequency $f$ (Hz) Experimental tests	Frequency $f$ (Hz) Numerical model
2.3	2.32
2.6	2.58
2.9	-
3.4	3.25
3.6	3.65

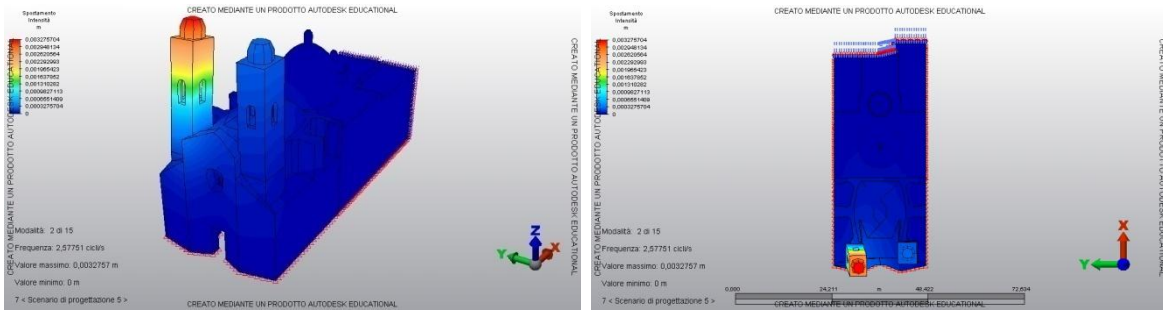
Table 5.3: Experimental and numerical frequencies.

The experimental mode at 2.9 Hz was not shown by the Finite Element analysis, mainly due to lacks of information related to the structural features and the wide uncertainties affecting the materials used to build the church and to restore the structure after the war. Similar difficulties to match the theoretical results with the experimental data have been discussed in other studies where the influence of the foundations design has been also evaluated to improve the results of the mechanical simulations (Castellaro et al., 2013). However this result highlights the advantages provided by in situ measurements in order to study the vibration mode of the structures. In order to evaluate how the physical properties of the materials can affect the experimentally observed difference on the dynamic behaviour of the towers, even a Finite Element Model characterised by the same subdomain properties for both towers was built. In this configuration the dynamic free undamped vibration analysis was performed again. First natural frequency of the model resulted to be 2.26 Hz and corresponded to a transversal bending modal shape showing maximum displacements on the tower A. The second mode at the frequency of 2.44 Hz was a bending mode with main deformations along the longitudinal direction, especially present on the tower B. Moreover the higher frequencies, corresponding to 2.50 Hz and 2.61 Hz, were linked to a transversal mode and a longitudinal mode, respectively. In this case, the model showed maximum displacement on the tower B at 2.50 Hz and on the tower A at 2.61 Hz.

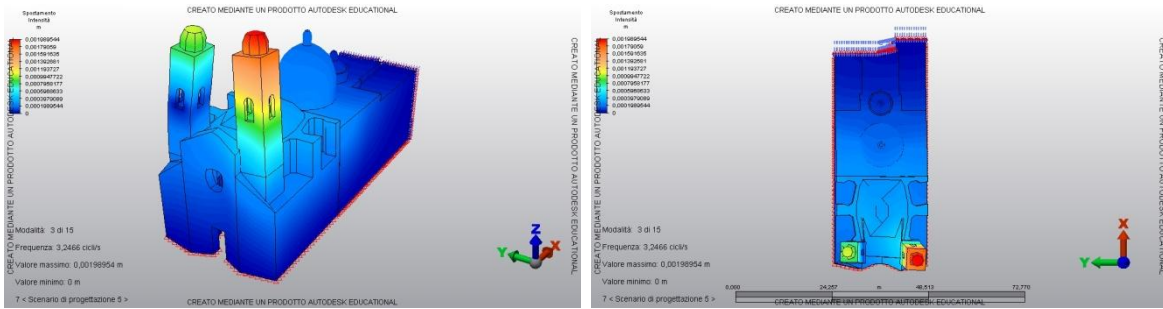
### Mode I $f=2.32$ Hz



### Mode II $f=2.58$ Hz



### Mode III $f=3.25$ Hz



### Mode IV $f=3.65$ Hz

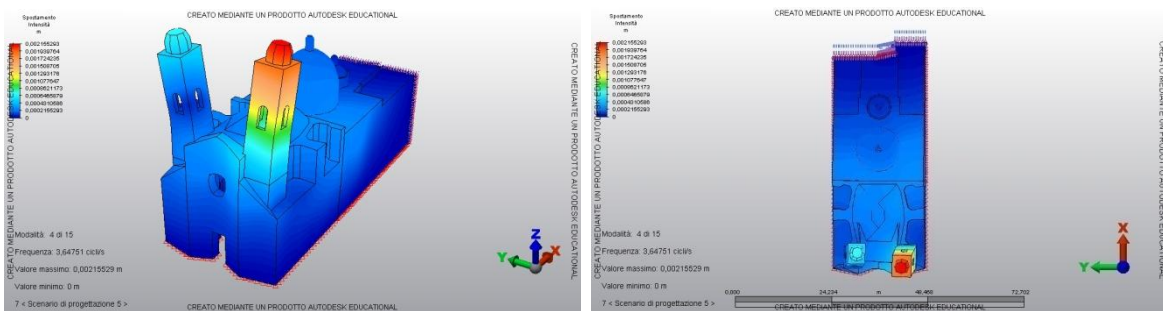


Figure 5.21: First four modal shapes of the model: perspective view (left); horizontal plane view (right).

The numerical results highlighted that the small difference of the dynamic responses between the two towers, as it was calculated assuming the same material properties could be related to the smallest width of the walls measured in the higher level of the tower B (about 85 cm for the tower B vs 120 cm

for the tower A, measured at the level of the external clocks, and 60 cm for the tower B vs 90 cm for the tower A, measured at the open level of the bells).

## 5.5 CONCLUSIONS

This chapter has presented the results of a study composed of ambient vibration tests and Finite Element Modelling, both aimed to estimate the main vibration parameters of two twin bell towers characterised by different mechanical properties. The experiments were performed by means of two kinds of contact velocity sensors: first a three-channels high sensitive instrument and, as second, two horizontal synchronous seismometers. Non-destructive tests were also carried out using a coherent radar system to acquire the displacement time series related to the upper parts of the towers which were not easily accessible to install any contact device. The microtremor time histories were acquired along both longitudinal and transversal axis of the church on different levels. Seven coupled sensors configurations were done to collect the phase relationship between the displacements of different points of the structures. Vibration data were processed in frequency domain using Standard Spectral Ratios, Power Spectral Density functions and coherence spectra to identify the dynamic features of both towers such as resonance frequencies, damping ratios and natural modal shapes.

The experimental frequency response was different for the two towers. We can summarise that the first and the second vibration mode of the whole church included two flexural deformed shapes with prevalent displacements, oriented in transversal and in longitudinal direction respectively, above the Tower A. Conversely, these modes showed only limited effects on the Tower B. Furthermore, it can be observed that the spectral components at 3.4 and 3.6 Hz were mainly amplified on the tower B. The component at 2.9 Hz was probably related to a mode shape involving the entire structure of the church. This component didn't show high amplification values on the two towers although it was measured even on them.

Finally the experimental dynamic response of the structures was compared to the numerical modal parameters obtained for a discrete model. The comparison highlighted a substantial agreement between experimental data and numerical results although some deviations, probably related to not well defined physical properties assigned to each subdomain of the structure model, were found. However, these uncertainties were partially reduced calibrating the physical properties in order to match the first vibration modes of the model with the observed behaviours and by means of sonic velocity measurements carried out above the bell towers.

Thus, the experimental results obtained by means of the ambient vibration tests represent a further confirmation of the advantages provided by these methods for non-destructive evaluation of cultural heritage structures. The integrated use of a triaxial single acquisition station, a dual spatially configurable horizontal station and a non contact instrument proved to be particularly effective to

define vibration properties of the two geometrically similar structures which were only partially accessible. Contact measurements proved to be more effective to define structural dynamic behaviour for elements at short heights which had lower amplitude vibrations while the radar approach was uniquely working for the parts at the top of the structures, not provided by stairs and with higher amplitude vibrations. Remote sensing technique was effective only for front side acquisition positions while for lateral ones the projected displacement on the Line Of Sight was too low and under the background noise level.

Furthermore experimental approach revealed also operational conditions not easy to be simulated and modelled mainly due to complexity and variability of constraints and structures features.

## **REFERENCES**

Bayraktar A., Türker T., Sevim B., Can Altunisik A., Yildirim F. (2012). Modal parameter identification of Hagia Sophia Bell-Tower via Ambient Vibration Test, *Journal of Nondestructive Evaluation*, 28, 37–47. doi:10.1007/s10921-009-0045-9

Bendat J.S., Piersol A.G. (1993). *Engineering applications of correlation and spectral analysis*. Wiley, New York; 1993.

Benedettini F., Gentile G. (2007). Ambient vibration testing and operational modal analysis of a masonry tower. *Proceedings of the 2<sup>nd</sup> International Conference on Operational Modal Analysis (IOMAC)*, Copenhagen, 451–460. doi:10.1016/j.engstruct.2008.06.001

Bongiovanni G., Buffarini G., Clemente P. (1998). Dynamic characterisation of two earthquake damaged bell towers. *Proceedings of the 11<sup>th</sup> ECEE European Conference on Earthquake Engineering (Paris, September)*, Balkema, Rotterdam.

Bongiovanni G., Clemente P., Buffarini G. (2000). Analysis of the seismic response of a damaged masonry bell tower. *Proceedings of the 12<sup>th</sup> WCEE World Conference on Earthquake Engineering; 2000; ID 2189*. <http://www.nicee.org/wcee/index2.php>

Borcherdt R.D. (1970). Effects of local geology on ground motion near San Francisco Bay, *Bulletin of the Seismological Society of America*, 60, 29-61. <http://www.bssaonline.org/content/60/1/29>

Buffarini G., Clemente P., Rinaldis D. (2009). Experimental dynamic analysis of cultural heritage buildings. *Proceedings of the 3<sup>rd</sup> IOMAC'09 International Operational Modal Analysis Conference* 459-466.

Bui Q.B., Hans S., Boutin C. (2014). Dynamic behaviour of an asymmetric building: Experimental and numerical studies, *Case Studies in Nondestructive Testing and Evaluation*, 2, 38–48. doi:10.1016/j.csndt.2014.07.001

Calcina S.V., Eltrudis L., Piroddi L., Ranieri G. (2014). Ambient Vibration Tests of an arch dam with different reservoir water levels: experimental results and comparison with Finite Element Modelling, *The Scientific World Journal*, vol. 2014, article ID 692709. doi:10.1155/2014/692709

<http://dx.doi.org/10.1155/2014/692709>

Cappellini A., Cigada A., Vanali M., Leva D., Rivolta C. (2014). Advantages and drawbacks in the use of non-contact radar techniques to perform dynamic measurements. *Journal of Civil Structural Health Monitoring*, 4, 4, 303-311. doi:10.1007/s13349-014-0080-9

Castellaro S., Mulargia F. (2010). How far from a building does the ground motion free field start? The cases of three famous towers and of a modern building, *Bull. Seism. Soc. Am.*, 100, 2080–2094. doi:10.1785/0120090188

Castellaro S., Padrón L.A., Mulargia F. (2013). The different response of apparently identical structures: a far-field lesson from the Mirandola 20th May 2012 earthquake, *Bulletin of Earthquake Engineering*, 12, 5, 2481-2493. doi:10.1007/s10518-013-9505-9

Cunha A., Caetano E. (2006). Experimental modal analysis of civil engineering structures, *Sound and Vibration*, 6, 40, 12-20.

Foti D., Ivorra Chorro S., Sabbà M.F. (2012). Dynamic investigation of an ancient masonry bell tower with Operational Modal Analysis. A non-destructive experimental technique to obtain the dynamic characteristics of a structure, *The open construction and building technology journal*, 6, 384-391. doi:10.2174/1874836801206010384

Gallipoli M.R., Mucciarelli M., Castro R.R., Monachesi G., Contri P. (2004). Structure, soil–structure response and effects of damage based on observations of horizontal-to-vertical spectral ratios of microtremors, *Soil Dynamics and Earthquake Engineering*, 24, 487–495. doi:10.1016/j.soildyn.2003.11.009

Gentile C., Saisi A. (2007). Ambient vibration testing of historic masonry towers for structural identification and damage assessment, *Construction and Building Materials*, 21, 6, 1311–1321. doi:10.1016/j.conbuildmat.2006.01.007

Ivanovic S.S., Trifunac M.D., Todorovska M.I. (2000). Ambient vibration tests of structures – A review, *Journal of Earthquake Technology*, 37, 4, 165-197.

Ivorra S., Pallarés F., Adam J.M. (2009). Dynamic behaviour of a modern bell tower - A case study. *Engineering Structures*, 31, 1085-1092. doi:10.1016/j.engstruct.2009.01.002

Ivorra S., Pallarés F., Adam J.M. (2011). Masonry bell towers: dynamic considerations. *Proceedings of the Institution of Civil Engineers Structures and Buildings*, 164, February 2011, Issue SB1, pages 3–12. doi:10.1680/stbu.9.00030

Julio E.N.B.S., Rebelo C.A.S., Dias-da-Costa D.A.S.G. (2008). Structural assessment of the tower of the University of Coimbra by modal identification, *Engineering Structures*, 30, 12, 3468–3477.

Kirova T.K., Masala F., Pintus M., Huen R.E. (1994). *Cagliari. Quartieri Storici: Stampace*, Silvana Editoriale, Cinisello Balsamo, Milano, Italy; 1994. ISBN:88-366-0393-9

Lagomarsino S. (1993). Forecast models for damping and vibration periods of buildings, *Journal of Wind Engineering and Industrial Aerodynamics*, 48, 221–239. doi:10.1016/0167-6105(93)90138-E

- Mucciarelli M., Gallipoli M.R. (2007). Non-parametric analysis of a single seismometric recording to obtain building dynamic parameters, *Annals of Geophysics*, 50, 2, 259-266. doi:10.4401/ag-3079
- Nakamura Y. (1989). A method for dynamic characteristics estimation of subsurface using microtremor on the ground surface, *QR Railway Tech. Res. Inst.*, 30, 1.
- Pieraccini M., Dei D., Betti M., Bartoli G., Tucci G., Guardini N. (2014). Dynamic identification of historic masonry towers through an expeditious and no-contact approach: Application to the “Torre del Mangia” in Siena (Italy), *Journal of Cultural Heritage*, 15, 275-282. doi:10.1016/j.culher.2013.07.006
- Pieraccini M. (2013). Monitoring of civil infrastructures by interferometric radar: a review, *The Scientific World Journal*, vol. 2013, article ID 786961. doi:10.1155/2013/786961  
<http://dx.doi.org/10.1155/2013/786961>
- Rainieri C., Fabbrocino G. (2012). Estimating the elastic period of masonry towers. Proceedings of the 30<sup>th</sup> International Modal Analysis Conference (IMAC-XXX), Society for Experimental Mechanics, Jacksonville, Fla, USA, 2012.
- Ramos L.F., Marques L., Lourenço P.B., DeRoeck G., Campos-Costa A., Roque J. (2010). Monitoring historical masonry structures with operational modal analysis: Two case studies, *Mechanical Systems and Signal Processing*, 24, 1291–1305. doi:10.1016/j.ymssp.2010.01.011
- Stabile T.A., Perrone A., Gallipoli M.R., Ditommaso R., Ponzo F.C. (2013). Dynamic survey of the Musmeci bridge by joint application of ground-based microwave radar interferometry and ambient noise standard spectral ratio techniques, *IEEE Geoscience and Remote Sensing Letters*, 10, 4, 870-874. <http://dx.doi.org/10.1109/LGRS.2012.2226428>
- Schmidt T. (2007). Dynamic behaviour of twin bell towers. Proceedings of 2<sup>nd</sup> International Conference on Operational Modal Analysis (IOMAC), Copenhagen, 261–268.
- Wilson J.M., Selby A.R. (1993). Durham cathedral tower vibrations during bell-ringing. In *Engineering a Cathedral* (Jackson MJ ed.). Thomas Telford, London; 1993.



## ***CHAPTER 6***



## AMBIENT VIBRATION TESTS OF AN ARCH DAM WITH DIFFERENT RESERVOIR WATER LEVELS: EXPERIMENTAL RESULTS AND COMPARISON WITH FINITE ELEMENT MODELLING

---

### **Abstract**

*This chapter deals with the ambient vibration tests performed in an arch dam in two different working conditions in order to assess the effect produced by two different reservoir water levels on the structural vibration properties. The study consists of an experimental part and a numerical part. The experimental tests were carried out in two different periods of the year, at the beginning of autumn (October 2012) and at the end of winter (March 2013), respectively. The measurements were performed using a fast technique based on asynchronous records of microtremor time-series. In-contact single-station measurements were done by means of one single high resolution triaxial accelerometer and two low-frequency seismometers, placed in different points of the structure. The Standard Spectral Ratio method has been used to evaluate the natural frequencies of vibration of the structure. A 3D finite element model of the arch dam-reservoir-foundation system has been developed to verify analytically determined vibration properties, such as natural frequencies and mode shapes, and their changes linked to water level with the experimental results.*

## 6.1 INTRODUCTION

The knowledge of the structural response of buildings following the application of dynamic actions represents a key element to evaluate the buildings performance, especially in the case of extreme environmental conditions, mainly represented by earthquakes actions, or in the case of structures located near to the areas affected by mining activities (quarry explosions and other excavation activities) or underground constructions (e.g., tunnels and subways). In general, it is possible to observe that the dynamic behaviour of the structures is mainly influenced by the design features and by the geometry of the buildings and the interaction effects with the foundation soil and with other existing structures. Several authors show that the experimental dynamic response contributes to the assessment of structural or geotechnical damage identification and they use experimental vibration properties of the buildings for Structural Health Monitoring procedures implementation. Numerous papers are focused on the study of the behaviour of buildings in terms of seismic response of structures. These studies deal with the complex interaction phenomena between the foundation soil and the earthquake input (to assess the seismic performance of the buildings) and the seismic wave propagation (transmission and reflection) at the boundaries of the foundation level by means of both inertial and kinematic interaction (Kramer, 1996). Experimental dynamic behaviour plays an extremely important role for structures of public interest such as school buildings, hospitals, roads, and railway infrastructures (such as bridges and viaducts); structures of economic importance to land and water resources management; and for the electricity production as dams and artificial reservoirs. Furthermore, dynamic analysis methods of structures are required to assess the safety of existing structures and to evaluate proposed designs for the construction of new dams that are located in areas with significant seismicity. These studies are also performed to determine when structural modifications proposed are suitable and effective solutions to improve the seismic performance of old structures. The prediction of the actual vibration response of arch dams to dynamic loadings is a very complicated issue and depends on several factors including intensity and characteristics of the design input, the interaction of the dam with the foundation rock and reservoir water; the computational modelling technique used to simulate the behaviour of the structure; and the material properties used for the analysis. Main recommendations to perform correct dynamic analysis procedures are provided by Ghanaat (1993). In particular, the study of the dams dynamic properties involves the assessment of the interaction with rock foundation along the section and the water reservoir mass influence acting on the upstream side. The interaction problem between the dam body and the water impounded reservoir is an important factor affecting the dynamic response of arch dams when the ground shakes during an earthquake. Therefore this problem has been discussed by several authors. The first formulation has been proposed by Westergaard (1933). He simulated the effect of the water by means of the added mass concept, as a mass attached to the dam. A more appropriate representation of this concept is obtained using a finite element formulation able to describe the interaction and also for complicated

geometry of the arch dam and the water reservoir (Kuo, 1982). However, both methods ignore the water compressibility and the energy losses caused by the radiation in the upstream direction and the reflections and refractions at the reservoir bottom of the pressure waves. These phenomena have been included in a more refined formulation (Fok and Chopra, 1986). These approaches require high computation efforts to determine frequency-dependent hydrodynamic pressure terms and to consider a range of reservoir-bottom reflection coefficients. Aminfar et al. (2011) have developed the added-mass concept, first proposed by Westergaard (1933). These authors have observed that the interaction effects between an arch dam and the contained water-reservoir lead to an increase in the dam vibration periods, because the water moves with the dam increasing the total mass that is in motion. Furthermore the added water mass can determine the partial absorption of pressure waves at the reservoir boundaries and this fact may be the fundamental cause of an increase in structural damping properties. In other works the proposed model highlights the earthquake response change of the dam and this behaviour as depending on the mass of the impounded water inside the reservoir. Sevim et al. (2010) have investigated the water level effects on the dynamic response of the dams by means of ambient vibration testing on a prototype arch dam reservoir-foundation model performed in a laboratory. These authors observe that the difference between the first natural frequencies measured with an empty reservoir and with a full reservoir ranges from 20% to 25%. Analytical models have often been developed in order to get the dynamic characteristics of the dams or to assess the correlation between experimental dynamic response (obtained by means of measurements of displacements, velocities, or accelerations acquired on the structure body) and numerical simulations (Mivehchi et al., 2003; Sevim et al., 2011). Generally an elastic or failure physical model may be used, depending on the purposes of the research. The identification of natural frequencies and the estimation of modal shapes and structural damping can be achieved by means of numerical simulations based on an elastic physical model. Conversely, in order to study the structures behaviour to strong actions (e.g., seismic actions), we must use more complex failure physical models able to reproduce the possible opening of joints and cracking of the concrete dams (Roşca, 2008). Other authors have used continuous ambient vibrations recordings to monitor the effects of the varying water level throughout the testing period (Darbre and Proulx, 2002). This part of the work aims to assess the influence of different water level heights on dynamic properties on a double curvature arch dam real structure by means of in situ experimental ambient vibration tests carried out with one single-station high sensitive triaxial tromometer and with two short-period seismological seismometers. The stored traces have been compared and processed in order to perform spectral, short-time, and directional Fourier analyses. The microtremor time-series are analysed using Standard Spectral Ratio method (Borcherdt, 1970) to enhance the spectral components related to the dynamic response of the dam. In this work spectral ratios are calculated, respectively, for radial, tangential, and vertical components of the motion. In order to attempt an explanation for the different behaviour achieved by the experimental surveys in both conditions, a dynamic numerical analysis of the dam

was done using a 3D finite element model of the system composed by structure-foundation rock-reservoir, obtained imposing different reservoir water levels.

## 6.2 THE SITE OF STUDY

The structure of Punta Gennarta Dam is a Reinforced Concrete variable radius arch dam located on the Canonica river in South-West Sardinia, Italy (as shown in Figure 6.1), at the northern side of Iglesias town. The actual structure was built over four years (1959–1962) using about 58,600 m<sup>3</sup> concrete for its body. It retains about  $12.70 \cdot 10^6$  m<sup>3</sup> reservoir water (named Corsi Lake). The structure is characterized by variable radius and angles that provide an asymmetrical geometry along crown cantilever. It is 57 metres in height (above foundation) and has 254 metres crest length. Its crest length to height ratio is 4.46. The thickness of the crown cantilever ranges between 2.30 metres at the crest and 9.90 metres at the base. It is provided with two galleries inside its body. The first one is located in the upper part and is used to keeping the measurement equipment such as strainmeters, jointmeters, extensometers, and other monitoring tools. The second tunnel is placed in the lower part of the structure and it is accessible through a narrow central opening. Some pictures of Punta Gennarta Arch Dam are shown in Figure 6.2. Other geometric features are summarized in Table 6.1. The site of the structure is classified in Class IV of the Italian seismic zonation, corresponding at very low seismic hazard areas. The dam is built on a weak, narrow valley characterized by geological metamorphic formations mainly consisting of metasandstones (lower Cambrian). The characteristics of easy accessibility of the site and the possibility of installing sensors into small niches opening on the downstream side of the dam are suitable for the experimental surveys and to obtain vibration data distributed all along the structure body.

Description	metres s.l.m.
Max height of reservoir water level	255.30
Shallow spillway altitude	249.00
Bottom spillway altitude	204.50
Lower walkway altitude	224.00
Upper walkway altitude	242.00
Crest altitude	257.50

Table 6.1: Geometric features of Punta Gennarta Arch Dam



Figure 6.1: Location of Punta Gennarta Dam and satellite image of the water reservoir Corsi Lake.



Figure 6.2: Some pictures of Punta Gennarta Arch Dam.

## 6.3 EXPERIMENTAL VIBRATION TESTS AND RESULTS

### 6.3.1 Description of Data Acquisition and Processing

The experimental dynamic characterisation of Punta Gennarta Dam was conducted only with passive survey mode through ambient vibration measurements, in agreement with the widespread NIMA techniques (Noise Input Modal Analyses). Ambient vibration tests represent an effective, fast, and relatively economical method of estimating fundamental dynamic features of the structures. In the last years several authors have proposed different methods that aimed to improve passive dynamic characterization techniques of structures using records of natural microtremor (Snieder and Safak, 2006; Gallipoli et al., 2009; Castellaro et al., 2013; Ditommaso et al., 2013; Vidal et al., 2013). The different number of sensors used to configure the experimental layout (from a single triaxial sensor to a multiple sensors network) affects the information degree that we can obtain by the surveys

(Ditommaso et al., 2010). During this experiment one digital high resolution tromograph Tromino has been used for ambient vibration record. This tridirectional sensor was oriented with one horizontal axis in the same direction of the dam local curvature radius. In other words, for each acquisition station, the displacement field was acquired along three components, respectively, radial, tangential, and vertical component. The acquisition setup is composed by fourteen asynchronous ambient vibration recording stations placed on the dambody. The distribution of the measurement points on the structure is shown in Figure 6.3 for seven stations placed on the crest level and in Figure 6.4 for all stations (frontal view of the downstream side of the structure). The measurements were performed in a relatively short time (about two hours) in order to ensure the condition of maximum stationarity of the noise seismic field. Ten-minute time-series were sampled with 0.002 seconds sample interval.

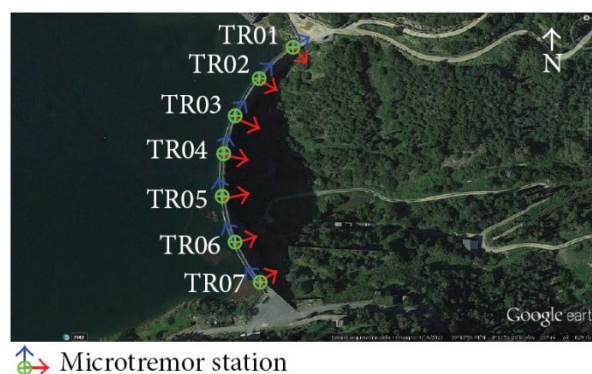


Figure 6.3: In-contact sensor stations placed on the dam crest.

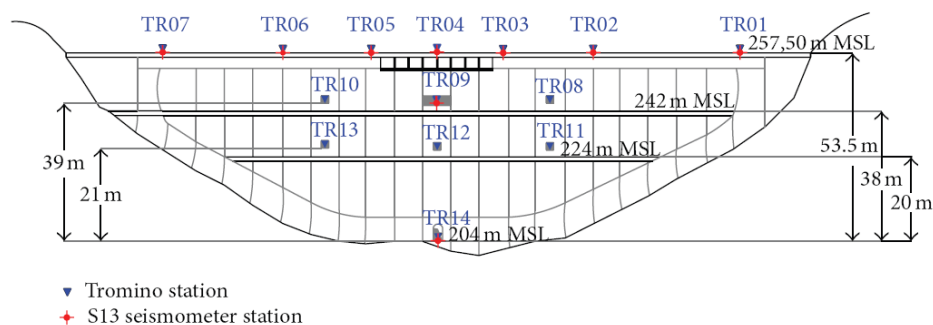


Figure 6.4: In-contact microtremor stations placed at different floors of Punta Gennarta Arch Dam, downstream side view (blue triangles indicate Tromino stations; red circles mark S13 stations).

Only at the topmost of the dam longer microtremor time-series (30 minutes) were acquired to enhance structural damping estimation procedures. Ambient vibration tests were repeated using the same acquisition geometry with two dam operational conditions characterized by different water reservoir levels. In both cases, the modal parameters obtained were natural frequencies, mode shapes, and damping ratios. The first measurement campaign was carried out in October 2012 with about 27-metre (231m s.l.m) water level height. The next measurements were collected in March 2013 with 43-



metre (247m s.l.m) water level height. In order to compare the achieved experimental results, the acquisitions were done with similar weather conditions. Before performing the spectral analysis the signals were equalized, padded, de-trended, and tapered with Bartlett window to reducing leakage effects. Natural frequencies of vibration were extracted by means of the Horizontal to Horizontal Spectral Ratio method (HHSR). Empirical dynamic response in radial, tangential, and vertical, respectively, direction assumes the following expression:

$$SSR_{rad}(\omega) = \frac{|H_i(\omega)|}{|H_{ref}(\omega)|} \quad (6.1)$$

where  $|H_i(\omega)|$  indicates the microtremor amplitude spectrum of the  $i^{\text{th}}$  measurement station and  $|H_{ref}(\omega)|$  the amplitude spectrum of the [TR14] station, placed inside the lower tunnel and used as reference site. Its amplitude spectrum represents the inverse filter able to highlight the experimental dynamic characteristics of the dam. Infact looking at the spectral ratios in time domain, starting from the stationary linear systems theory, for each component of motion, the output signal on the top floor of the structure is in this way deconvolved with the input signal acquired at the ground floor of the structure, leading to the estimation of its empirical transfer function. This technique, developed in seismological context (Borcherdt, 1970), has been effectively applied to perform experimental dynamic analyses of civil structures such as residential buildings and towers using microtremor time-series and appears to be a reliable method for assessing natural frequencies (Gallipoli et al., 2009; Castellaro et al., 2013; insert other ref). Due to the higher sensitivity of the velocity transducers, velocity traces were used for SSR analysis. To estimate the damping ratio at the fundamental frequency of the structure a simplified non parametric method proposed by Mucciarelli and Gallipoli (2007) was applied. This technique is based on the general assumption that the first approximation of the dynamic behaviour of the engineering structures is provided by the Single-Degree-Of-Freedom oscillator model. This approach allows us to assess with good approximation the damping ratio associated with the first mode shape by means of only a ten minute recording of ambient vibration acquired at the topmost part of a building. To compare the experimental results obtained using Tromino with the results achieved by other measurement tools, we have also used two high resolution short-period seismometers (Teledyne Geotech Model S13). These moving coil electromagnetic velocity-transducers are mainly designed for geophysics research and are capable of meeting the noise and stability requirements of the most exacting studies. Their operation condition is convertible in both vertical and horizontal mode and, depending on the purposes of the survey, their natural frequency can be adjusted between 0.75 Hz and 1.1 Hz. To perform this study, one sensor has been configured to acquire the horizontal component of motion (along the radial direction of the dam), whereas another geophone has been used in vertical operation mode. Both horizontal and vertical signals were recorded by one Single Geode seismograph unit (Geometrics). For each station we have acquired twenty time-histories of 32 s (maximum time acquisition length with 2 ms sample interval).

The seg2 files are next merged and converted in ASCII format to be analysed in the Matlab environment. The relatively bulky size of the S13 sensors doesn't allow the placement of the instrumental tool at some station points. In particular for three stations located at the lower walkway level and for those to the left and right of the upper walkway. All S13 microtremor stations are marked with red circles in Figure 6.4.

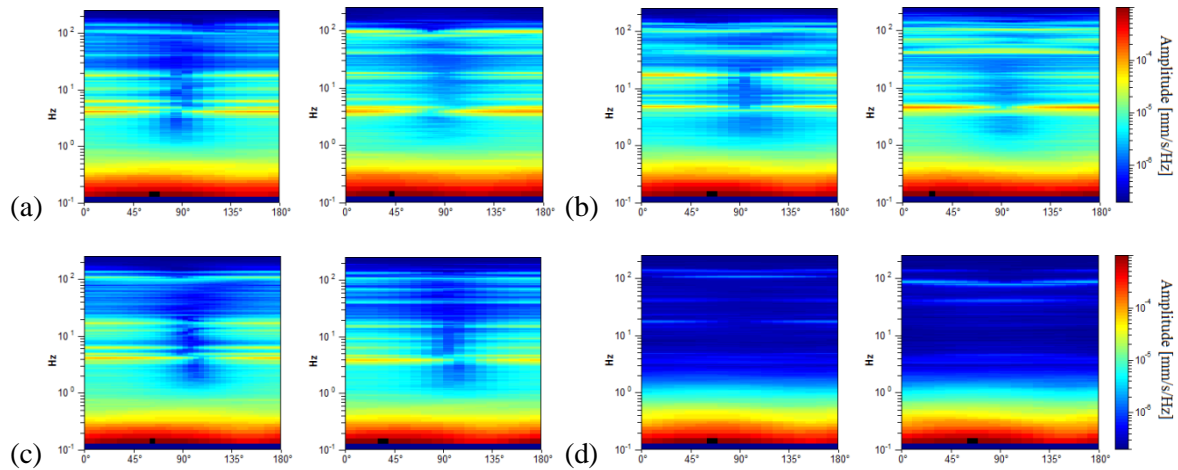


Figure 6.5: Directional spectra derived for the TR03 (a), TR04 (b), TR05 (c) and TR14 (d) microtremor horizontal traces acquired during both passive surveys.

### 6.3.2 Tests results and discussion

Natural frequencies are highlighted by amplitude peaks in both radial and tangential horizontal spectra of the recorded time-histories at several floors of the Punta Gennarta Dam. Amplitude spectra used for this analysis were derived only by velocity time-histories for the higher sensitivity and very low instrumental self-noise of the velocimeter transducers. Spectral analyses have been performed only selecting the time intervals not affected by transients using Gabor's transform. All amplitude spectral ratios were obtained by filtering the amplitude spectrum of each microtremor trace with the reference amplitude spectrum computed for the signal acquired at [TR14] station, collected above the foundation level of the dam, within the lower tunnel. Directional spectral analysis of all microtremor data puts in evidence that radial displacements represent the main vibration components of the arch dam motion. Thus, the traces acquired in this direction can be used to effectively evaluate the empirical transfer function of the dam. To demonstrate this fact we can observe Figure 6.5 where the directional spectra of the horizontal components for some records are compared. Microtremor signals acquired at the topmost part of the structure are characterized by a strong directional effect of the main spectral components (corresponding to the natural frequencies of the dam). In these plots, 0° and 90° indicate radial and tangential directions respectively. Directional effects are progressively attenuated towards the lower levels of the structure until the base station, where the [TR14] angular plot doesn't show any anisotropic features of the noise field. Radial spectral ratios derived for all microtremor stations placed on the crest of the dam are included in Figure 6.6 and in Figure 6.7.

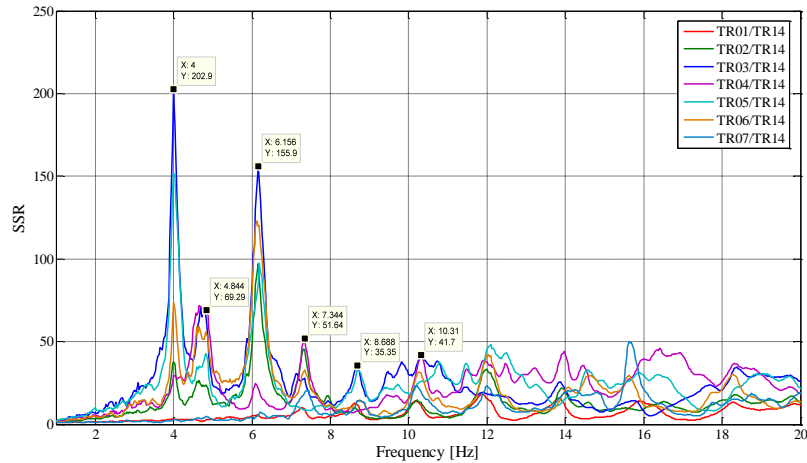


Figure 6.6: Radial spectral ratios at the dam crest (October 2012).

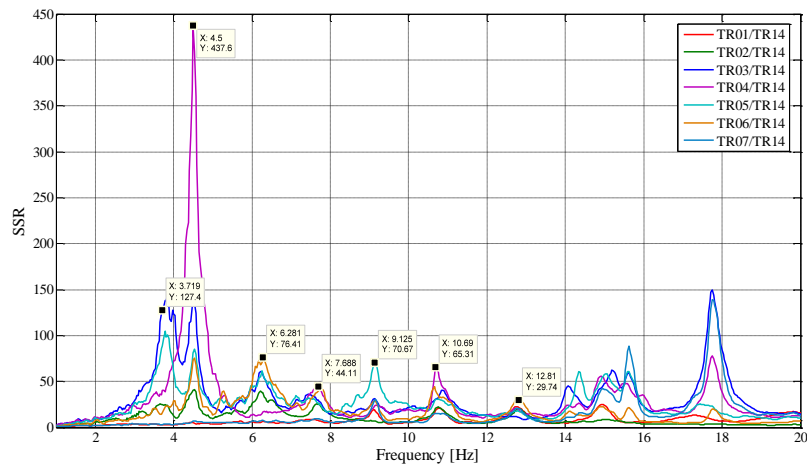


Figure 6.7: Radial spectral ratios at the dam crest (March 2013).

As we can observe, results obtained in October 2012 highlight the fundamental frequency of vibration at about 4 Hz considering the radial component of the motion. The peak related to the fundamental mode is characterized by maximum amplitude in correspondence with the [TR03] and [TR05] microtremor stations. Conversely, this frequency shows negligible amplitude in the spectral ratio derived from the [TR04] station placed in the central position at the crest of the dam, as can be seen in both figures. The amplitude of this frequency peak is strongly attenuated in the signals acquired at stations [TR01] and [TR07], measurements performed near to the abutments of the dam. These records are not affected by the main vibration frequencies of the structure, rather their spectra are characterized only by frequency peaks above 7 Hz, related to structural higher modes of vibration. The absence of the vibration component with frequency of 4 Hz in the [TR04] recording allows us to assume that the first vibration mode shape of the structure is not represented by a simple flexural mode but is characterized by one node in the central part of the dam. This hypothesis is also supported by the characteristics of the spectral ratios relative to the measurements taken in both upper and lower

walkways, where the spectral peak associated with the first vibration mode shows larger amplitude in the side positions of the structure rather than in two central positions, where it is negligible or missing (like for the [TR09] and [TR12] stations). Furthermore, the spectral ratios show a clear peak centered at the frequency of 4.8 Hz. This component could be associated with the second mode of vibration of the structure. In this case the mode shape retrieved at 4.8 Hz is not provided by one node in correspondence of the central acquisition station [TR04], where the amplitude of this component is at its maximum. An additional spectral peak at the frequency of about 6.2 Hz is probably related to a higher vibration mode. The frequency range between 7 Hz and 20 Hz is instead characterized by other frequency peaks of further vibration structural modes of the dam. The measurements carried out in March 2013 supply evidence that the first frequency of vibration is now about 3.7 Hz. The frequency shift from 4 Hz to 3.7 Hz between the conditions of two reservoir water levels corresponds with a reduction of about 7.5 %. Because the structure features were not modified during the two surveys (few months), this variation is directly related to different water pressure acting on the upstream side of the dam. The second frequency of vibration is 6.25 % lower than the value measured in October 2012, reducing from 4.8 Hz to 4.5 Hz. Higher frequencies of vibration are either not clearly affected by this effect, or the observed variation is negligible. The first experimental mode shape of vibration for the crest arch of the dam is shown in Figure 6.8. In both cases we can observe an anti-symmetric fundamental mode shape with maximum displacements at the [TR03] and [TR05] microtremor stations. Several empirical relationships proposed in literature can be used to assess fundamental frequency of arch dams by the geometric features of these structures.

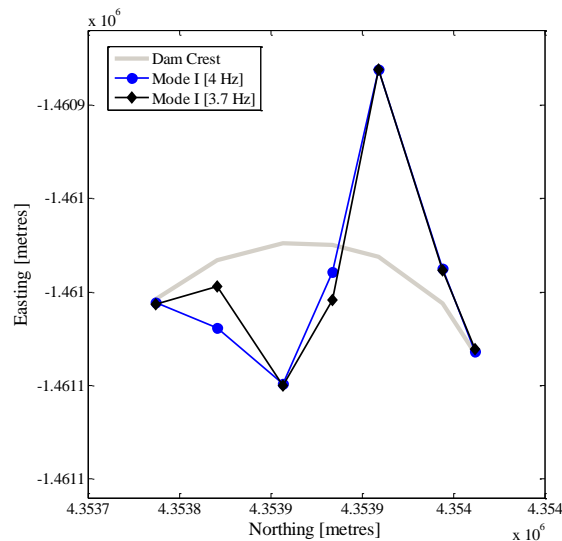


Figure 6.8: Normalised crest plot of the empirical first mode shape derived by the ambient vibration surveys with 27 metres water level (4 Hz) and 43 metres water level (3.7 Hz).

In particular, Priscu et al. (1985) present the natural fundamental frequency of arch dams corresponding at the full reservoir condition by means of the following equation:

$$f_0 = \frac{1}{0.1 + 0.2 \left( \frac{H}{100} \right)} \quad (6.2)$$

where,  $f_0$  indicates the natural fundamental frequency and  $H$  (in metres) is the dam height. The natural frequencies of Punta Gennarta Dam, obtained from the two ambient vibration tests, are summarized in Table 2 and Table 3. As can be seen in these tables, the natural frequencies are close to each other. We have compared experimental vibration properties with expected values using the above empirical formulation. According to the equation (6.2), the natural fundamental frequency of Punta Gennarta Dam is 4.6 Hz while the reservoir is full. Whereas the natural fundamental frequency obtained from ambient vibration test is 3.7 Hz. However, this value is not obtained for full reservoir condition, but for the highest water level during the analysed periods (corresponding to about 83.8 % of the maximum reservoir height). Furthermore, the above equation doesn't account for the aspect ratio of the dam, completely neglecting both the crest length and the thickness of the structure. Therefore, this kind of difference may be accepted. This result shows that the reservoir water interaction phenomena have more importance on the dynamic behaviour of these structures. Further evidence of the experimental results obtained from the recordings acquired with the digital tromograph Tromino comes from the comparison with the microtremor spectra recorded through the S13 Teledyne seismometers. In fact, it is possible to detect the same frequency components using both instrumental tools, as we can see in Figure 6.9, where radial spectral ratios related to the crest stations acquired using S13 geophones are shown. By observing these spectra it is possible to note that all frequency peaks are very close to those identified using the other sensor. Only the frequency of the second vibration mode shows smaller amplitudes, except for the midpoint crest station [TR04].

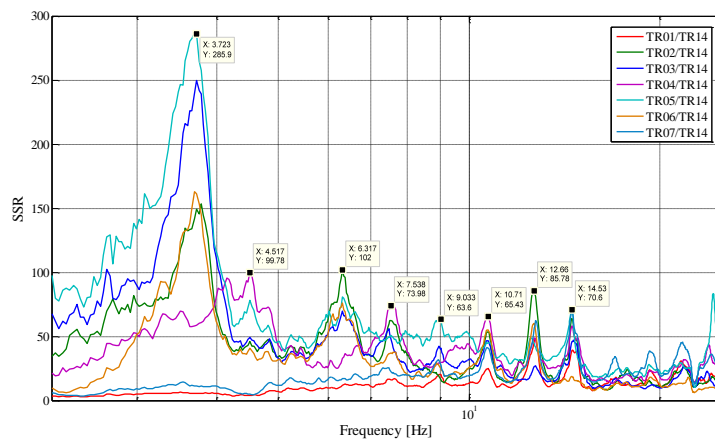


Figure 6.9: Amplitude spectral ratios derived for the crest stations using S13 seismometers time-recordings with 43 metres water level height.

The water level variation effect is also highlighted by the different behaviour of several points of the structure body during two test conditions. The experimental mode shapes are obtained by comparing

the measurements acquired along four floors of the structure, above the foundation level (taken as reference point at 0 metres), at the lower and at the higher walkways (21 and 39 metres), and at the crest of dam (53.5 metres) respectively. Radial spectral ratios derived for these points are used to assess the relative amplification effect of vibration produced from the base to the top of the dam, along its crown cantilever section (Figure 6.10) and two side sections, at the left (Figure 6.11) and at the right (Figure 6.12) of the structure.

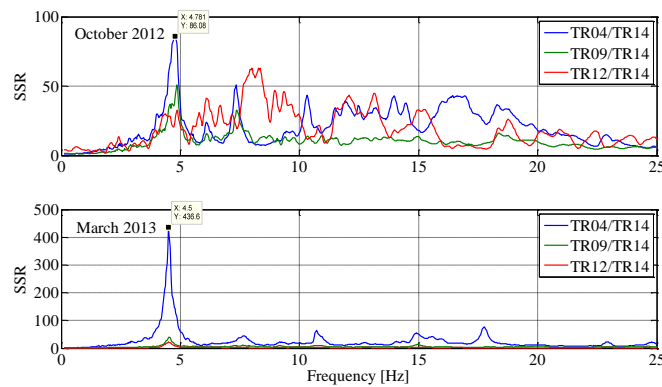


Figure 6.10: Empirical transfer function derived for the crown cantilever vertical section during both ambient vibration tests.

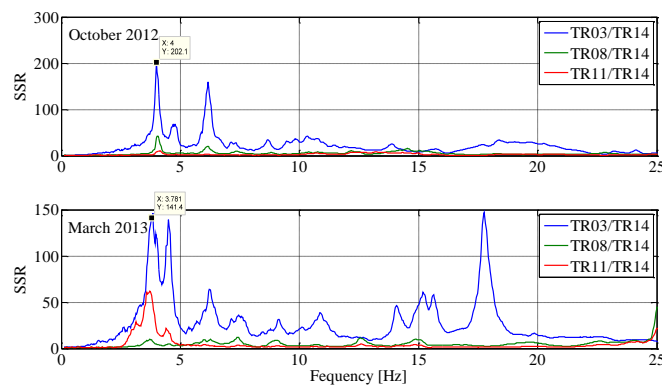


Figure 6.11: Radial spectral ratios derived for the left side of the dam.

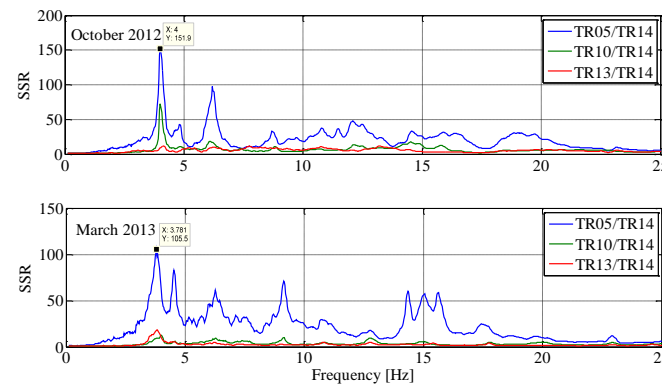


Figure 6.12: Radial spectral ratios derived for the right side of the dam.

The relative amplitudes have been compared to measurements collected on different days, although with analogous environmental and weather conditions. The comparison is shown in Figure 6.13 where we can see that during the test carried out with the lower water level (27 metres) all considered points of the dam are characterized by an amplification effect, progressively increasing from the base to the crest for both first and second natural frequencies.

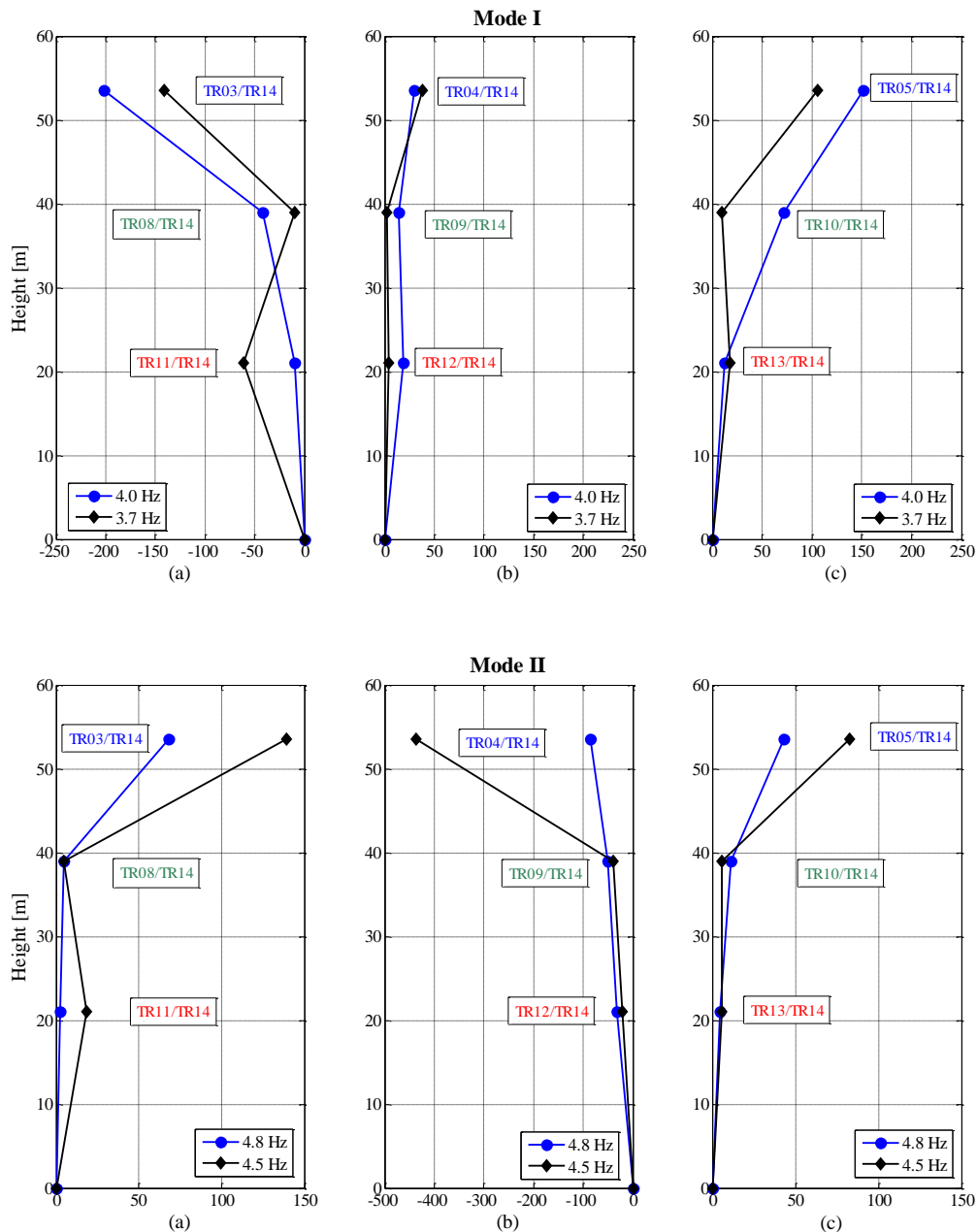


Figure 6.13: Comparison between the experimental mode shapes evaluated in terms of relative amplification effect, derived for: (a) the left side of the dam; (b) the crown cantilever vertical section; (c) the right side of the dam.

Conversely, results obtained in the next ambient vibration test (with 43 metres water level height) highlight a deviation from the previous behaviour and we can observe that there is a greater

amplification of the motion at the lower walkway level. This behaviour can be observed in both sides of the structure for the fundamental frequency of vibration, but it is more marked in the left side of the dam. Along the crown cantilever section we can observe that the central section of the dam is mainly affected by the second vibration mode (at the frequency of 4.8 Hz in October 2012 and 4.5 Hz in March 2013). Moreover the experimental dynamic behaviour of the dam associated with higher water level is characterised by greater amplification at the dam crest rather than the case of lower water level. Damping ratios derived for the first and second vibration mode of the dam are also summarized in Table 6.2 and Table 6.3. These values have been obtained by means of the matrices shown in Figure 6.14. In these plots, maximum amplitudes indicate the percentage of modal damping related to each natural frequency of vibration detected. However, in contrast to natural frequencies, damping ratios do not show a significant change with two different water levels.

Mode No.	Frequency $f$ (Hz)	Damping ratio $\xi$ (%)
1	4.0	1.64
2	4.8	1.91
3	6.2	-
4	7.3	-

Table 6.2: Experimental vibration properties of Punta Gennarta Dam – October 2012

Mode No.	Frequency $f$ (Hz)	Damping ratio $\xi$ (%)
1	3.7	1.73
2	4.5	1.82
3	6.3	-
4	7.5-7.7	-

Table 6.3: Experimental vibration properties of Punta Gennarta Dam – March 2013

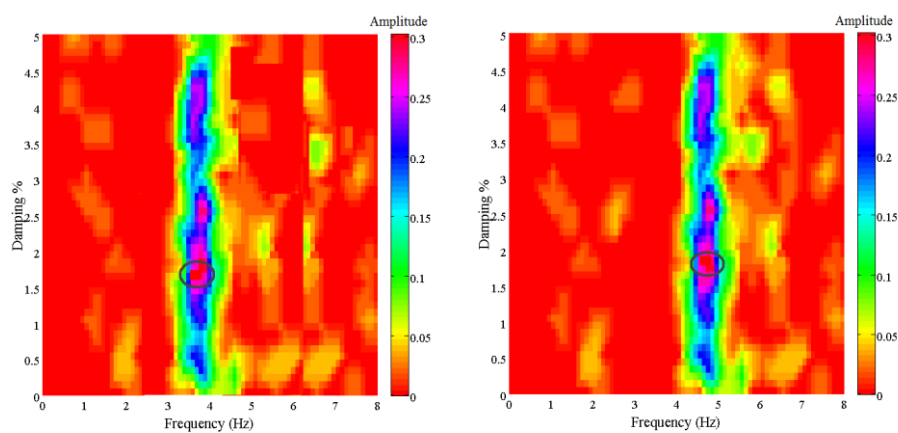


Figure 6.14: Exemple of NonPaDAn damping estimation performed for the first (left) and second (right) vibration mode of the dam. Maximum values, indicated by means of a black ellipse, correspond to each natural frequency and to the related modal damping.



## 6.4 FINITE ELEMENT MODELLING AND ANALYSIS

### 6.4.1 Discrete model of Punta Gennarta Dam

In order to explain whether the differences observed in the fundamental frequencies are really related to variation in the water level reservoir a numerical dynamic analysis was carried out, taking into account the foundation rock-structure-reservoir interaction. 3D Structural Mechanics Module (eigenfrequency analysis solver) of Comsol Multiphysics® package was used to calculate the mode shapes and the undamped natural frequencies. The finite element model of the Punta Gennarta Dam is built with variable radius curvature geometry obtained through the interpolation of seven vertical sections of the structure in 3D space. In fact, all authors highlight that arch dam structures must be modelled as three dimensional objects to obtain a realistic representation of their structural behaviour. The discrete model used to predict dynamic vibration properties does not consider the openings of the structure. The mesh size is established in agreement with literature guidelines (USACE, 2003). The dam body is built by means of 4,734 tetrahedral 3D elements. These elements compose the base mesh of the discrete model and each node of the model has three degrees-of-freedom, corresponding to translations in x, y, and z directions. The total number of degrees-of-freedom amounts to 26,799 for the extended mesh. In the finite element model the compatibility and equilibrium conditions are automatically satisfied at the nodes along the interfaces between Dam-Reservoir-Foundation because the displacements are assumed as variables in both the reservoir and the dam, following classic Lagrangian approach. Domain properties defined for the analysis are density, elasticity modulus and Poisson's ratio. The density was taken to be  $2,300 \text{ kg/m}^3$ , the Young's modulus  $25\text{E}09 \text{ N/m}^2$  and Poisson's ratio was assumed to be 0.33. Some views of the finite element model of the Punta Gennarta arch dam are shown in Figure 6.15.

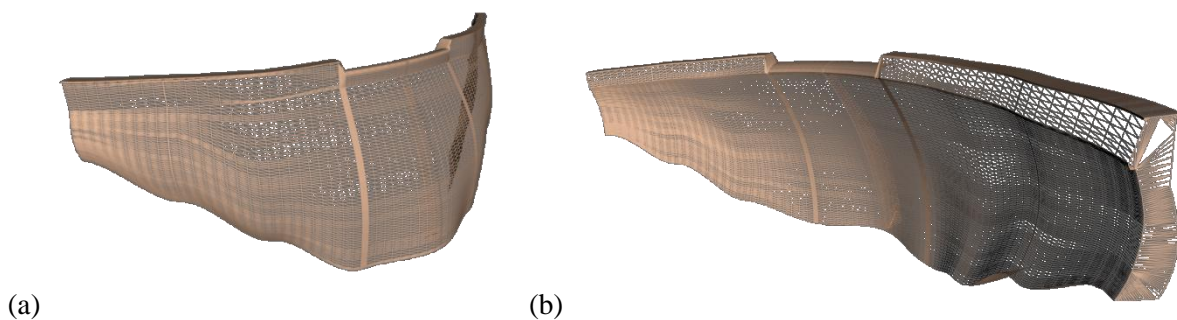


Figure 6.15: Some pictures of the 3D mesh used for the finite element analysis of Punta Gennarta Dam (a) upstream side view; (b) downstream side view.

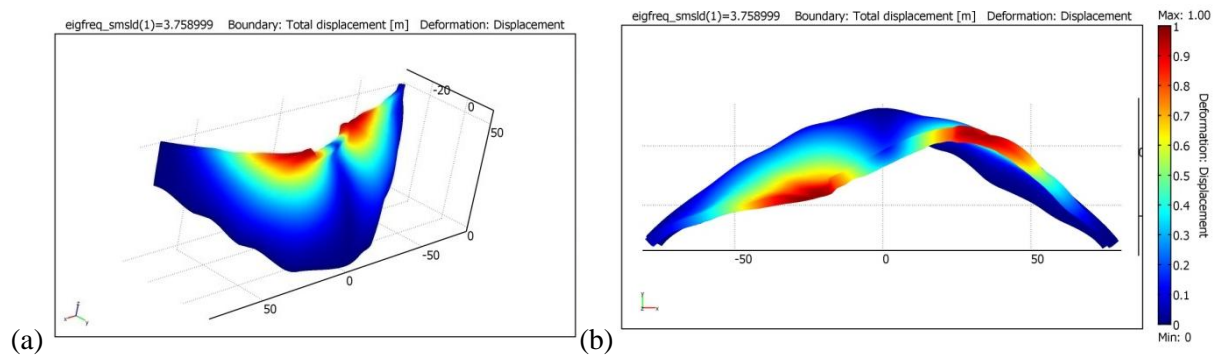
### 6.4.2 Numerical results

The Finite Element code solves the generalized eigenvalues problem to describe free undamped vibrations of a finite element linearly elastic system. This problem is defined by the following equation:

$$(K - \lambda_n M)\Theta_n = 0 \quad n = 1, \dots, N \quad (6.3)$$

where  $K$  and  $M$  are the stiffness matrix and the mass matrix of the structure respectively and  $N$  represents the total number of degrees of freedom of the discrete model. The solution leads to define  $N$  eigenvalues  $\lambda_n$  and the corresponding eigenvectors  $\Theta_n$ . Eigenvalues are related with natural frequencies ( $\omega_n = \lambda_n^{1/2}$ ) and each eigenvector describes one single mode shape. The mode shapes obtained for this model are plotted in Figure 16. This numerical model allows us to predict the vibration properties of the dam with both considered water levels.

### Mode I



### Mode II

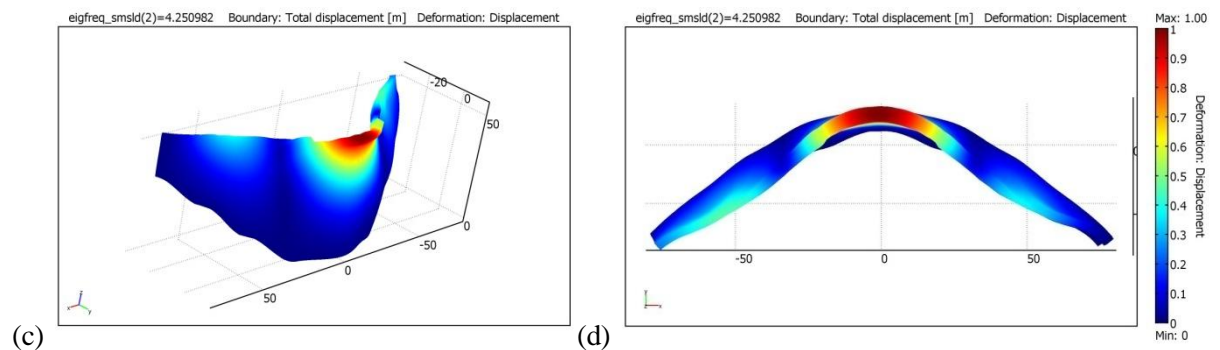


Figure 6.16: First two mode shapes of vibration according to Punta Gennarta Dam model: (a, c) perspective view; (b, d) horizontal plane view. The color scale indicates the normalized total displacement of each mode shape.

Water level effect has been simulated by means of different boundary conditions on the upstream surface of the structure finite element model. In particular, at the nodes of the mesh placed along the contact surface with the water reservoir only vertical displacements are allowed. In other words, to taking into account the water pressure acting on the upstream surface of the structure, we have built the finite element model approximating the curvature of the upstream surface with several faces characterized by variable curvature and fixed height. In this way, we have imposed only vertical displacement boundary condition at the nodes placed along the faces in contact with the water reservoir. Conversely, the free boundary condition has been assumed for the faces placed above the

water level table. The interaction between the dam structure and the rock foundation corresponds with the fixed nodes boundary condition (zero displacements and rotations along the interface between structure and rock foundation). The mode shapes can be generally classified into symmetrical, anti-symmetrical and vertical modes respectively. We can see that the fundamental mode shape of the structure is an anti-symmetrical vibration mode and it shows a node at the midway point of the dam crest, corresponding about to the [TR04] microtremor station position. There are no displacements along the crown cantilever section for this mode shape. The second vibration mode is characterized by a more complicated shape with maximum displacement localised in the upper part of the crown cantilever section. Thus, the second mode is classified as a symmetric mode shape. The first natural frequency of the dam model results in 4.03 Hz and 3.75 Hz considering the different water level height. These values are very similar to those derived by vibration spectra. Conversely, there is a small difference for the second natural frequency of the finite element model with results of 4.56 Hz and 4.25 Hz respectively, therefore in both cases lower than those experimentally measured. This fact could be related to more complex interaction phenomena not fully modelled through Finite Element analysis or to assigned material properties, not perfectly matching true values. These limitations could be probably overcome also improving numerical simulation of the fluid-structure interaction effects using more complex multiphysics models. However, for the purposes of this research, despite the above small differences, we can consider that numerical results confirm the experimental dynamic behaviour of the dam and the observed frequency shift following the changes of the water height.

## **6.5 CONCLUSIONS**

Through the passive survey method we have derived the main vibration properties of a double curvature arch dam by considering two different water levels. Experimental vibration analyses carried out by means of a simple instrumental layout (composed of a single tri-directional tromometer and two short period seismometers) have allowed us to observe the variation of the first two natural frequencies of the dam related to the effect produced by the impounded water within the artificial reservoir. Fourteen microtremor recording stations have been chosen above the structure on the downstream surface. Natural frequencies are derived using Standard Spectral Ratio method modified for the purposes of this research into radial, tangential and vertical spectral ratio respectively. The radial component of the motion is that mainly affected by the vibration properties of the dam and it has been used for eigenfrequency peak picking. Observed frequency shift for the first vibration mode results 7.5 % passing from 4 Hz to 3.7 Hz. Also the second mode shows the same variation (about 6.25 % from 4.8 Hz to 4.5 Hz). Higher modes do not appear significantly influenced by this effect. Furthermore, although we have acquired only asynchronous time-histories, the measurements have allowed us to define the shape of the fundamental vibration mode. In order to validate experimental evidences, a numerical dynamic analysis has been performed by finite element modelling of the structure. This numerical model has allowed us to observe the water interaction effect imposing

several boundary conditions at the nodes of the 3D mesh along the interface between the upstream side and water volume stored within the reservoir. The obtained results have shown a good agreement with vibration data and have confirmed the hypothesis about the shape of the fundamental vibration mode.

## **REFERENCES**

- Aminfar M. H., Mafi-Kandi H., Ahmadi H. (2011). Improving the seismic performance of arch dams using segmentation - a case study of Karun 4 Arch Dam, Iran, *Journal of Engineering Science and Technology*, 6(4), 397-410.
- Borcherdt R. D. (1970). Effects of local geology on ground motion near San Francisco Bay, *Bulletin of the Seismological Society of America*, 60, 29-61.
- Castellaro S., Mulargia F., Padrón L. A. (2013). The different response of apparently identical structures: a far-field lesson from the Mirandola 20th May 2012 earthquake, *Bulletin of Earthquake Engineering*, 2013. (doi:10.1007/s10518-013-9505-9)
- Darbre G. R. and Proulx J. (2002). Continuous ambient-vibration monitoring of the arch dam of Mauvoisin, *Earthquake Engineering and Structural Dynamics*, 31, 475–480. (doi: 10.1002/eqe.118)
- Ditommaso R., Vona M., Mucciarelli M., Masi A. (2010). Identification of building rotational modes using an ambient vibration technique, *Proceedings of the 14<sup>th</sup> European Conference on Earthquake Engineering*, Ohrid, Macedonia, August 30 – September 03, 2010.
- Ditommaso R., Vona M., Gallipoli M. R., Mucciarelli M. (2013). Evaluation and considerations about fundamental periods of damaged reinforced concrete buildings. *Natural Hazards and Earth System Sciences*, 13, 1903–1912.
- Fok K. L. and Chopra A. K. (1986). Earthquake analysis of arch dams including dam-water interaction, reservoir boundary absorption and foundation flexibility, *Earthquake Engineering and Structural Dynamics*, 14, 155–184.
- Gallipoli M. R., Mucciarelli M., Vona M. (2009). Empirical estimate of fundamental frequencies and damping for Italian buildings. *Earthquake Engineering and Structural Dynamics*, 38, 973–988.
- Ghanaat Y. (1993). Theoretical manual for analysis of arch dams, *Instruction Report ITL-93-1*, U.S. Army Engineer Waterways Experiment Station, Vicksburg, MS.
- Kramer S. L. (1996). *Geotechnical Earthquake Engineering*, Prentice Hall, Upper Saddle River, New Jersey, 1996.
- Kuo J. S. H. (1982). Fluid-Structure interactions: added-mass computations for incompressible fluid, Report No. UCB/EERC-82/09, University of California Earthquake Engineering Research Center, Berkeley, CA.
- Mivehchi M. M., Ahmadi M. T., Hajmomeni A. (2003). Effective techniques for arch dam Ambient Vibration Test: application on two Iranian dams, *Journal of Seismology and Earthquake Engineering*, 5(2), 23-34.
- Mucciarelli M. and Gallipoli M. R. (2007). Non-parametric analysis of a single seismometric recording to obtain building dynamic parameters, *Annals of Geophysics*, 50, 259–266.
- Prisic R., Popovici A., Stematiu D., Stere C. (1985). *Earthquake engineering for large dams*. New York, Wiley, 1985.

Roşca B. (2008). Physical model method for seismic study of concrete dams, *Buletinul Institutului Politehnic Din Iaşi*, 54(58), Fasc. 3, 2008.

Sevim B., Bayraktar A., Altunişik A. C., Adanur S., Akköse M. (2010). Determination of water level effects on the dynamic characteristics of a prototype arch dam model using Ambient Vibration Testing, *Experimental Techniques*, 36, 72–82. (doi:10.1111/j.1747-1567.2010.00671.x)

Sevim B., Bayraktar A., Altunişik A. C. (2011). Finite element model calibration of Berke Arch Dam using operational modal testing, *Journal of Vibration and Control*, 17(7), 1065–1079. (doi: 10.1177/1077546310377912)

Snieder R., Safak E. (2006). Extracting the building response using seismic interferometry: theory and application to the Millikan Library in Pasadena, California. *Bulletin of Seismological Society of America*, 96, 586–598.

USACE, Time-History Dynamic Analysis of Concrete Hydraulic Structures, Engineering and Design EM 1110-2-6051, 200 p (2003).

Vidal F., Navarro M., Aranda C., Enomoto T. (2013). Changes in dynamic characteristics of Lorca RC buildings from pre- and post-earthquake ambient vibration data. *Bulletin of Earthquake Engineering*, 2013. (doi:10.1007/s10518-013-9489-5)

Westergaard H. M. (1933). Water pressure on dams during earthquakes, *Transactions of the American Society of Civil Engineers*, 98, 418-433.

## ACKNOWLEDGMENTS

The completion of the Ph.D thesis would not have been possible without the cooperation and the help of a great many people.

First I thank my supervisor Prof. Gaetano Ranieri for his stimulating discussions and for his invaluable advice and support during the last years.

I'm very grateful to Luca Piroddi for his fundamental contribution to the researches and especially for the helpfulness shown during the different phases of the work.

I would also like to acknowledge the great working group of applied geophysics and in particular way Antonio Trogu, Luigi Noli and Mario Sitzia. I thank all the aforementioned people for their essential support.

Finally, I gratefully acknowledge Sardinia Regional Government for the financial support of the Ph.D. scholarship (P.O.R. Sardegna F.S.E. Operational Programme of the Autonomous Region of Sardinia, European Social Fund 2007–2013—Axis IV Human Resources, Objective 1.3, Line of Activity 1.3.1.).

*Sergio Vincenzo Calcina*